THESIS FOR THE DEGREE OF DOCTOR OF PHILOSOPHY

Development of a Hydrometallurgical Process for Recycling Steel Grinding Sludges into Iron Chloride

Thomas Ottink

Department of Chemistry and Chemical Engineering

Chalmers University of Technology

Gothenburg, Sweden 2026

Development of a Hydrometallurgical Process for Recycling Steel Grinding Sludges into Iron Chloride

Thomas Ottink

ISBN: 978-91-8103-395-3

Doktorsavhandlingar vid Chalmers Tekniska Högskola
Ny serie nr 5852
ISSN: 0346-718X
DOI: https://doi.org/10.63959/chalmers.dt/5852

Nuclear Chemistry and Industrial Materials Recycling
Department of Chemistry and Chemical Engineering
Chalmers University of Technology
SE-412 96 Gothenburg
Sweden
Telephone +46 (0)31-772-1000

Cover illustration: Open-loop recycling of grinding sludges via production of iron chloride solutions for water treatment and battery material synthesis

Profile picture: Ateljé Marie Fotostudio AB, Fotograf Peter Nilsson

Printed by:
Chalmers digitaltryck
Gothenburg, Sweden 2026

Development of a Hydrometallurgical Process for Recycling Steel Grinding Sludges into Iron Chloride

Thomas Ottink

Industrial Materials Recycling
Department of Chemistry and Chemical Engineering
Chalmers University of Technology

Abstract

Almost 2 billion tons of steel are produced annually, accounting for 7.2% of global greenhouse gas emissions, and recycling plays a crucial role in reducing this impact by conserving energy and materials. Grinding sludge is a hazardous metal waste generated during machining processes throughout the steel value chain. Due to limited recycling options, it is widely incinerated and landfilled today, representing a significant environmental and economic burden for its producers, with disposal fees up to 1000 €/ton. New waste management strategies are needed, and given that the sludges contain 50-80 wt% iron, an open-loop hydrometallurgical recycling process to produce iron-based chemicals was developed in this work. It was shown that >95% of the iron could be recovered as ferrous ($FeCl_2$) or ferric ($FeCl_3$) chloride solutions, which are vital in water treatment and other sustainability-related applications. This was achieved by first washing the sludges with a solvent to recover lubricant oils and removing abrasive wheel materials by magnetic separation. Cleaned swarf was then leached with hydrochloric acid (HCl) or $FeCl_3$ to convert iron into soluble $FeCl_2$. Codissolved impurities, including chromium, copper, nickel and residual lubricant oils, were removed directly from the slurry with grinding swarf as a precipitation agent, and made separable from the solution by filtration. Purified $FeCl_2$ solutions were converted to $FeCl_3$ via pressure oxidation with oxygen or electrolysis, with the coproduction of hydrogen gas (H_2), yielding a solution of 36 wt% $FeCl_3$ that met drinking water coagulant purity standards. Further assessments showed that the recycled product performed comparably to a commercial 40 wt% $FeCl_3$ solution in water treatment and synthesis of iron phosphate for lithium-ion batteries. A net profit of 520 €/ton sludge recycled was estimated, with $FeCl_3$ and H_2 representing 71% and 8% of the process revenue streams. This can generate significant income, serving as a stable foundation for grinding sludge recycling.

Keywords: Grinding sludge, Swarf, Recycling, Hydrometallurgy, Ferric chloride

List of publications and manuscripts

This thesis is based on the following papers and manuscript:

(1) Ottink, T., Vieceli, N., Foreman, M. R. S., Petranikova, M. (2022). Novel approach to recycling of steel swarf using hydrometallurgy. Resources, Conservation and Recycling, 185, 106450.

Contribution: Main author and responsible for experimental work and data analysis.

(2) Ottink, T., Petranikova, M. (2026). Hydrometallurgical Recycling of Steel Grinding Swarf via Hydrochloric Acid Leaching and Precipitation for Production of High Purity Iron Chloride Coagulants and Hydrogen Gas. Resources, Conservation & Recycling Advances, 200320.

Contribution: Main author and responsible for experimental work and data analysis.

(3) Ottink, T., Garjulli, F., Lumetzberger, M., Espinosa, D. C., Petranikova, M. (2025). Hydrometallurgical recycling of steel grinding swarf via oxidative leaching using ferric chloride. RSC Advances, 15(48), 40675-40686.

Contribution: Main author and responsible for conceptualisation and data analysis.

(4) Ottink, T., Ahlberg, E., Rouquette, L. M. J., Petranikova, M., (2026). Development and Economic Assessment of a Recycling Process for Production of Ferric Chloride and Hydrogen Gas from Steel Grinding Sludges. Manuscript submitted to Chemical Engineering Journal.

Contribution: Main author and responsible for experimental work and data analysis.

Related publications and patent application not included in the thesis:

Vieceli, N., **Ottink, T**., Stopic, S., Dertmann, C., Swiontek, T., Vonderstein, C., ... & Petranikova, M. (2023). Solvent extraction of cobalt from spent lithium-ion batteries: Dynamic optimization of the number of extraction stages using factorial design of experiments and response surface methodology. Separation and Purification Technology, 307, 122793.

Großwendt, F., Bram, M., Treppmann, M., Keszler, M., **Ottink, T**., & Weber, S. (2025). Materials scientific challenges of a circular economy of high-alloy tool steels. Practical Metallography, 62(9-10), 634-649.

Ottink, T., Petranikova, M., Process for recycling steel swarf sludge to produce an iron chloride solution. WO 2025/058553 A1, Published Mar. 20, 2025

Abbreviations and definitions

The following abbreviations and definitions are used throughout the thesis:

a	Thermodynamic activity
AEM	Anion exchange membrane
ANOVA	Analysis of variance
a.u.	Arbitrary unit
CBN	Cubic boron nitride
CV	Cyclic voltammetry
DI	De-ionised
DOE	Design of Experiments
E	Electrode potential
EAF	Electric arc furnace
EC	Electrochemical
E_{cell}	Cell potential
EDS	Energy dispersive X-ray spectroscopy
EIS	Electrochemical Impedance Spectroscopy
EN 888	$FeCl_3$ coagulant standard
EWC	European waste codes
FP	Iron phosphate
FTIR	Fourier Transform Infrared Spectroscopy
GCD	Glassy carbon disc electrode
GCR	Reticulated glassy carbon electrode
GHG	Greenhouse gas
HSAB	Hard-soft acid-base theory
I	Current
ICP-OES	Inductively Coupled Plasma Optical Emission Spectroscopy
K	Equilibrium constant
L/S	Liquid to solid ratio
L/S_i	Initial liquid to solid ratio
LFP	Lithium iron phosphate
LOD	Limit of detection
LOF	Lack of fit
LSV	Linear sweep voltammetry
OPEX	Operating expense
ORP	Redox
PQ	Precipitant quantity
Q	Reaction quotient
R^2	Coefficient of determination
R^2_{adj}	Adjusted coefficient of determination
R_{cell}	Cell resistance
RE	Reference electrode
rpm	Rotations per minute
SATP	Standard ambient temperature and pressure
SEM	Scanning Electron Microscopy
SiC	Silicon carbide
t	Time
T	Temperature
TC	Total carbon
TN	Total nitrogen
TOC	Total organic carbon
V	Volume
WE	Working electrode
wt%	Weight percentage
x_i	Coded variable
x_M	Mass fraction of metal M
XRD	X-ray Diffraction
XRF	X-ray Fluorescence
β	Cumulative stability constant
ΔG_r	Gibbs free energy of reaction
ΔH_r	Enthalpy of reaction
ΔS_r	Entropy of reaction
ε	Experimental variability
η_F	Faradic efficiency
σ	Standard deviation
%E	Leaching efficiency
$\%E_s$	Percentage of input solids dissolved in output
$\%E_{tot}$	Percentage of input dissolved in output
%FC	Percentage of filter cake
%R	Removal efficiency
[M]	Concentration of metal M

Constants

Faraday constant (F)	96485 A s/mol
Gas constant (R)	8.3145 J/K mol

Table of contents

1 Introduction

Iron is perhaps the single most important element in our modern society. This dependence becomes obvious when trying to imagine a product that contains no iron or has not involved any form of iron in its production. It can today be found everywhere, from construction materials to vehicles and household appliances. Most of our technological progress in the past 200 years is owed to advances in steelmaking during the Industrial Revolution. Steel production has seen an exponential increase since then, and was close to 2 billion tons in 2025 [1]. This number more than doubled over the past 25 years, driven by the developments in China, where 50% of all steel is produced today. Chinese steel is expected to peak between 2020 and 2030, but global production is predicted to increase further to 2.5-3 billion tons by the 2100s due to growing Indian, Latin American, and African economies [2].

Because of its magnitude, energy use, and coke consumption, steelmaking is today responsible for 7.2% of global greenhouse gas (GHG) emissions [3]. Significant amounts of waste are also generated along the value chain, posing serious health and environmental threats, and an important strategy to reduce these impacts is to implement better waste management practices. The European Union (EU) Waste Framework Directive (2008/98) defines the waste hierarchy as a general guideline for waste management, in which the preferred order of action is shown in Figure 1. Working towards higher tiers minimises energy use, material losses to landfills, and the need for natural resources. Following the hierarchy is especially important when managing hazardous waste, as these pose an added risk of contaminating local soil and groundwater when land-filled.

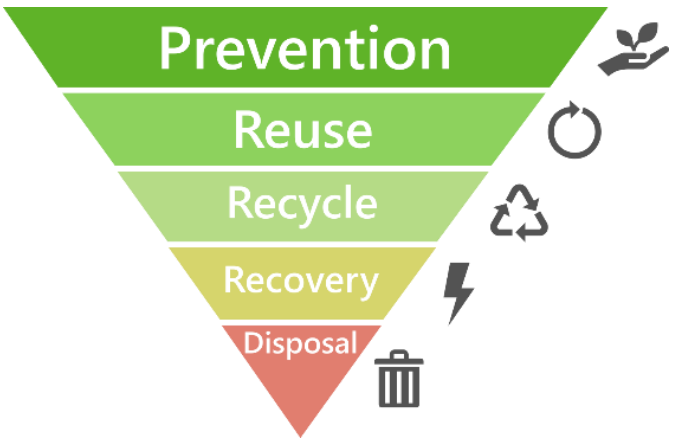

Figure 1: The waste hierarchy describing the most to least preferable approaches to waste management.

A particular waste generated across all steps of the steel value chain, but especially in workshops and foundries, is metallic swarf and machining sludge. Metalworking operations such as milling, turning, and grinding are used to shape a workpiece by cutting away excess material with a tool. The affected area is normally cooled

and lubricated with cutting fluids, which also wash away the swarf. The swarf particle size can vary considerably depending on the tool, lubricant, and processing conditions used, and determines the overall recyclability of these wastes. Operations such as milling, turning, and drilling produce large shavings that are easily separated from cutting fluids and remelted as scrap in steelmaking furnaces. Fine swarf from grinding and polishing, on the other hand, readily absorbs and retains cutting fluids, forming oily sludges. These sludges have low value, are generally classified as hazardous waste (European Waste Code 12 01 18), and few technologies exist to economically recycle them. Vast amounts are therefore incinerated and landfilled today, which is not only problematic from an environmental perspective but can also entail high disposal fees of 200-1000 €/ton for manufacturers [4, 5]. The worldwide production of grinding sludges can be estimated at roughly 10-12 million tons per year (see paper 2), and these numbers are expected to continue to grow as steel production increases.

New open-loop recycling strategies are needed to reach higher tiers in the waste hierarchy, given that recirculating grinding sludges to the steel industry has been attempted in the past decades without widespread adoption. In this context, this thesis proposes a novel hydrometallurgical approach to recycling by making iron-based chemicals. Steel grinding sludges typically contain 70-80 wt% iron and represent a promising feedstock for producing bulk chemicals such as iron chloride and sulphate solutions. These products are indispensable in water treatment, battery manufacturing, and other sustainability-related applications. The aim is to develop a process to produce ferrous chloride ($FeCl_2$) and ferric chloride ($FeCl_3$) solutions from low-alloy steel and cast iron grinding sludges, and assess the economic and environmental benefits of this recycling approach. Validating the applicability of recycled products is important, and the final $FeCl_3$ solution was tested as a water-treatment coagulant and precursor to iron phosphate for Li-ion batteries. Unlocking new applications for grinding sludges outside the steel industry can potentially be the key to making recycling more economical and preventing thousands of tons of hazardous waste from ending up in landfills.

2 Background

2.1 A brief history of steelmaking and current applications of iron

Human relations with iron go back as far as 5000 years, with the earliest applications involving the use of meteoric iron in tools and weapons [6]. Man-made iron was first produced in bloomeries, which could reach 1200°C to smelt iron ore and produce blooms that could be hammered into wrought iron with 0.04-0.08 wt% carbon. This malleable but strong material largely replaced bronze tools and became a commodity during the Iron Age. Due to the difficulty of smelting and limited production, iron was considerably more valuable than it is today, and recycling can be assumed to have been an important aspect of ironmaking already during this period. Towards the end of this era, the Chinese developed the first high-temperature furnaces capable of producing significantly harder, but brittle cast iron with a carbon content of 2.0-4.3 wt% [7]. Steel has the combined ductility and strength of wrought and cast iron with a carbon content ≤2 wt%, and requires partial decarburisation of the cast iron. Despite the early discovery of this material shortly after the Iron Age, steelmaking would remain limited until 2000 years later [6]. At the start of the Industrial Revolution, major advances were made to meet the rising demand for iron. Charcoal was replaced by cheap mineral coal, and the development of new furnaces enabled the mass production of steel from low-grade iron ores [8]. This made steel much more affordable, which was the key to unlocking further industrial developments.

Metallic iron and steel remain the largest and most important applications of iron by far. A myriad of grades and alloys are available today, specially tailored to each application. In modern steelmaking, iron ore is typically smelted in a blast furnace with coke and flux to produce pig iron, which can be poured as cast iron or refined into crude steel in a basic oxygen furnace. Around a third of current steel demand is met today by secondary production from scrap, typically in electric arc furnaces (EAFs) [2]. Crude slabs, billets, and blooms from the steel mill can be remelted and cast into more advanced shapes in foundries. Blasting and roughing machining operations, such as milling, are common here to remove defects and provide detail to the cast product. Further grinding and polishing are also necessary for precision applications, such as gears and bearings, and are typically done in workshops where the finished goods are assembled. Recent awareness of climate change and environmental pollution problems has sparked one of the greatest transform-ations in iron and steelmaking since the Industrial Revolution. Key strategic actions

include a shift towards scrap-based production and minimisation of coke use by replacing traditional blast furnaces with direct-reduction furnaces that use H_2 for smelting iron ore [2, 9]. Unlike the reaction between carbon and iron oxides, which forms CO_2, direct reduction mainly generates water vapour as a byproduct. This can reduce GHG emissions in primary production by 95% if H_2 is generated via water electrolysis with renewable energy.

Other important uses of iron in the chemical industry have emerged during the 1900s. Ferric ($FeCl_3$ and $Fe_2(SO_4)_3$) and aluminium coagulants are widely used in water treatment today to remove phosphorus and other contaminants, including microplastics and heavy metals [10], [11], [12]. This is essential to prevent local water eutrophication as our urbanisation and the use of chemical fertilisers in agriculture intensify [13]. Around 2 million tons of iron-based coagulants are used annually in Europe, and this number is expected to increase significantly following a recent amendment to the EU urban wastewater directive (2024/3019) [14]. Other common uses of these iron-based chemicals include etching of printed circuit boards and hydrometallurgy, where Fe(III) can serve as a strong oxidiser capable of dissolving nobler metals such as Cu and Au [15–18].

Moving forward, iron is also expected to play an essential role in the ongoing green energy transition. In anaerobic digestors for biogas production from organic wastes such as sewage and manure, iron oxides and $FeCl_3$ are already added to inhibit the formation of toxic and corrosive H_2S [19, 20]. The battery industry is another fast-developing field where iron cathode and anode active materials can make a difference. Stationary energy storage solutions are required as green, intermittent solar and wind power become more common. Sodium-ion batteries (SIB) with iron oxide or cyanide electrodes, and iron-air batteries are expected to play important roles as affordable solutions [21–23]. Lightweight batteries for electric vehicles are also necessary and have to a large extent been lithium-ion batteries based on Ni, Mn, and Co oxides [24]. However, due to high supply risks and the unethical production of conflict minerals such as Co, many electric vehicle batteries today use cheaper lithium iron phosphate (LFP) cathodes. The most common raw material for LFP and SIB is $FeSO_4$, but other chemical iron sources, such as $FeCl_3$ and $Fe(NO_3)_3$, can also be used [25].

2.2 The grinding process

Grinding is used in iron and steel metalworking for fine machining, surface finishing, and sharpening applications. Its most extensive application is in the automotive industry for powertrain components such as cast-iron crankshafts, camshafts, drive shafts, and engine parts, as well as in gear cutting and the manufacturing of steel bearings. In foundries and steel mills, it can also be used to remove casting defects and to control the size and quality of hot- and cold-rolling rolls. Small-scale grinding applications include sharpening knives, saws, and blades for aerospace and energy generation turbines.

The grinding tool is an abrasive material in the form of loose particles, coated on a sandpaper disc or belt, or bonded in a wheel with binders [26]. Manual grinding is suitable for single jobs, but most larger workshops use computer numerical control to achieve high precision and consistency with short processing times. Cutting fluids are used in these high-throughput settings to cool, lubricate, wash away metal swarf, and protect the metal workpiece from corrosion [27]. Cooling is especially important in grinding as friction between the tool and workpiece creates high temperatures that drastically shorten the abrasive tool's life. The affected area is therefore commonly flooded with a jet of lubricant, as seen in Figure 2. The next sections focus on abrasives and cutting fluids to provide a deeper understanding of the components present in grinding sludge.

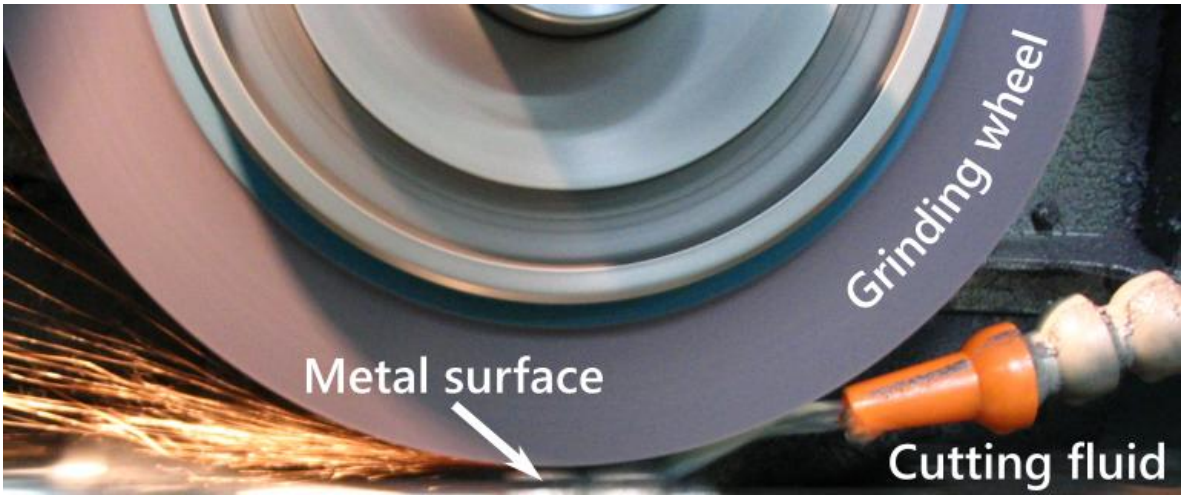

Figure 2: Grinding process with flood lubrication (*Grinding Process,* Solaris2006, Wikimedia Commons, CC BY-SA 3.0).

2.2.1 Grinding wheel abrasives and binders

The choice of abrasive for grinding depends on its cost, the hardness and type of workpiece material, and operating conditions. A well-performing abrasive is significantly harder than the workpiece and exhibits high chemical and thermal resistance to prevent degradation and maintain its sharpness over time [28]. Both natural and synthetic abrasives are used for grinding, but natural abrasives are typically softer and are rarely used in metalworking. Synthetic abrasives can be divided into conventional and superabrasives, as shown in Figure 3.

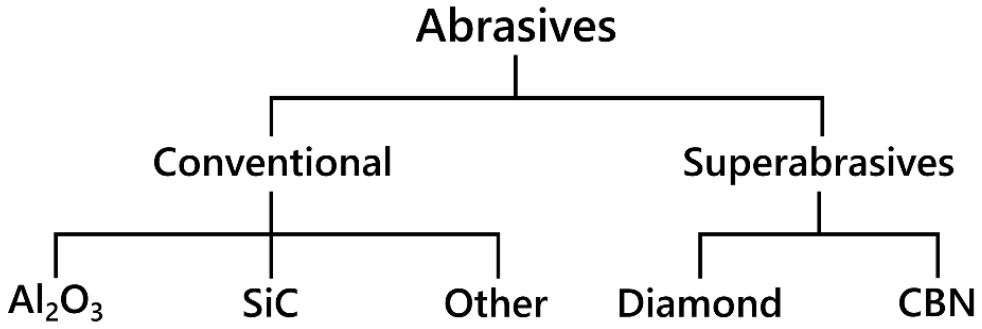

Figure 3: Conventional abrasive and superabrasive types used in grinding applications [28].

Alumina (Al_2O_3) and silicon carbide (SiC) are the most commonly used abrasives in grinding applications [28]. In metalworking, Al_2O_3 is used for general-purpose grinding of steel, while SiC is harder and is typically used for grinding cast iron components. Superabrasives are the hardest known materials used in grinding and include diamond and cubic boron nitride (CBN). Diamonds are important in the dressing of grinding wheels but are rarely used for machining ferrous metals due to their tendency to react with Fe. This is not the case for CBN, which is widely used for grinding hardened steels and cast iron. Superabrasives are expensive, and when grinding softer steels, cheap conventional abrasives are often preferred. These wheels can, however, wear out 40 times faster than CBN, and up to 4-20 wt% abrasives and binders may be found in grinding sludges with Al_2O_3 [29].

The abrasive grains in grinding wheels are held together through vitrified, resin, or metal bonds [26]. In vitrified wheels, abrasives and binders make up the bulk of the tool. This is accomplished by sintering or vitrification of the grains with clay, glass frit, or flux binders at high temperatures. A similar variant is also available with organic epoxy, phenolic, or polyamide resin binders. Phenolic binders are the second most common for conventional abrasives after vitrified bonds. Mono- or multilayer wheels with abrasives deposited on a steel or bronze core are also used, but this binder is exclusive to superabrasives, which degrade more slowly.

2.2.2 Cutting fluids

Cutting fluids can be divided into water-soluble fluids, neat oils, and gases, as shown in Figure 4 [27]. The choice of cutting fluid depends primarily on the workpiece material and machining process [30]. High-speed operations, such as grinding, require efficient swarf and heat removal to prevent tool degradation, which is why water-based fluids are most commonly used for their excellent cooling properties. Neat oils are occasionally used for grinding hard materials such as high-speed steels, whereas gas-based fluids have so far primarily been proposed in research but currently lack commercial applications in grinding [31]. Cutting fluids have a major impact on the recyclability and classification of grinding sludges, and the different types are described in more detail below.

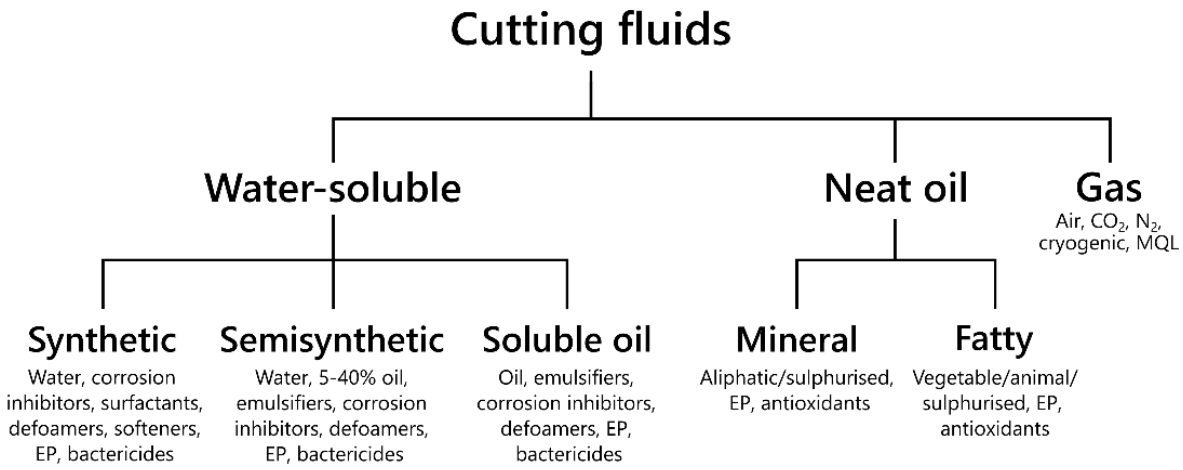

Figure 4: Water-soluble, neat oil, and gas-based cutting fluids and their respective subcategories with typical constituents [27, 32].

Water by itself is corrosive to ferrous metals and a poor lubricant and is therefore normally complemented with various chemical additives. Synthetic water-based fluids are transparent, completely oil-free solutions that rely on surfactants and other chemicals for lubrication. These fluids are occasionally used in grinding, but many formulations contain small amounts of emulsified oil to improve lubricity [27]. Soluble oils contain mineral or fatty oils with emulsifiers and are typically diluted to 2.5-10 wt% oil-in-water to form milky solutions. The oils provide good lubricity, reducing friction between the tool and workpiece. Semisynthetic fluids are popular intermediates that contain lower amounts of oil and form stable microemulsions in water. In general, cutting fluids with higher oil content can be expected to result in higher oil content in grinding sludges, which can adversely affect recyclability and lead to classification as hazardous waste.

In addition to oils, water-soluble fluids generally contain additives to improve performance [27]. Corrosion inhibitors are substances that deposit on the metal surface as a film, separating the surface from corrosive environments [33]. When grinding ferrous metals, amines, carboxylic acids, and inorganic molybdates are commonly included in the formulation. Borates and sodium nitrate have also been used extensively but are being phased out due to their respective reproductive toxicity and tendency to form carcinogenic nitrosamines [32]. Other additives include defoamers, softeners, and bactericides that prevent microorganisms from growing and degrading the lubricant. Extreme pressure additives (EP) are sulphur, chlorine, or phosphorous compounds that protect the workpiece under harsh conditions by reacting with the metal surface. These additives are most commonly used in heavy-duty machining applications.

The second, less common group of cutting fluids in grinding are neat oils, which are water-free and based on mineral oil from petroleum or fatty oils from animal or vegetable fats. These fluids are more expensive and less effective as coolants, but provide excellent lubricity and natural corrosion protection [27]. They are therefore used with few or no additives. For heavy-duty grinding, the base oil may be sulphurised, or EP can be included. Antioxidants are also required in fatty oils, which are susceptible to rancidification. This has led most oil-containing cutting fluids to be based on mineral oils [31]. These oils and many additives are, however, poorly biodegradable and represent significant environmental hazards when landfilled [32]. Grinding sludges containing neat oils can thus be considered among the most difficult to handle from a waste management perspective.

Gas-based lubrication is a promising alternative to the flood lubrication systems that require high liquid flow rates. Air, CO_2 or N_2 can be used as coolants and to blow away swarf, but gases generally have poor lubricity [27]. To compensate for this shortcoming, oil-based cutting fluids can be sprayed into the compressed gas stream [34]. This so-called Minimum Quantity Lubrication (MQL) reduces liquid consumption by more than 1000x compared to flood systems [31]. Despite its popularity in research, this technology is unlikely to see industrial application in grinding due to its inferior cooling and cleaning performance compared to water. However, if implemented, this technology could reduce the oil content of grinding sludges, facilitating recycling.

2.3 Grinding sludge handling in workshops

In industrial grinding processes with flood lubrication, swarf and abrasive wheel particles are collected in large volumes of cutting fluid. Recirculation of fluids is normally prioritised, as the purchase and disposal of machining lubricant are major expenses for manufacturers. Most workshops have filtration, centrifugation or magnetic separation equipment to separate out swarf and abrasives from the grinding slurry [35]. Filtered grinding sludges appear as a spongy powder and typically still contain between 15-40 wt% cutting fluids (see Table 6), as the grinding swarf has a large surface area that readily absorbs and retains liquids. Pictures of filtered grinding sludges in storage are shown in Figure 5.

Figure 5: Stockpiling of filtered grinding sludges with cutting fluid runoff (left), and briquetted grinding sludges (right).

Even more lubricant can be recovered by compacting the filtered sludge in a briquetting machine [35]. Liquids are extruded when pressing the swarf, thereby reducing transport and waste management costs. This can significantly reduce the sludge's liquid content and make the metal fraction eligible for recycling. The relative amount of cutting fluid recovered by briquetting is small, however, and investing in the necessary equipment is therefore rarely economical for small to medium-sized workshops [4]. In these cases, filtered grinding sludges are typically collected by a third party for further waste treatment. Larger workshops, with several hundred to thousands of tons of grinding sludge per year, can, on the

other hand, significantly reduce their cutting fluid demand and disposal costs. Despite these obvious economic and environmental benefits, briquetting has not yet become common practice everywhere. This is partly due to high uncertainty and limited recycling options for the grinding sludge.

2.4 Waste management problems and solutions

A main challenge in recycling is that the cumulative generation of grinding sludges is high, but distributed across many smaller workshops [4]. This is both a logistical challenge and makes the waste highly heterogeneous due to the different workpiece materials, tools, cutting fluids, and recovery methods used at each site. Even within a single workshop, different grinding sludges may be generated, and these fractions may be mixed with each other or with other similar wastes. Another common issue with sludges containing water-soluble cutting fluids is that they can self-ignite when stockpiled under uncontrolled conditions [36]. The metal fraction is slowly oxidised in contact with water and air, generating heat that accelerates further oxidation. This can lead to runaway reactions in which the lubricant oils or metal eventually ignite, resulting in an industrial fire. Self-ignition is less common with neat oils, which provide natural corrosion protection, but these oils also make the sludge more flammable overall.

To homogenise and reduce the waste complexity, some recyclers use mechanical pretreatment methods to separate components [4]. These processes may include drying, screening, and magnetic separation to separate abrasives and ferrous metals into different fractions, which can be sold as raw materials for the steel and cement industries. Manufacturers may still pay a gate fee of around 200 €/ton for this disposal method, but at least part of the material can be recycled. More details regarding current recycling, recovery, and disposal methods are discussed below.

2.4.1 Recycling in the steel industry

The swarf content in filtered grinding sludges is typically 50-80 wt%, rising to 80-90 wt% after briquetting (see Table 6). A logical recycling alternative is therefore to remelt it as scrap in the steel industry. At high temperatures, cutting fluids and organic wheel binders evaporate or are combusted, and non-metallic abrasives and oxides end up as slag or furnace dust. Swarf generated in foundries and steel mills is often recycled this way when the steel grade and contaminants are well known. Internal recycling is not an option for workshops where most product finishing typically takes place, however. These actors rely on third-party recyclers and on steelmakers' willingness to use grinding sludge as a raw material. While

such collaborations are occasionally established, the solutions are seldom permanent or complication-free.

A prerequisite for remelting finer scrap and swarf in most furnaces is that the material is properly briquetted. This ensures that the material density is high enough to keep it submerged in the melt and prevents loose particles from being oxidised and ending up in the slag and off-gases [37]. Briquetting of grinding sludges is no easy task, however, and projects from the past 30 years show that the briquette integrity is easily reduced by oils and oxides on the swarf's surface [38–40]. A particular complication mentioned is the presence of tramp oils from leaking machinery, which frequently contaminates cutting fluids, leading to irregular grinding sludge oil contents and briquette qualities [41]. This causes them to crack and crumble easily, as seen in Figure 5, which is especially problematic during transportation and furnace charging, where scrap is sometimes dropped from heights of several meters. Sturdier briquettes can be obtained by mixing grinding sludge with a binder or by combining it with larger swarf at up to 20% by volume.

Contaminants are another concern when remelting grinding sludges. Combustion of lubricant oils can produce black smoke, flames, and explosions, which can damage steelmaking equipment. The metal product may also be negatively affected by S, P, and Cl from sulphurised oils and EP additives, which can cause steel embrittlement and corrosion. While such problems should be less severe with sludges containing water-based cutting fluids, the swarf is typically more corroded, reducing product yields and increasing slag and dust formation. Abrasives can also be a concern, where Al_2O_3 has been found to damage acidically lined furnaces, drastically shortening their lifespan [38].

Briquetting difficulties, low metal yields, contaminants, and fire hazards all make grinding sludges relatively unattractive for steelmaking. Moreover, the sludge volumes generated by individual workshops are usually insignificant compared to a steel mill's output. This creates little economic incentive for recycling and rarely makes the added risks of using grinding sludges as a raw material worthwhile. The situation may look different for high-alloy grinding sludges, where the value of the metal itself can justify additional recycling efforts, but for the more abundant low-alloy cast iron and steels studied in this work, waste management is often limited to options lower in the waste hierarchy (Figure 1).

2.4.2 Recycling in the cement industry

Another common recycling route is to include grinding sludges in cement production [42]. When added to a cement kiln, the metal fraction is combusted, along with lubricant oils, and incorporated into the clinker product as a filler. Part of the material can be recovered this way, but the valuable metal fraction is essentially lost. This strategy should therefore be considered downcycling, somewhere between energy recovery and recycling (Figure 1). One limitation of using steel swarf as a filler is the low tolerance for Cr in Portland cement [43]. This metal partially oxidises to carcinogenic Cr(VI) in the kiln and can potentially leach from the concrete product over time. The addition of grinding sludges to cement is therefore prohibited in some countries.

2.4.3 Energy recovery and disposal

Decontamination and disposal are a last resort when the above solutions fail and can be carried out in various ways, depending on local regulations, costs, and the waste composition. The EU Landfill Directive (2018/850) states that landfilling of biodegradable waste should be reduced, and many countries today have bans on landfilling flammable materials and waste with high total organic carbon (TOC) contents [44]. This prevents landfill fires that release toxic gases and particles into the surrounding environment, and anaerobic production of methane, which is both flammable and a strong GHG. Grinding sludges are occasionally eligible for direct landfilling, but typically require decontamination due to their flammability and hazardous constituents, including lubricants and metals. This is most commonly done via incineration with or without energy recovery, and disposal of the ashes in landfills [4]. Similar results can also be achieved by composting to digest the organic fraction. Either way, the material value is lost, and manufacturers can be forced to pay up to 1000 €/ton for the disposal, depending on whether the original sludge or ashes are classified as hazardous waste [5].

2.4.4 Previous research and developing technologies

Lubricant oils are a major reason grinding sludges are difficult to recycle and are frequently classified as hazardous waste. Previous research has therefore mainly focused on techniques to eliminate cutting fluids from swarf to facilitate remelting in the steel industry. Aqueous washing has so far received most attention due to the low cost and inherent safety of water as a solvent [45–49]. In these studies, grinding swarf was washed in one or multiple stages using surfactants to lower

surface tension and emulsify and liberate lubricant oils. These could then be separated from the steel by filtration and thereafter recovered by demulsification or membrane filtration. Partial water recirculation was proposed to minimise wastewater generation. Oil contents <3 wt% were generally reported for washed sludges and were considered acceptable for steel production. Several of the works also included economic assessment, which showed that aqueous washing may be economically feasible.

Similar publications on cleaning with organic solvents instead of water are also available [50, 51]. These solvent degreasing systems are also used in workshops for cleaning manufactured parts and utilise solvents with lower boiling points than cutting fluids, enabling easy distillation and recirculation of the washing media. Water consumption and wastewater generation are lower than in aqueous washing, but the energy consumption is higher. Many organic solvents are flammable or toxic, and should be selected in accordance with green chemistry principles [52]. One variant of solvent washing that has been proposed is supercritical CO_2 extraction [5]. Supercritical fluids have zero surface tension, making it possible to reach all parts of the swarf's complex surface. A drawback with CO_2 is that it primarily targets non-polar substances and is unsuitable for recovering water or polar additives on its own. A comparative study found that the cleaning efficiency was typically lower than in aqueous washing [45].

A common weakness in many degreasing studies is that the compatibility of cleaned grinding swarf in steelmaking is rarely verified. More recent works by Großwendt et al. and Hankel et al. took this extra step by studying magnetic separation, degreasing, and supersolidus liquid-phase sintering of high-Cr tool steel grinding swarf [5, 49]. The cleaned metal particles were fused directly to form a steel product, eliminating the need for energy-intensive remelting. Results indicated that new steel could indeed be produced this way, but the product only exhibited 40% of the original workpiece's compressive strength. This was found to be caused by oxides on the metal surface and by insufficient removal of Al_2O_3 abrasives, which prevented metallurgical bonding. These are the same problems observed in the briquetting of grinding sludges, where oxides also negatively affect the cohesion of swarf particles. The applicability of degreasing, and particularly aqueous washing, during which low-alloy ferrous metals may be corroded, is therefore questionable. This argument is supported by the limited implementation and the lack of businesses selling washing equipment.

2.4.5 Hydrometallurgical recycling

As seen so far, current recycling strategies largely rely on grinding sludge as a filler in existing steel and cement production but have frequently failed. This puts manufacturing workshops in an insecure position where they may be forced to switch to disposal at any time, incurring additional costs. Furthermore, these solutions are rarely even an option for small actors with annual sludge volumes of <100 tons. This calls for the development of a more specific technology to recycle low-alloy ferrous grinding sludge. Ideally, such a process should be flexible enough to handle waste from different sources, account for daily variations, and be economical even on a smaller scale.

Hydrometallurgy is a method that is well-suited for the small-scale recovery of metals from low-grade ores and waste [53]. It is based on processing metals in aqueous solutions using chemicals and can achieve efficient metal separation with lower energy consumption and gas emissions than traditional pyrometallurgical processes. Main uses of hydrometallurgy in waste management include the recovery of metals from spent batteries [54, 55], electronic wastes [56, 57], and municipal solid waste incineration ashes [58]. In relation to steelmaking, it has also been proposed as an alternative for the decontamination and recycling of slags and furnace dusts [59–61]. In most of these applications, the goal is to recover more valuable metals than Fe, which is often considered an impurity. More particular studies on the recycling of steel pickling liquors and oily cold rolling mill sludges for the production of Fe-based chemicals can, however, also be found [62–64]. The latter waste is highly similar to grinding sludge and was considered as a raw material for Fe_2O_3 pigments and battery anode materials.

No specific research on hydrometallurgical recycling of grinding sludges has been reported, despite the obvious advantages this method can offer for these types of low-value waste. This thesis, therefore, aims to determine whether this method is a feasible strategy and whether the sludges can serve as raw materials for producing commercial-grade Fe-based chemicals. To this end, the focus is on optimisation and on studying the chemistry of the unit processes that convert Fe to $FeCl_3$, while also monitoring the effects of impurities arising from the grinding sludge.

3 Theory

Hydrometallurgy is a form of extractive metallurgy that takes place in water solutions. It relies on solution chemistry and reactions taking place in the aqueous phase or at the interface with another liquid or solid. These reactions are fundamentally driven by chemical equilibria, thermodynamics, kinetics and catalysis, and a brief introduction to these topics is therefore provided.

3.1 Chemical equilibria and thermodynamics

Chemical thermodynamic systems can be modelled to determine the feasibility of reactions at given conditions [53]. The chemical equilibrium for an arbitrary reaction aA + bB ⇌ cC + dD is given by Equation 1, where a_i is the chemical activity of species i.

$$K = \frac{a_C^c a_D^d}{a_A^a a_B^b} \approx \frac{[\mathrm{C}]^{\mathrm{c}}[\mathrm{D}]^{\mathrm{d}}}{[\mathrm{A}]^{\mathrm{a}}[\mathrm{B}]^{\mathrm{b}}} \quad (1)$$

Bracket notation is used to express concentrations, and the right-hand equality only holds for ideal systems. The equilibrium constant K describes the system when the species activities are in balance, and forward and backward reactions occur at equal rates. When this is not the case, K is replaced by the reaction quotient Q, and a net formation of products or reactants occurs depending on whether Q<K or Q>K. The driving force behind chemical reactions can also be described in terms of changes in Gibbs free energy (ΔG_r), as defined in Equation 2.

$$\Delta G_r = \Delta H_r - T\Delta S_r = \Delta G_r^o + RT\ ln\ Q \quad (2)$$

Here, ΔH_r and ΔS_r are the molar reaction enthalpy and entropy, respectively, T is the system temperature, and R is the gas constant. Standard energies of reaction $\Delta G_r°$ at 298.15 K and 1 bar (SATP) are calculated using Equation 3, where ν_i are reaction coefficients, and standard free energies of formation $\Delta G_i°$ for chemical species can be found in thermodynamic databases.

$$\Delta G_r^o = \sum_k^{Products} \nu_k \Delta G_k^o - \sum_n^{Reactants} \nu_n \Delta G_n^o \quad (3)$$

A reaction is considered spontaneous when $\Delta G_r<0$ (i.e. Q<K), meaning that reaction product formation will occur until an equilibrium is established and Q=K. At this point, $\Delta G_r = 0$, and Equation 2 simplifies to Equation 4.

$$\Delta G_r^o = -RT\ ln\ K \quad (4)$$

As mentioned earlier, the equivalence between activities and concentrations in Equation 1 generally holds under ideal conditions, which in solutions is typically valid only for pure liquids or highly dilute solute concentrations. An estimate of whether a solution is ideal can be made by determining its ionic strength using Equation 5.

$$I = \frac{1}{2}\sum_{i}^{n}[\mathrm{M}]_i z_i^2 \tag{5}$$

The sum is taken over all n ionic species M with charge z_i, and for an ideal solution $I<10^{-5}$ M. Most hydrometallurgical systems are non-ideal, in which more complex interactions may occur [53]. Chemical activities better describe the effective concentrations of species in these situations and are defined by Equation 6.

$$a_i = \gamma_i x_i \tag{6}$$

The mole fraction x_i of a species is corrected with an activity coefficient γ_i to describe deviations from ideality. Activities of pure liquids, solids, and ideal gases are usually defined as unity. Otherwise, molecular interactions can be modelled to determine γ_i based on the solution's ionic strength, e.g. by using the Debye-Hückel (I<0.01 M), Davies (I<1 M), or specific ion interaction theory (SIT; I<3.5 M) [53, 65]. The most sophisticated models can handle ionic strengths up to ~6 M.

3.1.1 Electrochemical reactions

The oxidation state of a metal can greatly affect its solubility and reactivity. Redox reactions are therefore important in hydrometallurgy and involve electron transfer between species or to or from an electrode. Electrochemical reactions can be described thermodynamically according to Equation 7, where E is the potential, n is the number of electrons transferred, and F is the Faraday constant.

$$\Delta G_r = -nFE \tag{7}$$

A correlation between E and Q can then be obtained by combining Equations 2 and 7, resulting in Equation 8.

$$E = E° - \frac{RT}{nF} ln\, Q \tag{8}$$

This is the Nernst equation, which can be used to calculate the potential of an electrochemical half-cell reaction at different conditions. The standard potential (E°) refers to the reduction potential relative to the standard hydrogen electrode (SHE) at SATP with aqueous species concentrations of 1 M. Equation 8 is especially

useful for assessing the feasibility of redox reactions by comparing the reduction potentials of the species involved using Equation 9.

$$E_{cell} = E_{red} - E_{ox} \quad (9)$$

The forward reaction is favoured when E_{cell}>0 V, the backward reaction when E_{cell}<0 V, and at equilibrium, E_{cell} = 0 V.

3.1.2 Pourbaix diagrams

Electrochemical potentials and chemical equilibria data can be used to construct Pourbaix (Eh-pH) phase diagrams that indicate the most stable form of an element at different E and pH values. This is a valuable tool for studying hydrometallurgical systems, and HSC Chemistry 10 ([66]) was used to model phase diagrams and chemical reactions throughout this work. The Fe-H_2O system at SATP with 1 mM Fe is shown in Figure 6, and more diagrams are available in Appendix Figure A1-A10. Vertical lines represent reactions that are independent of E, while horizontal lines symbolise pure redox reactions. Dashed lines indicate potentials for O_2 reduction to H_2O (upper) and H^+ reduction to H_2 (lower).

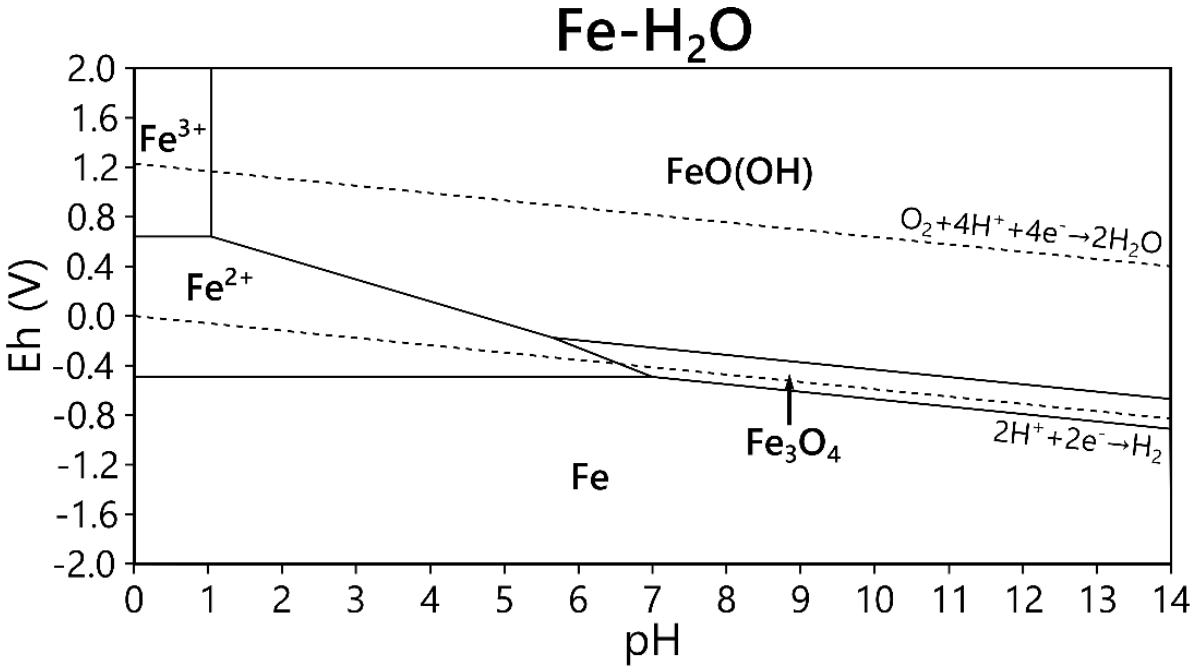

Figure 6: Pourbaix diagram for the Fe-H_2O system with 1 mM Fe at 25°C, indicating the stability of Fe species as a function of pH and redox potential.

A limitation is that these diagrams show only the dominant species at equilibrium, and the formation of a given species may still be kinetically limited and never occur in practice. Caution is also advised when modelling systems at high ionic strength, where activity modelling is required to accurately estimate chemical equilibria.

3.2 Kinetics and catalysis

Another concept that is needed to understand hydrometallurgical reactions is kinetics. No detailed kinetic studies or modelling were conducted during this work, but the necessary fundamentals are explained. Returning to the arbitrary reaction aA + bB ⇌ cC + dD from earlier, the forward reaction rate r can be described by Equation 10.

$$r = k[\mathrm{A}]^x[\mathrm{B}]^y \tag{10}$$

The exponents x and y determine the order of the reaction with respect to the concentrations of A and B, and the overall order of the reaction is given by x+y [53]. Often, x and y are equal to the reaction coefficients (i.e., a and b), but this is not always the case and determining the order requires a more detailed understanding of the reaction mechanisms. According to Equation 10, the rate is proportional to the forward rate constant k, and fast reactions generally have high k-values. For reversible reactions, however, the rate of the backward reaction must also be considered to determine the net formation of products. The temperature dependence of k is described by the Arrhenius equation (Equation 11), where A is the collision frequency factor, and E_a is the reaction activation energy.

$$k(T) = Ae^{-E_a/RT} \tag{11}$$

Reactions with large E_a values typically require high temperatures before they are likely to occur. A key function of catalysts is to reduce the activation energy, allowing a reaction to occur at lower temperatures (or at lower overpotentials in electrochemistry) than usual. Kinetics are, in most cases, governed not only by chemical reactions but also by mass transport of the reactants and products. The overall reaction rate is therefore determined by the rate-limiting step.

3.3 Solvation and coordination chemistry

Metal ions in an aqueous solution exist in a hydrated state, surrounded by water molecules in an arrangement that minimises the system's free energy [67]. Ions can sometimes achieve a more energetically favourable state by replacing water in their inner hydration sphere, and bonding with anionic, cationic, or neutral ligands (L) via Lewis acid-base reactions, as described in Equation 12.

$$\mathrm{M}^{2+} + \mathrm{L}^{-} \rightleftharpoons \mathrm{ML}^{+} \tag{12}$$

Chemical equilibria determine the stability of the formed complex, and the stability constant k_1 for Equation 12 is given in Equation 13.

$$k_1 = \frac{a_{ML^+}}{a_{M^{2+}} \cdot a_{L^-}} \tag{13}$$

When the activity of L^- increases, higher-order complexes may be formed, and a general stability k_n constant for the n^{th} complex is given in Equation 14 [68].

$$k_n = \frac{a_{ML_n^{(2-n)+}}}{a_{ML_{n-1}^{(2-n+1)+}} \cdot a_{L^-}} \tag{14}$$

The overall equilibrium from the ground state M^{2+} up to the n^{th} order complex is then defined by the cumulative stability constant β_n given in Equation 15.

$$\beta_n = k_1 k_2 \dots k_n = \frac{a_{ML_n^{(2-n)+}}}{a_{M^{2+}} \cdot a_{L^-}^n} \tag{15}$$

In general, a large stability constant indicates that formation of a complex is favourable. However, this also depends on the magnitude of other constants and the presence of other species forming even more stable complexes with L, thereby reducing $[L^-]$ in the solution.

Substances can be classified into four groups according to the hard-soft acid-base (HSAB) theory to predict the relative strength of formed complexes [69]. Hard Lewis acids (electron acceptors) and bases (electron donors) are small, weakly polarisable species with high electrical charge, while soft species have large ionic radii and are easily polarised. In terms of stability, hard acids typically form strong ionic or dipole-dipole bonds with hard bases and only have weak interactions with soft bases. Likewise, soft acids form stronger covalent bonds with soft bases and form weaker complexes with hard bases.

3.3.1 Iron complexation in chloride media

Iron has three common oxidation states: metallic Fe, ferrous Fe(II), and ferric Fe(III). Aqueous Fe^{2+} is classified as an intermediate Lewis acid and can react with Cl^-, a hard base, via Equation 16.

$$\mathrm{Fe^{2+} + nCl^- \rightleftharpoons FeCl_n^{(2-n)+}} \tag{16}$$

In acidic chloride media at room temperature, main Fe(II) species include Fe^{2+}, $FeCl^+$, and uncharged $FeCl_2^0$ [70]. Higher order complexes are typically formed with increasing $[Cl^-]$ and temperatures, and $FeCl_4^{2-}$ has also been observed at temperatures >100°C in concentrated $FeCl_2$ brines [71]. Water can also act as a strong Lewis base, and under less acidic conditions, Fe^{2+} can be hydrolysed to aqueous $Fe(OH)^+$ or $Fe(OH)_2^0$ via Equation 17 [72].

$$Fe^{2+} + nH_2O \rightleftharpoons Fe(OH)_n^{(2-n)+} + nH^+ \quad (17)$$

The Fe^{3+} ion can undergo analogous reactions with Cl^- and water as described in Equations 18 and 19.

$$Fe^{3+} + nCl^- \rightleftharpoons FeCl_n^{(3-n)+} \quad (18)$$

$$Fe^{3+} + nH_2O \rightleftharpoons Fe(OH)_n^{(3-n)+} + nH^+ \quad (19)$$

Contrary to Fe^{2+}, this ion is classified as a hard Lewis acid and forms stronger hydroxide and chloride complexes [68]. The main species in acidic chloride solutions include Fe^{3+}, $FeCl^{2+}$, $FeCl_2^+$, $FeCl_3^0$, $FeCl_4^-$, $FeOH^{2+}$ and $Fe(OH)_2^+$, as well as a mixed $FeOHCl_2^0$ complex [73, 74]. Aggregation of hydroxide species has also been found to be possible, forming dimeric or higher-order polymeric species [75]. The strong hydrolysis reaction generally makes $FeCl_3$ solutions relatively acidic, as H^+ is formed in Equation 19. It also makes Fe^{3+} less stable than its Fe^{2+} counterpart, as solid FeO(OH) is easily formed, even under acidic conditions [76]. The Eh-pG diagram in Figure 6 shows that the stability pH for Fe^{3+} lies below pH 1-2, whilst Fe^{2+} is stable over a broader pH range in non-aerated solutions. High temperatures favour hydrolysis and shift the stability line towards even more acidic conditions. Cumulative stability constants for Fe(II) and Fe(III) species are summarised in Table 1 to demonstrate the different behaviours of the oxidation states, and how complexation increases with temperature.

Table 1: Cumulative stability constants for possible aqueous Fe(II) and Fe(III) species in acidic chloride media at 25, 40 and 60°C.

Species		Log(β)			Reference
		25°C	40°C	60°C	
Fe(II)	$FeCl^+$	-0.37	-0.20	0.02	[70]
	$FeCl_2^0$	-1.74	-1.56	-1.25	[70]
	$FeCl_4^{2-}$	-	-	-4.10	[70]
	$FeOH^+$	-9.43	-8.97	-8.42	[68]
	$Fe(OH)_2^0$	-20.51	-19.55	-18.39	[68]
Fe(III)	$FeCl^{2+}$	1.49	1.53	1.61	[74]
	$FeCl_2^+$	2.13	2.43	2.84	[74]
	$FeCl_3^0$	1.11	1.49	1.99	[74]
	$FeCl_4^-$	-1.26	-0.94	-0.33	[74]
	$FeOH^{2+}$	-2.21	-1.85	-1.43	[74]
	$Fe(OH)_2^+$	-5.67	-5.08	-4.39	[74]
	$Fe(OH)_3^0$	-12.28	-11.06	-9.63	[68]
	$FeOHCl_2^0$	-0.80	-0.94	-1.03	[74]

3.4 Hydrometallurgical processes

Unlike the hydrolysis and complexation reactions shown so far, most hydrometallurgical processes are heterogeneous and take place at the interface of two different phases [77]. One of these phases is normally an aqueous solution, and the other is either another liquid, a solid, or a gas. As metals in ores and waste typically occur as solids, the first and most important step is to extract and transfer them to a water solution via leaching.

3.4.1 Leaching and chemical dissolution

Leaching is a chemical dissolution process that occurs at the interface between a solid and an aqueous phase. In hydrometallurgy, the aim is to transform metals into water-soluble salts via chemical reactions, and this is achieved by contacting the solids with a water solution containing a leaching agent, typically an acid or base [53]. An example of Fe dissolution by H^+ is shown in Equation 20.

$$\mathrm{Fe} + 2\mathrm{H}^+ \longrightarrow \mathrm{Fe}^{2+} + \mathrm{H}_2(\mathrm{g}) \qquad (20)$$

Other relevant leaching reactions, along with their thermodynamic data at SATP, for partially corroded grinding swarf, are presented in Table 2. Transfer of reactants and products to and from the reaction interface takes place in several steps. The first step is convection and diffusion of leaching agents from the aqueous bulk to the solid-liquid boundary layer. Reactants are transported through the film by diffusion and may be adsorbed before reacting with the metal surface. Reaction products are then desorbed and diffuse back through the boundary layer to the bulk phase.

Limitations in either step control the overall kinetics of the leaching process. Suitable operating conditions thus need to be selected to facilitate mass transport and reactions. High pulp density (low liquid-to-solid ratio, L/S) typically inhibits mass transport by increasing viscosity and reducing the amount of reagent available per unit mass of metal. Transport rates can be increased by stirring, which favours bulk transport and can thereby reduce the boundary-layer thickness. High temperatures generally also improve mass transport by lowering viscosity and increasing diffusion rates, in addition to speeding up chemical reactions. Furthermore, sufficient leaching agents must be supplied, and suitable pH and redox potential should be maintained to prevent the precipitation of dissolved metals.

Table 2: Possible grinding swarf leaching reactions with thermodynamic data modelled with HSC Chemistry at 25°C and 1 atm [66].

Reaction	ΔH° (kJ/mol)	ΔS° (kJ/mol)	ΔG° (kJ/mol/K)	log(K)	Eq. (#)
$Fe + 2H^+ \rightarrow Fe^{2+} + H_2(g)$	-89.1	-34.3	-78.9	13.8	(21)
$Fe + 2Fe^{3+} \rightarrow 3Fe^{2+}$	-161.4	136.1	-202.0	35.4	(22)
$Fe(OH)_3 + 3H^+ \rightleftharpoons Fe^{3+} + 3H_2O$	-80.1	-183.4	-25.4	4.4	(23)
$Fe_2O_3 + 6H^+ \rightleftharpoons 2Fe^{3+} + 3H_2O$	-138.6	-454.1	-3.2	0.6	(24)
$Fe_3O_4 + 8H^+ \rightleftharpoons Fe^{2+} + 2Fe^{3+} + 4H_2O$	-222.8	-580.6	-49.7	8.7	(25)
$4Fe^{2+} + 4H^+ + O_2(aq) \rightarrow 4Fe^{3+} + 2H_2O$	-415.3	-573.3	-244.3	42.8	(26)
$Cr + 3H^+ \rightarrow Cr^{3+} + 1.5H_2(g)$	-242.9	149.7	-198.3	34.7	(27)
$Cr + 3Fe^{3+} \rightarrow Cr^{3+} + 3Fe^{2+}$	-351.4	106.0	-383.0	67.1	(28)
$Cr(OH)_3 + 3H^+ \rightleftharpoons Cr^{3+} + 3H_2O$	-124.7	-207.7	-62.8	11.0	(29)
$Cr_2O_3 + 6H^+ \rightleftharpoons 2Cr^{3+} + 3H_2O$	-205.9	-517.5	-51.7	9.1	(30)
$Mn + 2H^+ \rightarrow Mn^{2+} + H_2(g)$	-220.6	24.9	-228.0	40.0	(31)
$Mn + 2Fe^{3+} \rightarrow Mn^{2+} + 2Fe^{2+}$	-292.9	195.3	-351.2	61.5	(32)
$Ni + 2H^+ \rightarrow Ni^{2+} + H_2(g)$	-55.0	-30.9	-45.8	8.0	(33)
$Ni + 2Fe^{3+} \rightarrow Ni^{2+} + 2Fe^{2+}$	-127.4	139.6	-169.0	29.6	(34)
$Al + 3H^+ \rightarrow Al^{3+} + 1.5H_2(g)$	-538.8	-157.3	-491.9	86.2	(35)
$Al + 3Fe^{3+} \rightarrow Al^{3+} + 3Fe^{2+}$	-647.3	98.5	-676.6	118.6	(36)
$Al_2O_3 + 6H^+ \rightleftharpoons Al^{3+} + 3H_2O$	-259.3	-491.1	-112.9	19.8	(37)
$Cu + 2H^+ \rightarrow Cu^{2+} + H_2(g)$	64.9	-0.47	65.0	-11.4	(38)
$Cu + 2Fe^{3+} \rightarrow Cu^{2+} + 2Fe^{2+}$	-7.4	170.0	-58.1	10.2	(39)
$Co + 2H^+ \rightarrow Co^{2+} + H_2(g)$	-58.2	-8.4	-55.7	9.8	(40)
$Co + 2Fe^{3+} \rightarrow Co^{2+} + 2Fe^{2+}$	-130.5	162.1	-178.8	31.3	(41)
$Zn + 2H^+ \rightarrow Zn^{2+} + H_2(g)$	-153.4	-20.6	-147.3	25.8	(42)
$Zn + 2Fe^{3+} \rightarrow Zn^{2+} + 2Fe^{2+}$	-225.7	149.9	-270.4	47.4	(43)

Surface passivation is a highly undesirable phenomenon in leaching, where the metal surface is covered by an insoluble layer. This prevents contact between the metal underneath and the aqueous phase, thereby blocking mass transport of reactants and products. Passivation layers may already exist in the solid input material, but can also form during leaching when reaction products are strongly adsorbed to the metal surface (e.g., sulphur precipitates in the leaching of sulphide minerals [78]). Other examples of protective layers include Fe or Cr oxide scales on steel, noble metal coatings, and adsorbed inorganic or organic chemical corrosion inhibitors. Passivation is also important in corrosion science, where surface protection is normally welcomed [79].

Leaching yield

The efficiency (%E_M) of a leaching procedure is defined by the fraction of a metal M in the solid phase that has been dissolved, as given by Equation 44.

$$\%E_M = 100 \cdot \frac{[\mathrm{M}]_L V_L}{m_s x_M} \tag{44}$$

Here, V_L is the leachate volume, and x_M is the fraction of the metal in the initial solid phase with mass m_s. If the goal is to indiscriminately dissolve as much material as possible, a simpler efficiency estimate can be made using Equation 45.

$$\%FC = 100 \cdot \frac{m_{FC}}{m_s} \tag{45}$$

This requires separating the solid residues and leachate by filtration, then drying and weighing the filter cake (FC). Equation 44 is valid only when the leaching agent does not contain any M. This thesis, however, also explores oxidative leaching procedures where $FeCl_3$ is used to leach metallic Fe via the comproportionation reaction described in Equation 46.

$$\mathrm{Fe(s)} + 2\mathrm{FeCl_3(aq)} \longrightarrow 3\mathrm{FeCl_2(aq)} \tag{46}$$

Two other estimates of the leaching efficiency have therefore been defined to account for Fe in the reagent (R) and are shown in Equations 47 and 48.

$$\%E_{s,M} = 100 \cdot \left(\frac{[\mathrm{M}]_L V_L - [\mathrm{M}]_R V_R}{m_s x_M} \right) \tag{47}$$

$$\%E_{tot,M} = 100 \cdot \left(\frac{[\mathrm{M}]_L V_L}{m_s x_M + [\mathrm{M}]_R V_R} \right) \tag{48}$$

The first equation estimates the amount of M transferred from the solid phase to the leachate, excluding M added via the reagent. Equation 48, on the other hand, is a ratio of the amount of M transferred to the aqueous phase relative to the total input and is a measure of the overall atom economy.

Potentiostatic leaching

Leaching is often performed by mixing concentrated reagents with solids and allowing the system to react for a set period. It can, however, also be done with potentiometric control, where either pH or E is kept constant throughout the duration of an experiment [80, 81]. This method keeps the solution within a specific region of the Eh-pH diagram where the formation of particular species is more or less favourable. In some cases, selective extraction can be achieved during leaching, reducing the need for purification.

3.4.2 Leachate purification

Aqueous metal ions in a leachate can be separated via several hydrometallurgical techniques. Solvent extraction (SX), ion exchange (IE), and precipitation are used most extensively, but separation by adsorption, ultrafiltration, and other methods is also possible [53]. Both SX and IE rely on the selective scavenging of metals from solution, typically by forming complexes with organic or inorganic ligands. In the former, the aqueous solution is contacted with an immiscible solvent, typically containing extractant molecules that complex with specific ions, enabling the metal to distribute between the phases. In IE, the extractant is instead a solid such as a porous mineral or resin, through which the solution flows. In both cases, metals can be recovered from the extraction medium by stripping with another aqueous solution. The investment cost and complexity of these methods are usually relatively high, and simpler precipitation techniques may be preferable.

Precipitation relies on converting aqueous metal ions back into solids that can then be removed by filtration. Common methods include pH adjustment to precipitate metals as hydroxides or oxides, formation of insoluble metal sulphides with H_2S, or cementation of noble metals. These techniques are typically less selective than SX or IE, and can lead to coprecipitation or sorption of other impurities or products on the formed particles. Both hydroxide precipitation and cementation were investigated using swarf as a precipitation agent. Analogous to %E for leaching, a precipitation efficiency (%R) is defined in Equation 49.

$$\%R_{t,M} = 100 \cdot \left(1 - \frac{[M]_t}{[M]_i}\right) \tag{49}$$

The respective subscripts i and t denote concentrations in the initial leachate and after a given precipitation time.

Cementation

Cementation is a redox displacement reaction where electrons are transferred from a metallic ignoble element (A) to a nobler metal (B). Metal A is dissolved in the process, while metal B is reduced and deposited onto the metallic surface. The general cementation reaction is defined in Equation 50.

$$\mathrm{nA(s)} + \mathrm{mB^{n+}} \rightleftharpoons \mathrm{nA^{m+}} + \mathrm{mB(s)} \qquad K = \frac{a^n_{\mathrm{A^{m+}}}}{a^m_{\mathrm{B^{n+}}}} \tag{50}$$

In terms of kinetics, this reaction is similar to leaching, in which B is transferred from the bulk to the sacrificial metal surface via diffusion before being reduced

[82]. The dissolved metal A then diffuses back through the boundary layer to the bulk. A difference in nobility is the main driving force for Equation 50, and the feasibility of cementing different ions can be determined by comparing reduction potentials. The E° values (in V) for the reduction of Fe^{2+} and common alloying elements to their respective metallic states ($M^{n+}+ne^{-}\rightarrow M$) are shown below.

$$\begin{array}{cccccccc} Al^{3+} < & Mn^{2+} < & Zn^{2+} < & Cr^{3+} < & Fe^{2+} < & Co^{2+} < & Ni^{2+} < & Cu^{2+} \\ -1.68 & -1.18 & -0.76 & -0.74 & -0.44 & -0.28 & -0.26 & +0.34 \end{array}$$

Redox reactions between Fe^{2+} and metals with higher E° result in $E°_{cell}>0$ V and are spontaneous. In theory, it should therefore be possible to precipitate Co, Ni, and Cu from $FeCl_2$ solutions with metallic Fe, which is supported by the literature [83–85]. Other noteworthy cementable metals that were not encountered during this work study but may be relevant include Pb^{2+} (E^0 =-0.13 V) and Hg^{2+} (E^0 =+0.85 V) [86, 87].

Hydrolysis precipitation

As mentioned already in Section 3.3.1, metal ions can also be precipitated by forming stable solid hydroxide complexes. This occurs via hydrolysis of the metal ion in the aqueous phase, followed by a distribution of the complex between its aqueous and solid forms as described in Equations 51 and 52.

$$\mathrm{M^{n+} + nH_2O \rightleftharpoons M(OH)^0_n(aq) + nH^+} \qquad \beta_n = \frac{a_{\mathrm{M(OH)^0_n}} a^n_{\mathrm{H^+}}}{a_{\mathrm{M^{n+}}}} \tag{51}$$

$$\mathrm{M(OH)^0_n(aq) \rightleftharpoons M(OH)_n(s)} \qquad \mathrm{K} = \frac{1}{a_{\mathrm{M(OH)^0_n}}} \tag{52}$$

The overall equilibrium for these reactions is the solubility product (K^*_{sp}), which can be related to the commonly tabulated solubility product based on OH^- activity (K_{sp}), via the water dissociation constant $K_w = a_{H+}a_{OH-} = 10^{-14}$ to give Equation 53.

$$K^*_{sp} = \frac{K_w}{K\beta_n} = K_w \frac{a_{M^{n+}}}{a^n_{H^+}} = a_{M^{n+}} a^n_{OH^-} = K_{sp} \tag{53}$$

Many transition metals can form stable hydroxide precipitates (e.g., $Fe(OH)_3$) with low K_{sp} values [68]. Equations 51-53 are pH-dependent and represented in Eh-pH diagrams as vertical (or diagonal) lines. Comparing diagrams for different species (see Appendix Figure A1 to Figure A10) can indicate the region where selective precipitation of a particular element is possible. The HSAB rule can also indicate whether precipitation may be possible, since hard Lewis acids are more readily hydrolysed. A selection of metals has been compared in Table 3 [88].

Table 3: Classification of Lewis acids according to the HSAB theory.

Soft acid	Borderline acid	Hard acid
Cu^{+}, Hg^{+}, Cd^{2+}, Hg^{2+}	Co^{2+}, Cu^{2+}, Fe^{2+}, Ni^{2+}, Pb^{2+}, Sn^{2+} Zn^{2+}	Al^{3+}, Cr^{3+}, Fe^{3+}, Mn^{2+}, Mo^{6+}, Si^{4+}, V^{4+}, W^{6+}

Classification by hardness is useful but only a guideline, as some elements, such as Al^{3+}, are amphoteric and can hydrolyse beyond their neutral state to form soluble anions. This, however, usually occurs only in alkaline solutions, where Fe is also easily precipitated. Table 3 and Eh-pH diagrams indicate that it may be possible to selectively precipitate and separate Al, Cr, Mn, Mo, Si, V, and W from Fe(II). One drawback of hydrolysis precipitation is that filtration of silicates and hydroxides can be challenging, leading to potential complications when scaling processing equipment [89].

3.4.3 Iron oxidation

Both of the presented precipitation methods rely on having Fe in solution as Fe(II). Table 2 shows that mostly Fe^{2+} is expected to form when leaching metallic Fe via Equation 21, and that Fe^{3+}, formed by dissolution of oxides in Equations 23-25, can be expected to be reduced to Fe^{2+} via Equation 22. In an aerated solution, however, Fe^{2+} is inherently unstable and can be oxidised to Fe^{3+} by O_2 via Equation 26. This is also reflected in Eh-pH diagrams (Figure 6), where the entire Fe^{2+} region lies below the O_2 reduction line ($E_{O2/H2O}$=1.229-0.059·pH), and spontaneous formation of Fe^{3+} can thus be expected. This can be observed as a slow colour shift from blue to green to brown in concentrated $FeCl_2$, but the process is kinetically limited, and it can take days for even a fraction of $FeCl_3$ to form at SATP or temperatures of 80°C. Both a high activation energy and low solubility of O_2 can be rate-limiting factors, depending on the conditions [90].

From an industrial perspective, air oxidation is too slow, and additional efforts are needed to obtain completely oxidised Fe(III) solutions. One way to achieve this is to introduce a stronger oxidant, such as Cl_2, ClO_3^-, or ClO^- [91, 92]. These oxidants are relatively hazardous and unstable and require proximity to a chlorine plant. Non-chlorinated oxidisers, such as H_2O_2 or O_3, in combination with HCl, can therefore be preferable [93, 94]. Oxidation with pure O_2 is also an option but requires pressures >4 bar, temperatures >100°C, and good mixing of the gas and liquid phases. Small amounts of Cu(II) or Co(II) in solution catalyse the reaction of Fe(II) and can generally increase the oxidation efficiency [91, 95]. In addition to

chemical oxidisers, electrochemical oxidation is also possible, and can generate H_2 as a byproduct [96, 97]. Pressure oxidation with O_2 and electrolysis were tested in this work for their potentially low environmental footprints compared to chemical oxidisers [98].

Electrolysis

An electrochemical cell consists of an electrically connected anode and cathode, separated by a conductive electrolyte containing redox-active species that completes the circuit. In electrolysis, a potential is applied across the cell to drive non-spontaneous reactions and is typically higher than the theoretical E_{cell} value due to losses, including high activation overpotentials for chemical reactions, ohmic losses from electrolyte and electrical equipment resistances, slow mass transport, and parasitic reactions. Possible reactions with E°-values in the electrolysis of $FeCl_2$ with HCl as a chloride source are given in Table 4.

Table 4: Possible reactions in electrolysis of $FeCl_2$ with HCl.

Reaction	E° (V)	Eq. (#)
$Fe^{3+} + e^- \rightleftharpoons Fe^{2+}$	+0.77	(54)
$2H^+ + 2e^- \rightleftharpoons H_2(g)$	0	(55)
$Fe^{2+} + 2e^- \rightleftharpoons Fe(s)$	-0.44	(56)
$O_2(aq) + 2H^+ + 2e^- \rightleftharpoons H_2O_2(aq)$	+0.70	(57)
$O_2(aq) + 4H^+ + 4e^- \rightleftharpoons 2H_2O$	+1.23	(58)
$Cl_2(aq) + 2e^- \rightleftharpoons 2Cl^-$	+1.36	(59)
$MnO_2(s) + 4H^+ + 2e^- \rightleftharpoons Mn^{2+} + 2H_2O$	+1.22	(60)

Desired anodic and cathodic reactions are given by Equations 54 (backwards) and 55 (forwards), respectively. At high cathodic potentials, reduction of Fe^{2+} can occur as described in Equation 56, and other parasitic reactions reducing H_2 formation in aerated systems are given by Equations 57 and 58. At the anode, formation of O_2 and Cl_2 gas via Equations 58 and 59 is possible at high potentials, and MnO_2 can precipitate in solutions containing Mn^{2+} as described in Equation 60. An estimate of the charge-transfer efficiency and the influence of parasitic reactions is given by the Faradaic efficiency η_F in Equation 61.

$$\eta_F = \frac{\{\text{Observed product yield}\}}{\{\text{Theoretical yield}\}} \tag{61}$$

The observed yield is measured analytically while the theoretical yield n_F is calculated using Faraday's law of electrolysis in Equation 62.

$$n_F = \frac{\int_0^t Idt}{nF} \tag{62}$$

The integral gives the charge transferred in Coulombs as a function of the applied current I(t) over the time interval t, while n is the number of electrons required for the desired reaction. Faradic efficiencies range from 0 to 1, with lower values indicating that unwanted reactions may have occurred.

4 Methods and materials

4.1 Outline of methods and results

The different steps investigated for recycling Fe in grinding sludges into an $FeCl_3$ product are shown in Figure 7 alongside a typical hydrometallurgical (HM) processing scheme. Corresponding papers and sections in the thesis where each unit process is discussed are shown above each block. Two different leaching and oxidation approaches were compared, and the final $FeCl_3$ product was tested in water treatment coagulation and LFP synthesis. Mass and energy balances, and economic and environmental impact assessment, are not shown in the outline but were part of the work and are discussed in Section 5.7.

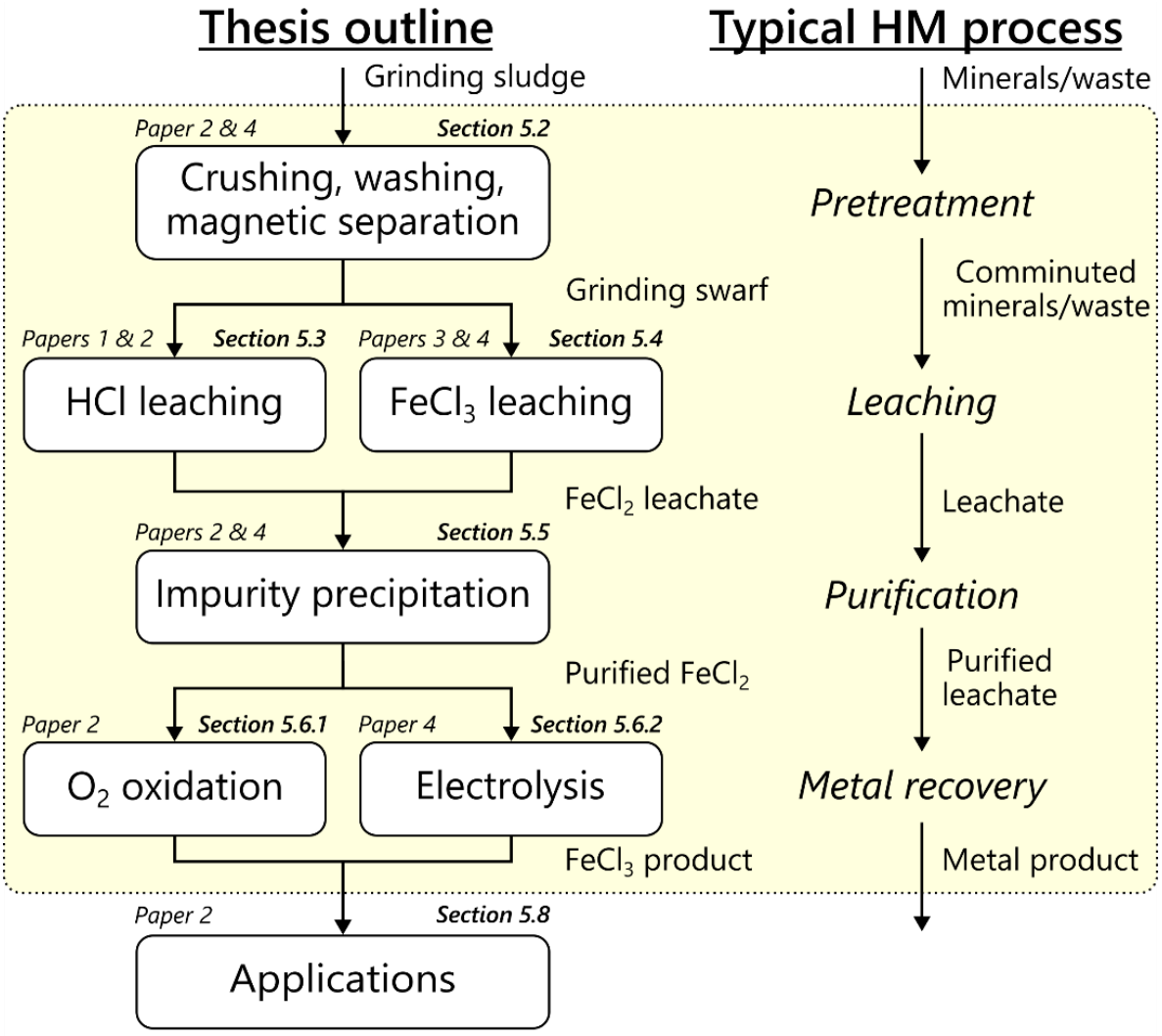

Figure 7: Outline of unit processes investigated in the thesis and comparison with a typical hydrometallurgical (HM) scheme.

4.2 Grinding sludge preparation and pretreatment

Grinding sludges were received as filtered or centrifuged, or as briquettes that were crushed into powder with a mortar and pestle. Pictures of filtered and briquetted sludges are shown in Figure 8. In several instances, the sludges were leached directly, but in later studies, pretreatment by washing and magnetic separation was also done to recover lubricants and abrasives prior to leaching.

Figure 8: Picture of filtered (left) and briquetted (right) grinding sludges from the steel bearings manufacturing, showing the powder-like nature of the material.

4.2.1 Sludge pretreatment

Cutting fluids were liberated from the swarf by washing with acetone or aqueous surfactant solutions. Grinding sludge was added to a heated, stirred reactor vessel and mixed with cleaning liquid for 15-30 min at 40°C. Swarf was then selectively removed by dipping a magnet into the slurry and dropping the adhered particles onto a filter, leaving non-magnetic particles behind. Washed swarf was rinsed with additional acetone or fresh water, then filtered and oven-dried. The remaining washing slurry was filtered to recover abrasives and other non-magnetic solids. This solid-free loaded wash liquid was then combined with rinse liquids and, if based on acetone, distilled to recover lubricants and cleaning fluids separately.

4.3 Leaching and impurity precipitation

All leaching and precipitation tests were conducted in jacketed glass reactors ranging in size from 200 mL to 5 L. The slurry temperature was controlled by an external hot or cold water flow, and mixing was done with an overhead propeller stirrer. A Metrohm Titrando 905 automatic titrator was used to pump concentrated

HCl or $FeCl_3$ into the reactor, to measure pH and temperature with a combined glass electrode, and to measure redox potential (ORP) with a combined Pt-ring electrode. A drawing and picture of the setup are shown in Figure 9.

Several experiments were performed with potentiometric control, in which pH or ORP was held constant. The titrator was programmed to make small additions of reagent whenever the electrode's measured potential was outside the target value. Leaching tests were therefore initiated with swarf in a water or $FeCl_2$ solution to enable pH and ORP determination. More details concerning each method are given in Sections 5.3 and 5.4. Precipitation was studied by adding small amounts of swarf to the leaching slurry and leaving the system to react. The purified $FeCl_2$ solution was separated from residual solids and precipitates by vacuum filtration.

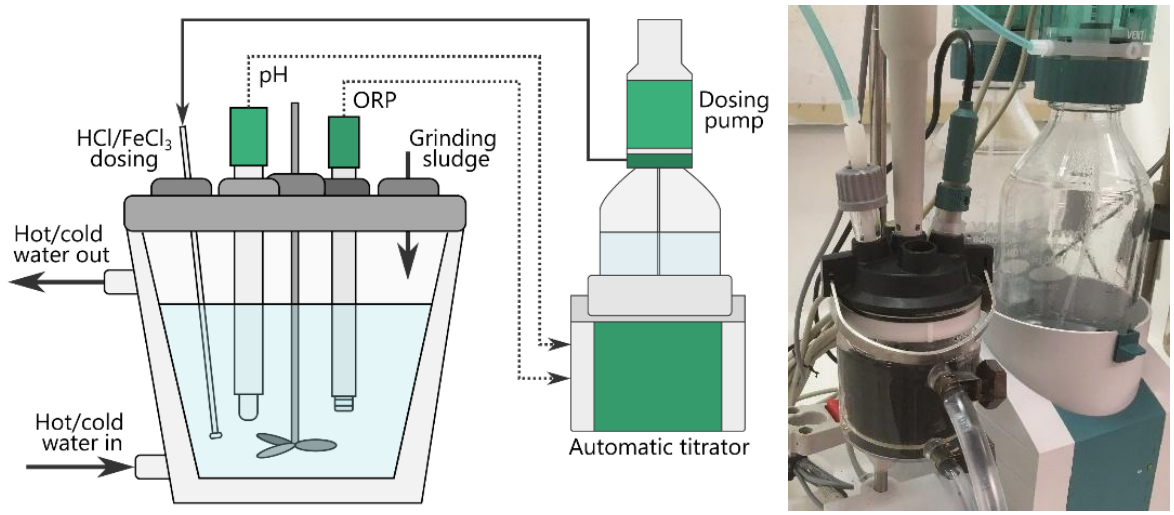

Figure 9: (Left) schematic drawing of the leaching and precipitation reactor with (right) a picture of the reactor, titrator and dosing pumps.

4.3.1 Electrode calibration

The pH electrode was calibrated with pH 2.00, 4.00 and 7.00 buffers. Several factors can influence the measurement of the hydrogen ion activity, including temperature and ionic strength [99]. The former was accounted for by calibrating at the experimental temperature, whereas ionic strength was uncontrollable and unaccounted for. The ORP electrode was calibrated by comparing its measured potential versus a 220 mV $[(Fe(CN)_6]^{3-}/[Fe(CN)_6]^{4-}$ standard.

4.3.2 Process optimisation by design of experiments

Design of experiments (DOE) was used to optimise leaching and precipitation parameters. With this method, multiple variables can be tested simultaneously, saving time and resources, and enabling investigation of variable interactions in

contrast to one-factor-at-a-time testing [100]. Experiments were conducted using spherical or face-centred composite designs with 2 or 3 factors. The experimental variability was estimated by including 3-4 centre point replicate experiments in the design, and all tests were run in random order to minimise experimenter bias. Variables were coded (x_1, x_2, ...) to allow evaluation of their relative impacts on a common scale.

Experimental response data were fitted with regression models using the least-squares method. The significance of regression models and lack-of-fit (LOF) was tested using analysis of variance (ANOVA) and F-tests at the 95% confidence level. Assessment of individual regression coefficients was performed using t-tests at the same confidence level. Redundant regression terms were removed by stepwise elimination of the least significant parameter. This optimisation was continued until a maximum adjusted coefficient of determination (R^2_{adj}), minimum LOF, and minimum standard deviation (σ) were obtained. Outlier identification and experimenter bias were assessed by analysing studentised residuals.

Response surface methodology was used to optimise experimental conditions. Regression models were plotted as 2D lines (1 significant variable) or 3D surfaces (≥2 significant variables). In cases where all three variables were significant, response surfaces were plotted for two variables while keeping the third constant at the low (x=-1), mid (x=0) and high (x=+1) level. Comparison of surfaces, e.g., across different elements, enabled identification of conditions with maximum leaching and precipitation efficiencies.

4.4 Oxidation methods

4.4.1 Pressure oxidation

Stoichiometric amounts of HCl (34 wt%) were added to a $FeCl_2$ solution, and 500 mL of the mixture was transferred to a 1 L jacketed glass reactor. The temperature was controlled at 100-120°C using an external oil flow, and the solution was pressurised to 5-6 bar with O_2 while mixing intensively with an overhead stirrer. Samples were taken regularly for analysis of Fe(II) contents.

4.4.2 Electrolysis in a divided cell

Electrolysis was performed in a 2x50 mL H-cell divided by a Fumasep FAA-3-50 anion exchange membrane (AEM) with Ø=16 mm, as shown in Figure 10. A glassy carbon disc (GCD; Ø=3 mm) working electrode (WE) was used in cyclic

voltammetry (CV), while a reticulated glassy carbon (GCR; Ø=20 mm, h=25 mm) WE was used in electrochemical impedance spectroscopy (EIS) and electrolysis. A Pt wire mesh was used as the counter electrode (CE) in all experiments. The anodic potential was controlled by a Biologic SP-300 potentiostat, relative to a saturated Ag/AgCl reference electrode (RE; E° = +0.222 V). Preparation methods for the AEM and electrodes are presented in Paper 4.

The anolyte was either 48 mL of 3.6 M $FeCl_2$ from swarf, or 3.6 M synthetic $FeCl_2$ prepared from Fe powder and concentrated HCl. An equivalent volume of 4 M HCl catholyte was used in both cases to provide sufficient Cl^- for the complete oxidation of Fe(II). This solution was, however, also replenished with additional catholyte during the experiments, as water osmosed from the catholyte to the anolyte. Electrolysis was conducted with a constant anodic potential of +1.5 V.

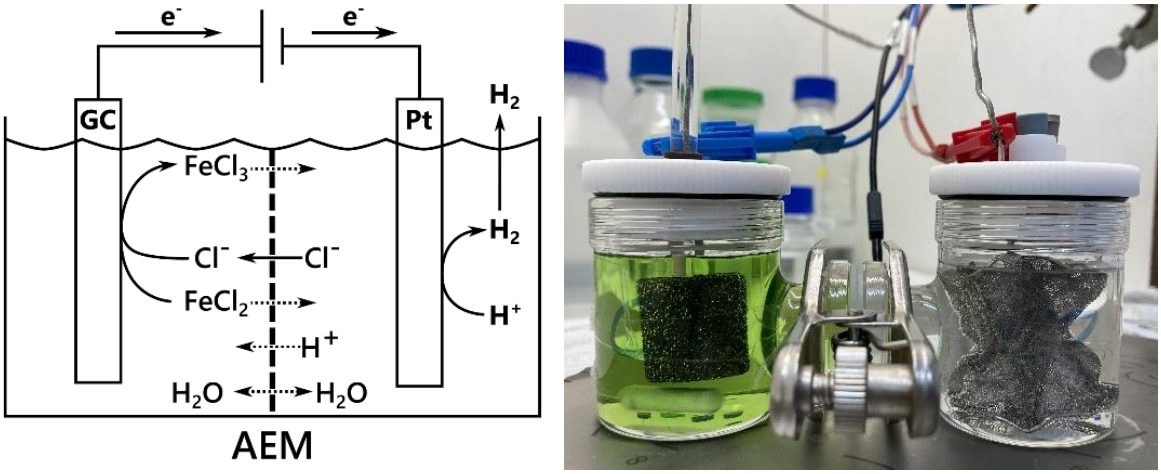

Figure 10: (Left) diagram of the electrolysis cell for oxidation of $FeCl_2$, with solid arrows showing desired reaction pathways and dotted arrows showing unwanted crossover. (Right) picture of the setup with the GCR anode in $FeCl_2$.

4.5 Analytical methods

Techniques used throughout the thesis for analysing liquids and solids are presented in Table 5. Detailed descriptions of how each method was applied can be found in the respective papers.

Table 5: List of analytical methods used for characterising liquids and solids.

Liquids			
Technique	Analytes	Analytical equipment	Source
ICP-OES	Elemental composition	iCAP™ PRO XP ICP-OES, Thermo Scientific™	Papers 1,2,3,4
1,10-Phenanthroline method	Fe_{tot}, Fe(II)	Lambda 25 UV/VIS, Perkin Elmer	Paper 3, [101]
Complexometric EDTA titration	Fe_{tot}	-	Appendix, [102]
Chromate redox titration	Fe(II)	-	Paper 4, [103]
Dean-Starke	H_2O	-	Paper 2
FTIR	Functional groups	Spectrum 3™ FTIR-ATR, Perkin Elmer	Paper 4
LSV/CV	EC reaction kinetics	Biologic SP-300, GCD WE	Paper 4
EIS	EC system characteristics	Biologic SP-300, GCR WE	Paper 4
Solids			
Technique	Analytes	Equipment	Source
Aqua regia digestion	Elemental composition	iCAP™ PRO XP ICP-OES, Thermo Scientific™	Papers 1,2,3,4
XRD	Crystal phase composition	D8 Discover XRD, Bruker	Papers 1,2,3
XRF	Elemental composition	Panalytical, Axios WDXRF	Paper 2
Combustion analysis	C, S	LECO CS744	Papers 1,2
SEM-EDS	Morphology	Phenom ProX™ SEM-EDS, Thermo Scientific™	Papers 2,3
FTIR	Functional groups	Spectrum 3™ FTIR-ATR, Perkin Elmer	Paper 4
Soxhlet extraction	Liquid content	-	Paper 2

5 Results and discussion

5.1 Grinding sludge characterisation

A total of 13 different grinding sludge samples were analysed during the study, which are shown in Table 6. Samples A-F and J-M stem from the bearing and automotive industries, where grinding processes are most extensively used, whereas G and H-I stem from tool manufacturing and a steel mill, respectively. More detailed descriptions of several samples can be found in the corresponding papers where they were tested, but general observations are summarised below.

The most common components found in the grinding sludges are also given in Table 6. Contents of Fe ranged from 50-80 wt%, but on average, around 70 wt% can be expected in the waste, based on the broad range of samples analysed. Sludges based on steel (A-I) typically contained more Cr, Ni and Mo, whereas cast iron sludges (J-M) contained more Mn, Si and V. Inorganic C is not shown but is generally more abundant in cast iron than steels. Abrasives were quantified by XRF in only a few cases, but generalisations regarding their presence across different samples can nevertheless be made based on the discussion in Section 2.2.1. Samples A-G were machined with Al_2O_3 and are assumed to contain 3-8 wt% abrasives based on available data. The remaining samples H-M were ground with harder SiC or CBN and can be expected to contain <1 wt% abrasives.

Cutting fluids were semi-synthetic in all sludges, except sample F, where a fully synthetic water-based lubricant was used for grinding. Filtered or centrifuged sludges had an average liquid content of 23 wt%, whereas the briquetted sample B contained only around 6 wt%. Other unidentified material in Table 6 include lubricants and abrasives for samples where these were not quantified, as well as oxygen in corroded metallic swarf. Differences in cutting fluids, abrasive contents and corrosion are the main reasons for large variations in Fe between sludges.

Typical XRD patterns for grinding sludges from samples B and G are given in Figure 11. Only peaks for ferrite, austenite, and alumina were identified, indicating that the swarf remained mostly metallic despite being stored for several weeks or months in humid conditions. This preservative effect was attributed to the lubricant oils and corrosion inhibitors in the cutting fluids, which protected swarf from the corrosive environment [104]. A similar analysis of samples A and J in papers 1 and 3 confirms that grinding swarf is typically well preserved.

Table 6: Summary of mild steel (S) and cast iron (CI) grinding sludge samples analysed by ICP-OES, Soxhlet extraction, and XRF (B = briquetted, F = filtered, C = centrifuged, CF = cutting fluid, ND = not determined).

Sample origin					Aqua regia digestion + ICP-OES (wt%)					Soxhlet & XRF (wt%)		
Company	Key	Country	Workpiece	Form	Fe	Cr	Mn	Ni	Mo	CF	Abrasives	Other
SKF AB	A[1]	SE	Bearings (S)	B	69.3±4.3	1.35±0.02	0.56±0.01	0.09±0.01	0.27±0.01	ND	~6.2	22.2
	B[2]	SE	Bearings (S)	B	78.4±0.8	1.13±0.01	0.37±0.01	0.10±0.01	0.09±0.01	~6.2	~7.8	6.0
	C	IT	Bearings (S)	F	60.2±1.1	0.58±0.04	0.32±0.02	0.04±0.01	0.02±0.01	~34.4	ND	4.4
	D	FR	Bearings (S)	B	57.5±1.6	0.88±0.02	0.43±0.01	0.08±0.01	0.05±0.01	ND	ND	41.1
	E	UK	Bearings (S)	B	71.2±2.8	1.01±0.02	0.24±0.01	0.04±0.01	<0.01	ND	ND	27.5
Tsubaki Nakashima	F[4]	IT	Bearing parts (S)	F	75.0±0.7	1.04±0.01	0.26±0.01	0.06±0.01	<0.01	~19.2	ND	4.4
Husqvarna AB	G[2]	SE	Chainsaw blades (S)	F	68.4±1.9	0.41±0.01	0.23±0.01	0.64±0.01	<0.01	~19.5	~3.1	7.7
SSAB	H[4]	SE	Cold rolling rolls (S)	F	82.3±1.8	2.94±0.05	0.24±0.01	0.16±0.01	0.35±0.01	ND	ND	14.0
	I	SE	Hot rolling rolls (S)	F	69.4±0.6	3.38±0.01	0.59±0.01	0.81±0.01	0.87±0.01	ND	ND	25.0
Scania AB	J[3]	SE	Crankshafts (CI)	F	64.0±1.5	0.18±0.01	0.94±0.01	0.04±0.01	0.04±0.01	~16.0	ND	18.8
	K[4]	SE	Crankshafts (CI)	F	70.0±4.7	0.18±0.01	0.96±0.06	0.04±0.01	0.04±0.01	ND	ND	28.8
	L	SE	Cylinder lining (CI)	F	52.6±1.2	0.32±0.01	0.37±0.01	0.04±0.01	0.05±0.01	~27.8	ND	18.8
Volvo trucks	M	SE	Crankshafts (CI)	C	69.0±2.0	0.45±0.01	0.73±0.02	0.06±0.01	0.02±0.01	~20.2	ND	9.5
				Average	68.3±8.2	1.07±1.01	0.48±0.26	0.17±0.25	0.14±0.24	20.0±8.3	4.6±2.9	-

[1,2,3,4]Studied in papers with the corresponding numbers.

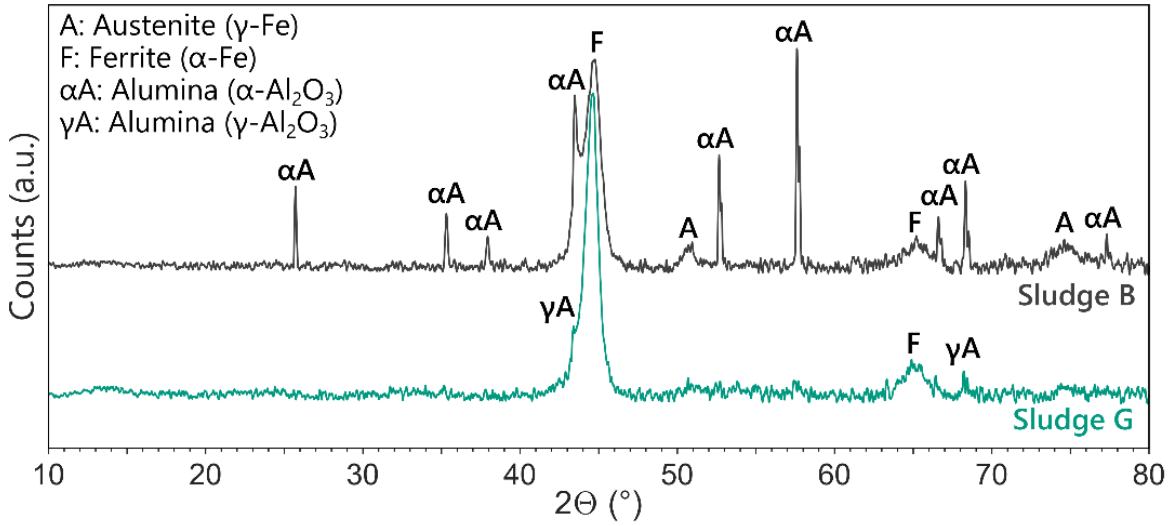

Figure 11: XRD analysis of grinding sludges B and G (Table 6).

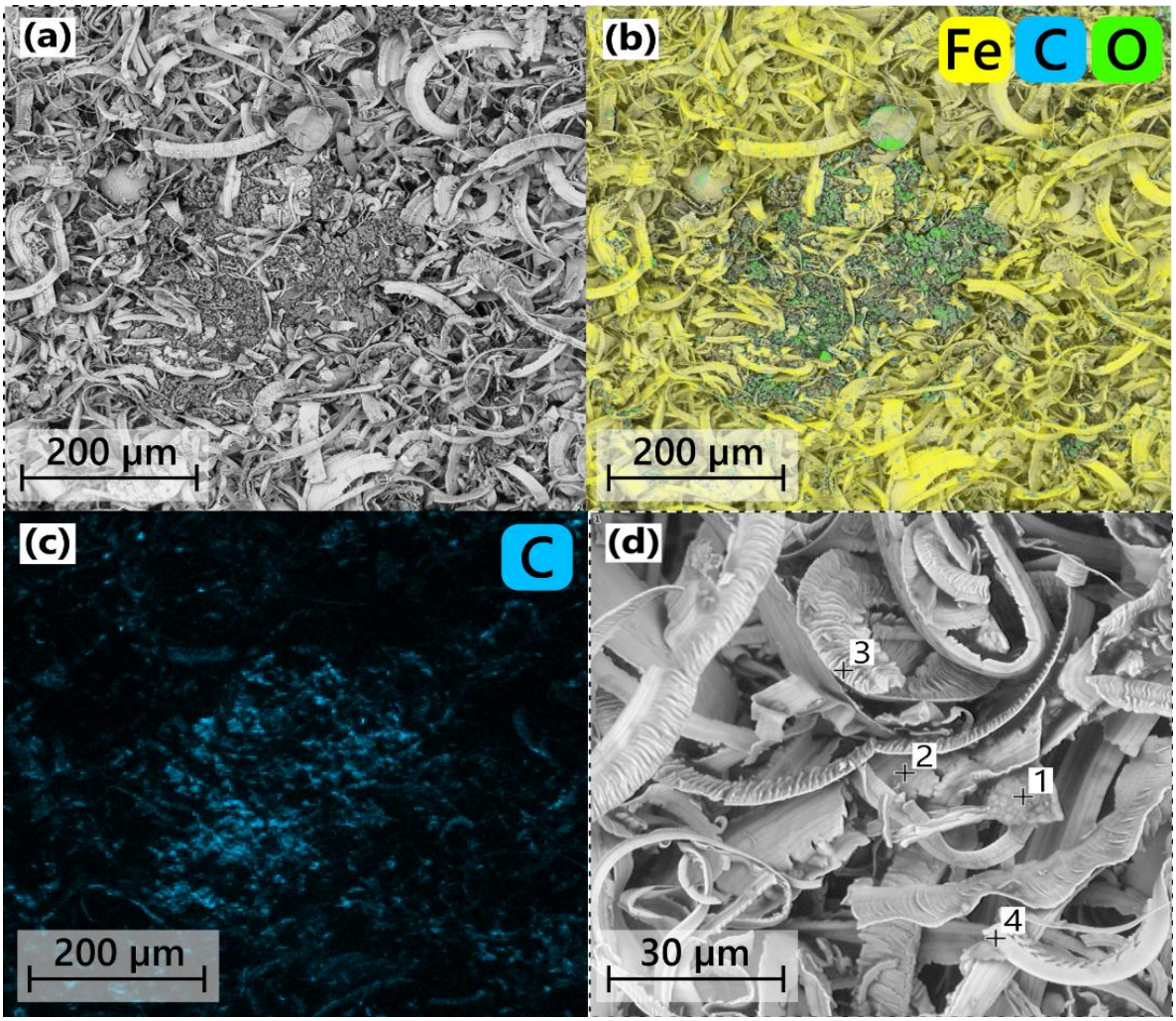

Figure 12: SEM analysis of grinding sludge sample J (Table 6). (a) Low magnification image of swarf around an oxide cluster and the same image with EDS mapping of (b) Fe, C and O, and (c) only C. (d) Spot analysis at high magnification with corresponding local compositions in Table 7.

Table 7: EDS analysis corresponding to the highlighted spots in Figure 12d.

Element	Spot 1 (wt%)	Spot 2 (wt%)	Spot 3 (wt%)	Spot 4 (wt%)
Fe	44	87	66	81
O	30	<1	<1	<1
C	26	12	32	18
Mn	<1	1	1	<1

A closer look at the swarf microstructure of sample J is provided in the SEM-EDS images in Figure 12. In general, the shavings were <200 µm long, <20 µm wide and <1 µm thick. The sickle-shaped particles tended to hook together, forming interconnected networks and giving the swarf a texture somewhere between a powder and steel wool. Fine grooves can be seen in the swarf's surface in Figure 12d, suggesting that it has a large surface area and explaining why it absorbs and retains fluids much like a sponge.

The Figure 12a-c focus on a corroded area where concentrations of oxides and hydroxides were high according to Fe/O ratios in EDS analysis. Corrosion seemingly started locally and grew outward to form larger clusters. A reason for this behaviour was given by Figure 12c, which shows an accumulation of carbon on the hydroxide particles. Similar results are seen from spot analysis in Figure 12d and Table 7 which confirms that carbon was concentrated on oxides and in grooves of the swarf. Organic cutting fluid components clearly preferred adsorbing onto polar corrosion products, leading to the migration and depletion of corrosion inhibitors in the vicinity. This made the surrounding swarf vulnerable to attack, leading to an outward-growing corroded area. While such an adsorption mechanism may accelerate corrosion, the overall extent of the process remained limited, as no oxides or hydroxides could generally be identified by XRD.

5.2 Washing and magnetic separation

Both aqueous and solvent washing were considered to remove cutting fluids prior to hydrometallurgical processing. This was done with the aim of preconcentrating Fe, homogenising the swarf to improve control over input materials, and reducing the risk of contaminating the final $FeCl_3$ product. Early removal of lubricant oils and corrosion inhibitors will also be demonstrated to increase Fe recycling rates and reduce secondary waste in later steps. Aqueous washing with a surfactant was tested as part of a scale-up demonstration project and proven feasible for this purpose. These results are unpublished and not discussed in detail; however,

pictures from the project are shown in Appendix Figure A12-A14, and general information regarding aqueous washing can be found in Section 2.4.4.

Washing with organic solvents was explored in papers 2 and 4, where ethanol and acetone were used, respectively. This selection was based on their relatively low boiling points (78°C and 56°C) that can facilitate distillation, intermediate polarities with potential to dissolve both water and less polar cutting fluid components, and classifications as relatively green solvents [105, 106].

In one instance, grinding sludges B and G were washed cyclically with ethanol via Soxhlet extraction. Their metal contents were analysed with aqua regia digestion and ICP-OES before and after washing, and are shown in Table 8. Both sludges contained Al_2O_3 abrasives and similar steels and semisynthetic cutting fluids (Hysol SL 35 XBB and Hysol SL 36 XBB; compositions in Table A3), with a main difference being that G contained 19.5 wt% liquid compared to 6.2 wt% in B. Each cleaned sample contained nearly identical amounts of Fe and swarf, as indicated by the similarity in Other substances in Table 8. This suggests that washing can account for day-to-day variations and differences between sludges from different sources, thereby granting the recycling process greater flexibility in input material.

Table 8: Comparative ICP-OES analyses of grinding sludges B and G (Table 6) before and after ethanol washing via Soxhlet extraction.

Element	Sample B (wt%)		Sample G (wt%)	
	Unwashed	Washed	Unwashed	Washed
Fe	78.4 ± 0.8	83.4 ± 4.7	68.4 ± 1.9	83.7 ± 2.9
Cr	1.13 ± 0.01	1.22 ± 0.03	0.41 ± 0.01	0.44 ± 0.01
Mn	0.37 ± 0.01	0.41 ± 0.01	0.23 ± 0.01	0.28 ± 0.01
Ni	0.10 ± 0.01	0.11 ± 0.01	0.64 ± 0.01	0.78 ± 0.01
Cu	0.10 ± 0.01	0.04 ± 0.01	0.04 ± 0.01	0.04 ± 0.01
Mo	0.09 ± 0.01	0.11 ± 0.01	<LOD	0.01 ± 0.01
Al	0.04 ± 0.01	0.07 ± 0.01	0.19 ± 0.01	0.15 ± 0.02
Co	0.01 ± 0.01	0.01 ± 0.01	0.01 ± 0.01	0.01 ± 0.01
Other	19.8	14.6	33.12	14.6

In another instance, grinding sludges F, H, and K were mixed in a 1:1:1 mass ratio and cleaned with acetone in a stirred beaker. Preliminary tests with solvent-to-sludge ratios ranging from 1 to 10 mL/g were conducted to estimate optimal washing conditions. At 1-2 mL/g, the swarf completely absorbed the solvent, and at least 3 mL/g was required for proper mixing. The swarf was well dispersed in

the solvent at ≥3 mL/g, and no secondary liquid phase formation was observed. The sludge weight reduction at 2, 3, 5, and 10 mL/g was 14.0%, 15.4%, 18.9%, and 20.0%, respectively, and 5 mL/g was determined to be a good trade-off between solvent consumption and cleaning efficiency. It should be noted that the washing conditions could be optimised further by using more industrially relevant equipment, such as a countercurrent screw conveyor [107]. In this case, however, washing served primarily to obtain more representative swarf samples for hydrometallurgical experiments. A larger batch of mixed sludge was washed at 5 mL/g, and swarf was thereafter recovered from the slurry by magnetic separation, filtered, and dried. Abrasives are chemically inert and were expected to have minimal impact on hydrometallurgical processing, but their removal was still important because their sharp edges could degrade equipment. The sludge compositions before and after pretreatment are shown in Table 9.

Table 9: Comparative ICP-OES analyses of grinding sludges F, H and K (Table 6), which were mixed in a 1:1:1 mass ratio and pretreated with acetone washing and magnetic separation to obtain mixed dry swarf (ND = not determined).

Element	Sample F (wt%)	Sample H (wt%)	Sample K (wt%)	Mixed 1:1:1 (wt%)	Mixed dry swarf (wt%)
Fe	75.0 ± 0.7	82.3 ± 1.8	70.0 ± 4.7	75.6 ± 2.4	90.6 ± 1.9
Cr	1.04 ± 0.01	2.94 ± 0.05	0.18 ± 0.01	1.39 ± 0.02	1.61 ± 0.02
Mn	0.26 ± 0.01	0.24 ± 0.01	0.96 ± 0.06	0.48 ± 0.02	0.60 ± 0.01
Mo	0.01 ± 0.01	0.35 ± 0.01	0.04 ± 0.01	0.13 ± 0.01	0.16 ± 0.01
Si	0.13 ± 0.01	0.13 ± 0.03	0.20 ± 0.02	0.15 ± 0.02	0.13 ± 0.01
Ni	0.06 ± 0.01	0.16 ± 0.01	0.04 ± 0.01	0.09 ± 0.01	0.12 ± 0.04
Cu	0.07 ± 0.01	0.07 ± 0.01	0.02 ± 0.01	0.05 ± 0.01	0.07 ± 0.02
V	0.01 ± 0.01	<0.01	0.07 ± 0.01	0.03 ± 0.01	0.03 ± 0.01
Al	0.06 ± 0.01	0.02 ± 0.01	0.01 ± 0.01	0.03 ± 0.01	0.03 ± 0.01
Zn	0.05 ± 0.01	<0.01	<0.01	0.02 ± 0.01	0.02 ± 0.01
Co	0.01 ± 0.01	<0.01	<0.01	0.01 ± 0.01	0.01 ± 0.01
Abrasives	ND	ND	ND	~1.5	ND
Lubricants	ND	ND	ND	~17.0	ND
Other	23.2	13.9	28.5	3.4	6.6

A swarf content of ~95 wt% with >90 wt% Fe was achieved in the dry material via pre-treatment according to Table 9, and approximately 18.5 wt% of the mixed swarf was removed, of which 1.5 wt% was abrasives, and 17.0 wt% cutting fluids. The washing liquid was distilled to recover lubricant oils and investigate whether the solvent could be recirculated. A clear distillate was obtained, and the raffinate was an emulsion that split into a lighter, transparent brown oil phase and a heavier,

cloudy yellowish water phase within 24 h. Both the distillate and raffinate phases were studied with FTIR, and their spectra are compared with those of water and acetone in Figure 13.

The raffinate oil mainly had peaks in the single-bond region (2500-4000 cm^{-1}) between 2800-3000 cm^{-1}, with matching peaks in the fingerprint region (600-1500 cm^{-1}) at around 1450 and 1380 cm^{-1}, corresponding to aliphatic compounds with C-H and C-C bonds [108]. Characteristic peaks for acetone were also identified, and the oil phase can therefore be assumed to consist mainly of cutting fluid oils with a small amount of solvent that was not properly distilled off. The same oil and

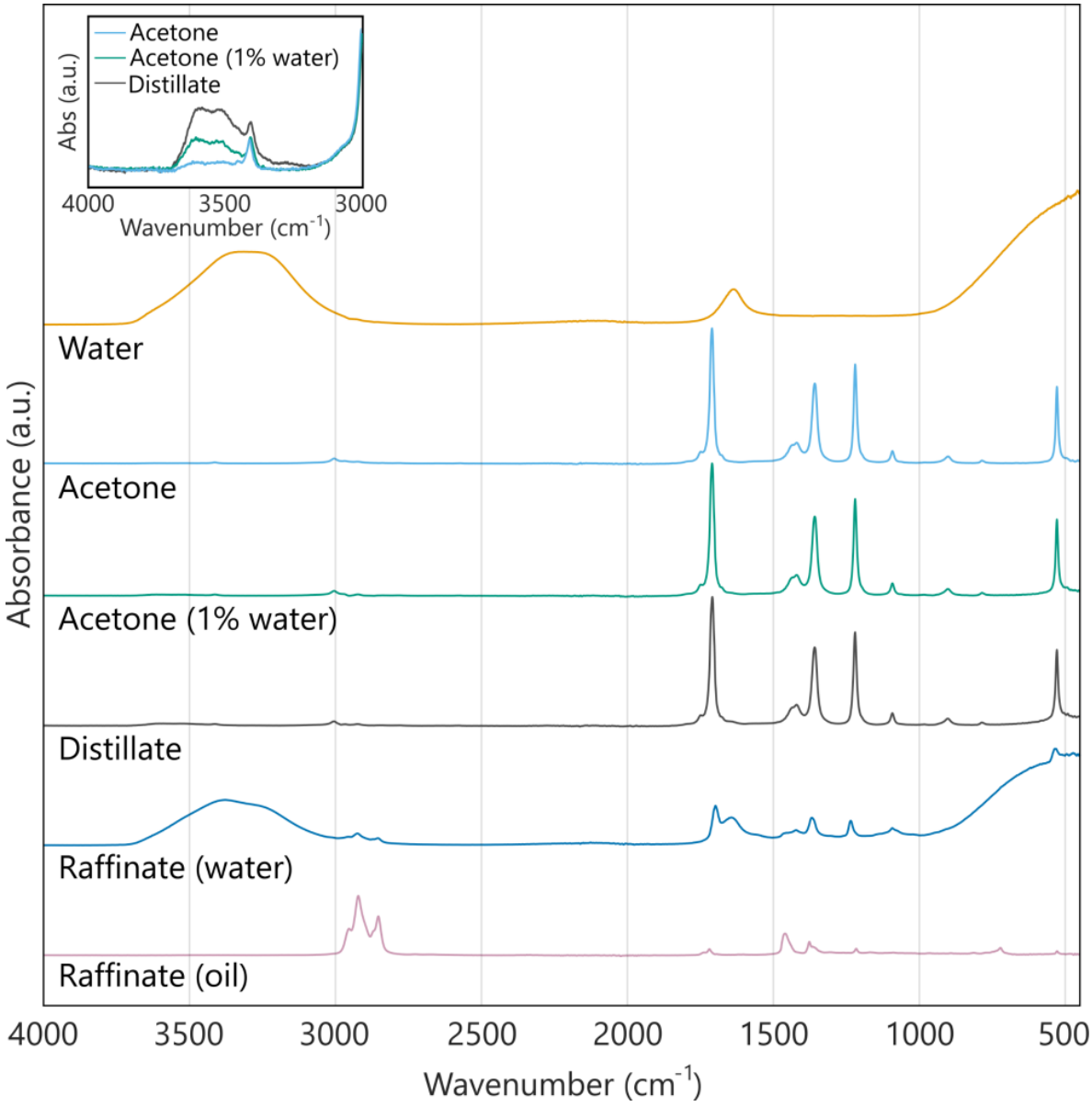

Figure 13: From top to bottom, FTIR spectra of pure water and acetone, acetone with 1 wt% water, and distillate and raffinate fractions after the distillation of loaded acetone from the washing of mixed grinding sludges F, H and K (Table 9). Detailed analysis of water peaks is shown for acetone and distillate samples.

acetone peaks were also detected in the raffinate water, indicating incomplete phase separation. The total raffinate mass was only ~50% of the mass of cutting fluids removed from the grinding sludge, which was attributed to the presence of >1 wt% water in the distillate (see top left box in Figure 13). Part of the water clearly boiled over, suggesting that an azeotrope may have formed during the distillation. Azeotropic behaviour is not expected in binary acetone-water systems, but can arise in ternary or higher order mixtures [109]. No peaks other than water and acetone were identified in the distillate, indicating that most of the cutting fluid oils and additives remained in the raffinate.

Based on these findings, a flowsheet for washing grinding sludges with acetone or another solvent is proposed in Figure 14. The solvent flows in a countercurrent cascade to minimise solvent use per unit sludge input, thereby reducing the heat

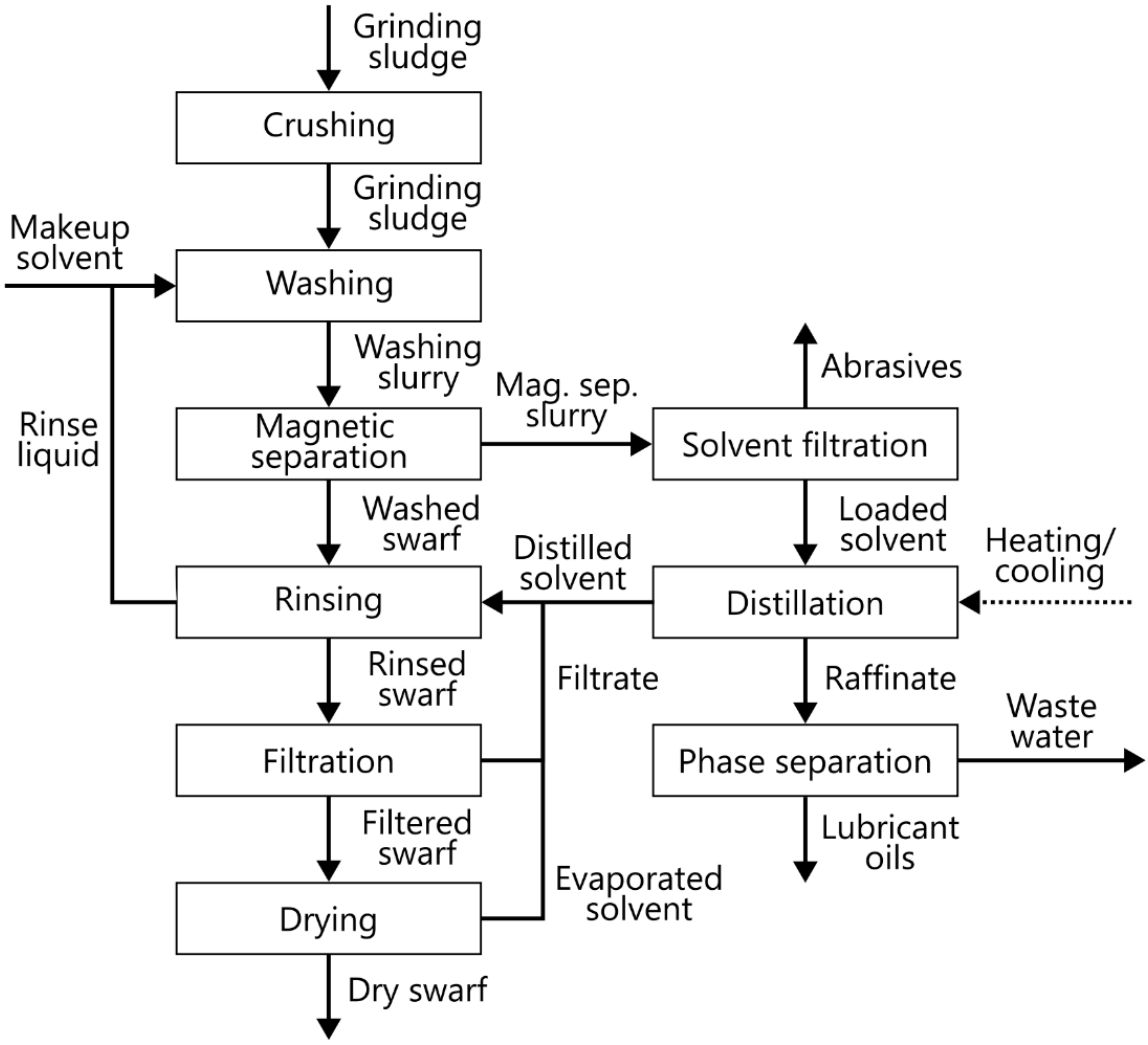

Figure 14: Proposed flowsheet for pretreatment of grinding sludges by solvent washing and magnetic separation prior to hydrometallurgical processing. Design choices are based on experimental observations from acetone washing, with a countercurrent solid-liquid flow and distillation to minimise solvent demand. Abrasives and lubricants can be recovered separately from the clean grinding swarf.

load in the energy-intensive distillation. The abrasives and relatively clean raffinate oils could potentially be recycled, while the oil-contaminated raffinate water is expected to be waste requiring further treatment. Part of the solvent is assumed to be lost to the raffinate and needs to be made up in the washing or rinsing step.

5.3 Acidic leaching with HCl

Conventional acid leaching was investigated first, as HCl is commonly used in industrial $FeCl_3$ production to dissolve magnetite and other Fe oxide materials. The main dissolution mechanisms during the leaching of grinding sludges with H^+ are listed in Table 2, and all reactions, aside from Cu dissolution, are exothermic and spontaneous with negative $\Delta H_r°$ and $\Delta G_r°$. Reactions between metallic elements and H^+ were expected to be most common, and significant H_2 formation was anticipated. However, as experiments were performed under air exposure, a pathway in which Fe^{2+} was first oxidised to Fe^{3+} via Equation 23 and then attacked the metal was also possible. This could potentially lead to dissolution of Cu via Equation 25, as Fe^{3+} is a stronger oxidant than H^+. Assuming the input material contains 70 wt% metal swarf and that all leaching occurs via Equation 21, around 2.1 mL of 37 wt% HCl per gram of sludge is theoretically required to achieve complete Fe dissolution.

Leaching of briquetted, unwashed grinding sludge A with HCl was investigated in a DOE optimisation study, with four centre-point replicates. The effects of temperature (T; x_1), pH (x_2), and initial liquid-to-sludge ratio (L/S_i; x_3) were evaluated, with leaching efficiencies ($\%E_M$) of Fe, Cr, Mn, Ni and Mo as responses. In each experiment, the sludge was added to 100 mL of DI water and leached at a static pH for t = 3 h with a stirring speed of 1500 rpm. Intense stirring was necessary to keep the swarf in solution in the small reactor during H_2 formation, but 300-400 rpm was generally sufficient for leaching in a ≥1 L reactor. Experimental data and regression analyses for the DOE are found in paper 1, and the final efficiency models are presented in Table 10, with validity between T = 20-60°C, pH 2-4, and L/S_i=20-50 mL/g. The dissolution of Mo was generally between 0% and 20% and was not modelled.

All regression models fit the experimental data well with R^2_{adj} values close to or exceeding 0.90. Some caution is advised when predicting efficiencies for Cr, as the standard deviation (σ) was relatively high. Graphical representations of the regression models are given as response surfaces in Figure 15. These contour plots

Table 10: Regression models for leaching efficiencies of Fe, Mn, Ni, and Cr based on the leaching of grinding sludge A (Table 6) with HCl in an experimental design. Coded variables: temperature (x_1), pH (x_2), initial liquid-solid ratio (x_3).

Regression model	R^2_{adj}	σ (%)	Eq. (#)
$\%E_{Fe} = 91.5 + 17.1x_1 - 19.8x_2 - 5.4x_3 + 7.6x_1x_2 - 5.9x_2x_3 - 13.1x_1^2 - 10.2x_2^2 + \varepsilon$	0.94	5.4	(63)
$\%E_{Mn} = 75.0 + 14.1x_1 - 17.0x_2 - 4.6x_3 + 5.4x_1x_2 - 4.4x_2x_3 - 9.2x_1^2 - 8.3x_2^2 + \varepsilon$	0.96	3.7	(64)
$\%E_{Ni} = 78.6 + 23.7x_1 - 20.7x_2 - 13.5x_3 - 18.2x_2^2 + \varepsilon$	0.86	5.6	(65)
$\%E_{Cr} = 37.8 - 25.0x_2 - 8.9x_1^2 + \varepsilon$	0.91	10.9	(66)

show leaching efficiencies as a function of temperature and pH, at high, intermediate, and low L/S_i levels. Only one surface is shown for Cr, which was valid at all L/S_i since the model in Equation 66 was independent of x_3.

Optimal leaching conditions were found to be between pH 2 and 3 and 40 and 60°C, where nearly 100% Fe could be dissolved. Around 95-100% of the theoretical amount of HCl needed was added under these conditions. More swarf was dissolved as T and $[H^+]$ increased, which was reasonable as kinetics and chemical equilibria were favoured under these conditions. Another observation was that the optimum pH decreased with L/S_i. This could be explained by variations in the acid-to-swarf ratio between 20 and 50 mL/g at a given pH, where less H^+ was available per metal at 20 mL/g, leading to slower dissolution. Low $\%E_{Fe}$ at combinations of high pH, and low L/S_i and T can therefore be explained by an incomplete reaction. Generally speaking, a steady state was reached only when T ≥ 40°C and pH ≤ 3, whereas under other conditions, significant acid addition continued after 3 h.

The behaviour of Mn was nearly identical to Fe, with the exception that $\%E_{Mn}$ was ~20% lower on average under the optimal leaching conditions, according to Figure 15. One possibility was that Mn in the swarf could have formed less soluble oxides (e.g., MnO or MnO_2) as this metal is less noble than Fe and more readily oxidised. Regardless, the conclusion was that coextraction of Mn could not be avoided in the investigated system. Leaching of Ni was also similar to Fe, but a significant $\%E_{Ni}$ decrease was observed with decreasing L/S_i. This could again be partially explained by incomplete swarf dissolution at low L/S_i, but another argument was that Ni was continuously cemented onto the remaining undissolved swarf. At 20 mL/g, a larger Fe surface area was available, leading to more efficient

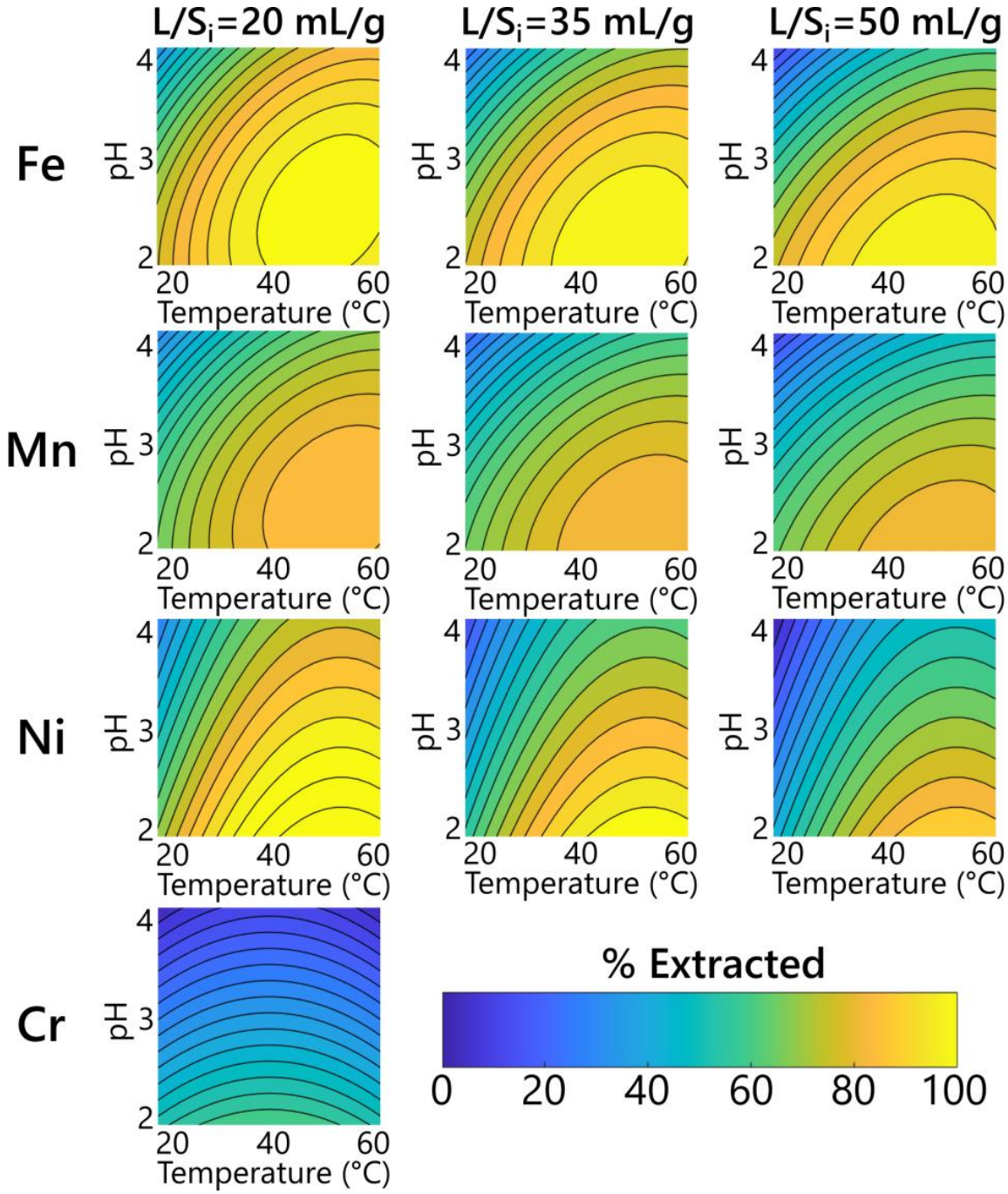

Figure 15: Response surfaces based on leaching efficiency models in Table 10. Efficiencies for Fe, Mn, and Ni are shown at three fixed L/S_i levels with varying temperatures and pH, while Cr was independent of L/S_i. All tests were conducted with a constant leaching time of 3 h, an initial water volume of 100 mL, 5 M HCl dosing, and stirring at 1500 rpm.

cementation. The response surface for Cr in Figure 15 is noticeably different, and $\%E_{Cr}$ was mainly influenced by pH, with 60% extraction at pH 2 and ~0% at pH 4. As with Mn, part of the Cr may have been present as acid-resistant oxides such as Cr_2O_3, which are well known to protect steel from corrosion. The dissolution of Cr is thermodynamically favoured over Fe when comparing $\Delta G°$ in Table 2, but Cr^{3+} is less stable than Fe^{2+}, Mn^{2+}, and Ni^{2+} and predominantly forms $Cr(OH)_3{\cdot}3H_2O$ at pH

≥2.5 according to the Eh-pH diagram in Appendix Figure A3. The assumed mechanism was that Cr was, in fact, partially dissolved but then precipitated via hydrolysis [110].

In conclusion, selective extraction and separation of Fe from Cr and Ni was possible by leaching at 60°C and pH 4 with a minimum L/S_i. Under these conditions, dissolution was slow, however, and only 80% Fe was extracted within 3 h. Maximum Fe recovery was preferred in the recycling process, and the optimal leaching conditions were therefore determined to be 60°C and pH <2. In later experiments, lower L/S_i of 1, 2, 3, 5, and 10 mL/g were also tested, and a minimum of 2-3 mL/g was found acceptable. The sludge completely absorbed the liquid at L/S_i <2, as observed during acetone washing, and turned into a rapidly expanding foam once HCl was added and H_2 began forming. This made mixing impossible and eventually led to the reactor overflowing. Foaming was also generally an issue at high L/S_i, as part of the swarf was lifted out of the slurry, preventing good contact with the HCl. The foam normally persisted for <1 h before disintegrating and being mixed back into the solution. To keep the L/S minimal throughout leaching, the added HCl should be highly concentrated.

5.3.1 Influences of cutting fluids on HCl leaching

Further HCl leaching experiments were conducted in paper 2 to study the effects of cutting fluids on swarf dissolution. Grinding sludges B and G in Table 8 were leached for 3 h in a 1 L reactor at 60°C and pH 2, with L/S_i = 10 mL/g, an initial DI water volume of 300 mL, and stirring at 400 rpm. As mentioned previously, steels and semisynthetic cutting fluids (see Appendix Table A3) in each sludge were comparable, but unwashed G contained over 3 times more fluid than B, according to Table 6. A comparison of $\%E_M$ over time is shown in Figure 16, indicating that <40% of unwashed G was dissolved, whereas unwashed B was more susceptible, with around 85% Fe dissolution in 3 h. This difference was also evident from analysis of the solid residues (see paper 2, Figure 3), where much of the metal swarf in G was intact after leaching, while only a dark brown sludge remained with B. To verify if this was due to cutting fluids, both grinding sludges were washed and leached using the same method. This resulted in a clear improvement, with both samples almost completely dissolved within 2 h, as shown on the right-hand side of Figure 16.

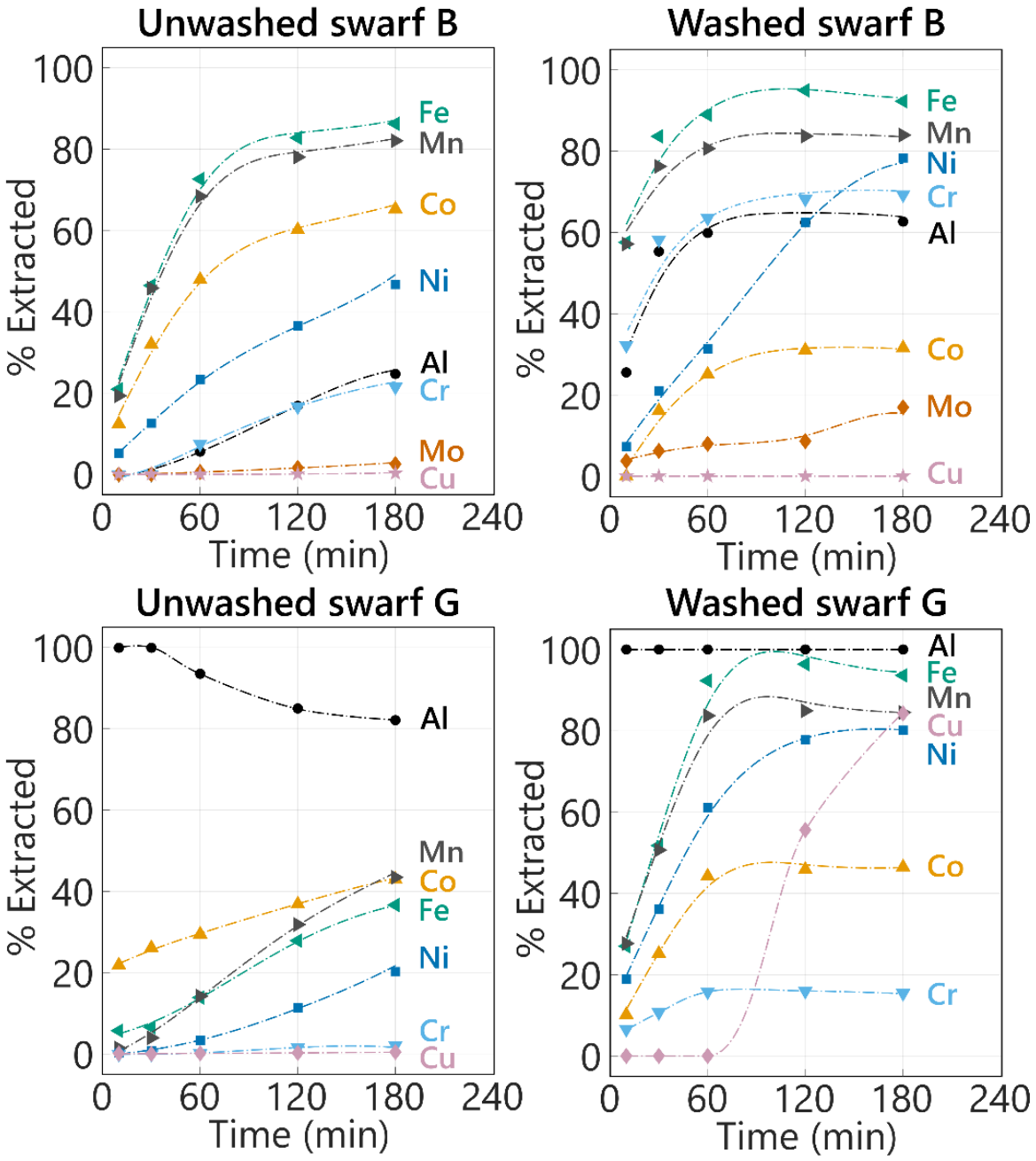

Figure 16: Leaching of briquetted sludge B and filtered sludge G before and after washing with ethanol (Table 8). Each test was conducted with an initial 30 g grinding sludge in 300 mL water, which was leached at 60°C and pH 2, with 12 M HCl dosing and stirring at 400 rpm.

Cutting fluids thus play a crucial role in achieving high Fe recovery, and the most likely explanation behind limited dissolution in unwashed swarf is passivation of the steel surface by organic corrosion inhibitors. These amphiphilic substances typically contain heteroatoms such as O, N, S, or P and conjugated π-bonds, and adsorb strongly onto metal surfaces under acidic conditions [104]. The base lubricants in sludges B and G contained multiple corrosion-inhibiting additives, including amines (ethanolamine, dicyclohexylamine, triethanolamine, etc.), carboxylic

acids and phosphates [111]. Sludge B also contained 0.1 wt% Mo, which can act as an anodic inhibitor by forming insoluble molybdate layers on steels [104].

In addition to organic corrosion inhibitors, lubricant oils in cutting fluids may also hinder leaching via coating of the metal surface, as well as through a less obvious demulsification and adsorption mechanism. The fluids were initially dissolved upon mixing grinding sludges with water, forming turbid solutions, as seen in Figure 17. During leaching, the solution gradually cleared, and the filtered $FeCl_2$ solutions were consistently transparent with no visible oil layer. This suggests that oils were destabilised and adsorbed by undissolved solids, including swarf, thereby blocking the metal surface. Previous work on the recovery of lubricant oils from water-based cutting fluids has shown that electrolytes disrupt the electrostatic forces that maintain the suspension of emulsified oils and other colloidal particles [112, 113]. This causes them to aggregate by coagulation and flocculation, forming a separate oil phase. Demulsification can be expected to occur at an ionic strength of 0.1 M, and given that the final [$FeCl_2$] was typically around 3.5 M, this process was assumed to be highly efficient during the leaching of grinding sludges. Other effects that have been shown to further promote destabilisation and were active during leaching include mixing and elevated temperature (≥40°C).

Figure 17: Water with 6 wt% semisynthetic oil emulsion cutting fluid (left), release of cutting oil emulsion from unwashed grinding sludge when mixed with water before leaching (middle), and $FeCl_2$ solution after leaching and filtration (right). The oil-free $FeCl_2$ indicates that emulsions are destabilised during leaching.

5.4 Oxidative leaching with $FeCl_3$

Leaching with HCl has so far proven to be a simple and efficient method for dissolving Fe, especially with washed grinding sludges. The formation of H_2 as a byproduct was assumed to be an advantage over current magnetite-based $FeCl_3$ production, where H^+ from HCl reacts to form H_2O. Theoretically, up to around 25 kg of H_2 can be generated per ton of sludge containing 70 wt% metallic swarf, potentially creating additional recycling value. Capturing this gas can prove relatively complicated if the process is small-scale, however. In a plant processing 1000 tons of grinding sludges per year, around 25 tons of H_2 would be generated. This number is insignificant compared to the current global H_2 use of 100 Mton, and predicted future demand of 660 Mton in the steel industry by 2050 [114, 115]. Economically speaking, compressing and storing these small volumes may be unfeasible with current technologies, especially if the gas is generated intermittently in a batch process. Furthermore, additional safety measures and ATEX-class equipment would be required in the process due to the explosion hazard H_2 represents according to EU directives (2014/34). These conclusions led to the development of an alternative leaching process that reduces H_2 formation by using $FeCl_3$ as a leaching agent.

Leaching reactions in Table 2 show that the dissolution of metallic elements by oxidation with Fe^{3+} is spontaneous and that no H_2 byproduct is formed. The molar ratio of Fe^{3+} to Fe is 2:1, the same as in leaching with H^+; however, concentrated $FeCl_3$ is typically around 3.5 M, while HCl can be found as 12 M solutions. This means the final slurry volume for the same amount of grinding sludge can be more than three times larger with $FeCl_3$. No direct effects of $FeCl_3$ were expected on oxides and hydroxides in the sludge, as these are already in a Fe(III) state and do not require oxidation to be leached.

Analogous to pH measurements during HCl leaching, monitoring ORP during $FeCl_3$ dissolution can provide valuable information about the Fe^{3+}/Fe^{2+} redox couple. The relationship between ORP and [Fe(III)]/[Fe(II)] was investigated in a synthetic iron chloride system at three different temperatures and constant $[Fe]_{tot}$ = 200 g/L, and is shown in Figure 18. When only Fe(II) was present, the ORP was between -200 and -300 mV, but as soon as 0.1% Fe(III) was introduced, the system rapidly became oxidising. This dramatic increase suggests that Fe(III) can be a good oxidiser even at low [Fe(III)]. From 1% Fe (III) and forward, log([Fe(III)]/[Fe(II)]) took on a linear relationship, described by the Nernst equation in Equation 67.

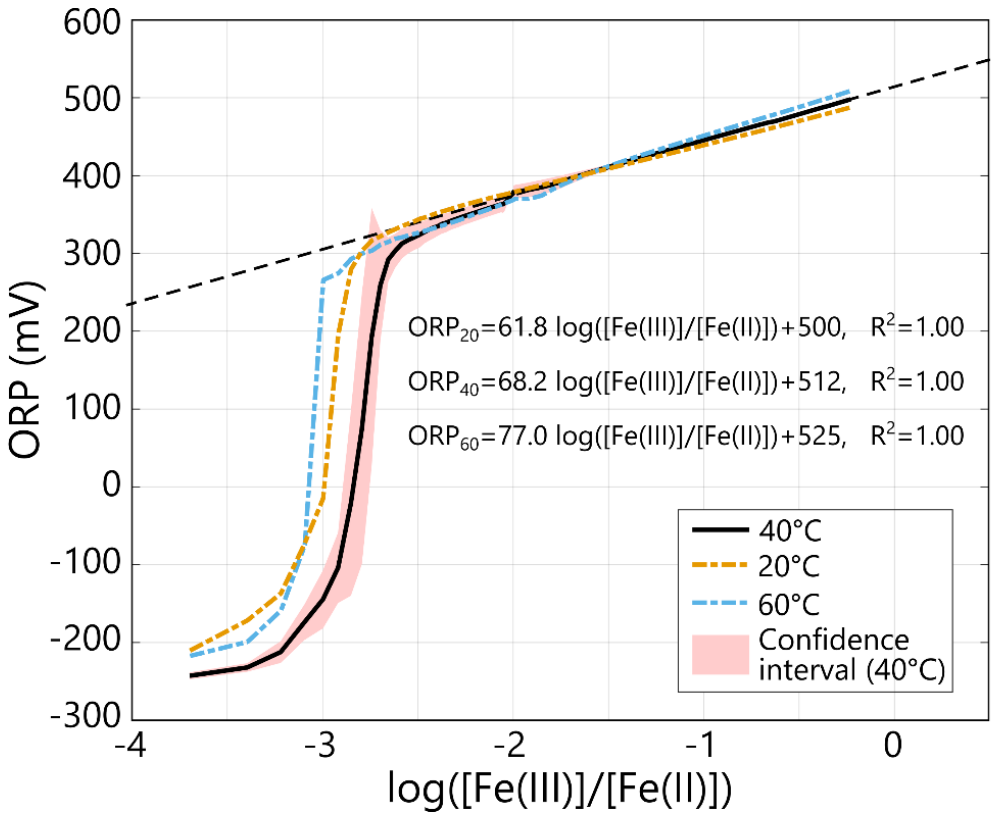

Figure 18: Relation between redox potential and relative concentrations of Fe(III) and Fe(II) in a chloride solution at 200 g Fe/L and 20, 40 and 60°C. The data was generated by dosing $FeCl_3$ into a 50 mL $FeCl_2$ at 0.4 mL/min. Regression models are provided for the linear regions at log([Fe(III)]/[Fe(II)])>-2.

$$E_{ORP} = E^o_{ORP} - \frac{RT}{nF}\ln\left(\frac{a_{\mathrm{Fe(II)}}}{a_{\mathrm{Fe(III)}}}\right) = E^o_{ORP} + \frac{2.302RT}{nF}\log\left(\frac{a_{\mathrm{Fe(III)}}}{a_{\mathrm{Fe(II)}}}\right) \qquad (67)$$

The confidence interval (95%) for 40°C in Figure 18 was narrow in the linear region, allowing good prediction of [Fe(III)]/[Fe(II)] based on ORP, and hence individual [Fe(II)] and [Fe(III)] if $[Fe]_{tot}$ is known.

5.4.1 Dissolution of grinding sludges in concentrated $FeCl_3$

A first approach tested in paper 3 was to leach unwashed grinding sludge J (Table 6) in concentrated $FeCl_3$. The benefits of washing were not fully evaluated at this point, and it was of interest to study whether the same passivation effects would be observed with a different leaching agent. Experiments were performed according to a DOE with three centre points. Temperature (x_1), time (x_2), and L/S_i (x_3) were the studied variables, with $\%E_s$ (Equation 47) for Fe as the response. The sludge was added to 35 mL of 32.5 wt% $FeCl_3$ solution, and pH and ORP were continuously monitored while stirring at 1500 rpm. The regression model for Fe, with R^2_{adj} = 0.77 and σ = ±10.6%, is shown in Equation 68 and is valid between T = 20-60°C, t = 15-105 min, and L/S_i = 6-10 mL/g.

$$\%E_{s,Fe} = 79.2 + 13.2x_2 + 19.5x_3 - 7.8x_2x_3 + 9.1x_2^2 - 18.2x_3^2 + \varepsilon \qquad (68)$$

Temperature effects were found to be insignificant, and a corresponding response surface shows how $\%E_{s,Fe}$ varied with t and L/S_i in Figure 19. Average pH, ORP, and T, during centre-point experiments (40°C, 60 min, 8 mL/g), are also presented with one standard deviation.

An optimum L/S_i was found between 9.0-9.5 mL/g, which was slightly higher than the theoretical amount of 8.7 mL/g required for swarf J containing 64 wt% Fe. The small excess required could be attributed to partial precipitation of the $FeCl_3$ reagent during leaching, as indicated by the formation of light-brown solids that increased solution turbidity. A time dependence was also observed in the response surface in Figure 19, where longer leaching had a positive effect on Fe dissolution.

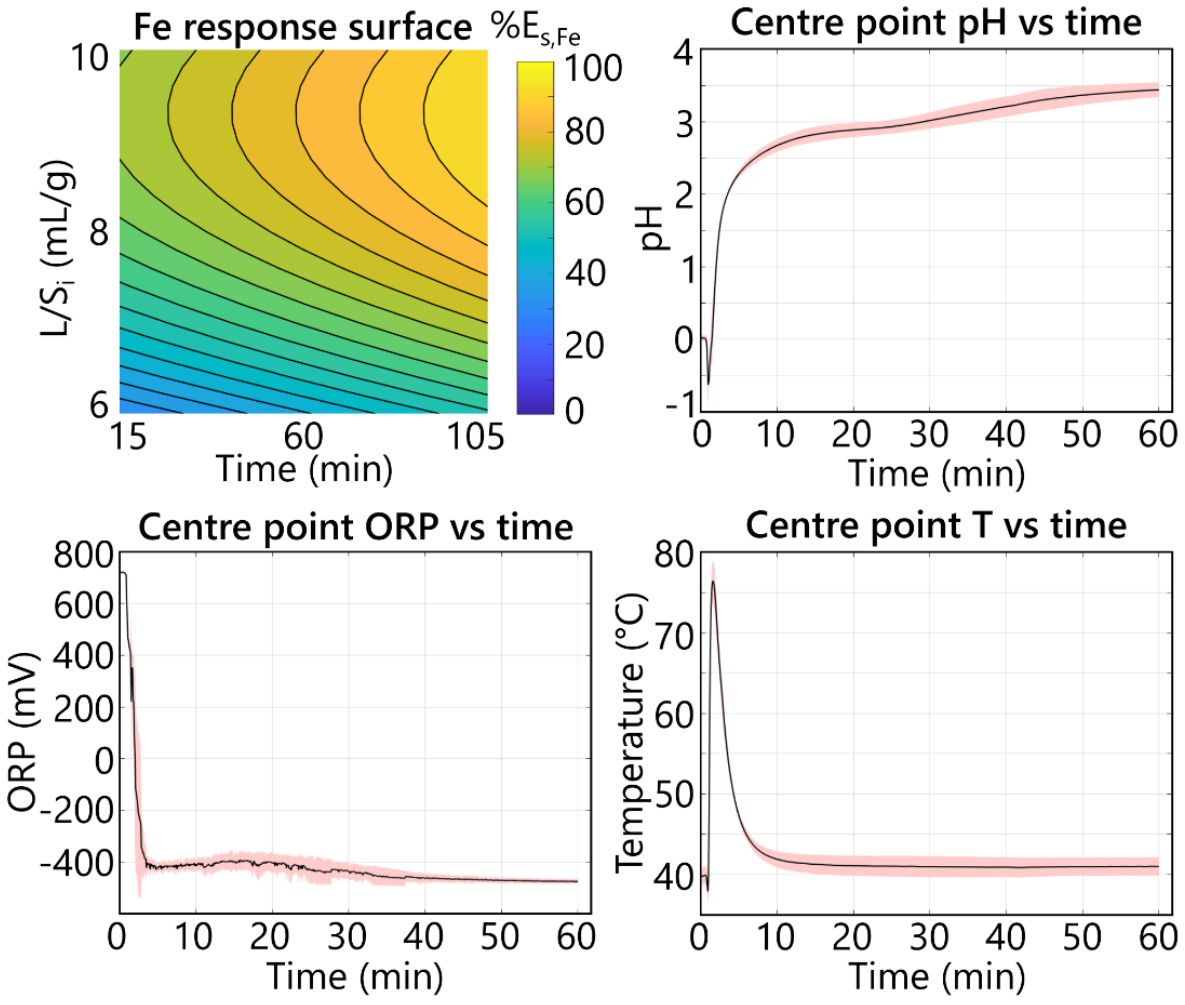

Figure 19: (Top left) Modelled leaching efficiencies for Fe based on Equation 68, when dissolving grinding sludge J (Table 6) in 35 mL, 32.5 wt% $FeCl_3$, while stirring at 1500 rpm. (Top right) measured average pH , (bottom left) redox potentials (ORP), and (bottom right) temperatures in centre-point tests (40°C, 60 min, 8 mL/g) are given, with shaded areas representing one standard deviation.

This was surprising, given that most Fe(III) was consumed within 5 min, as indicated by an ORP drop from +700 mV to -400 mV, and that little H^+ remained, based on a high pH of 2.8 after 15 min that rose only marginally to 3.5 after 105 min. Therefore, too few leaching agents were present to account for the observed 10-40% increase in $\%E_{s,Fe}$. Given that reactions were fast, this time effect was attributed to a slow diffusion of the $FeCl_2$ product into the bulk. Diffusion was likely hindered by the formation of mixed $FeCl_2$ and FeO(OH) at the swarf surface.

Reactions between Fe^{3+} and metallic elements were highly exothermic based on the large negative ΔH in Table 2, and Figure 19 shows a dramatic heat generation in the first 5 min. This was observed as intense sizzling and boiling in the solution, and local temperatures at the metal surface were assumed to be high, promoting hydrolysis and increasing the risk of precipitating the Fe^{3+} reactant. An indication of hydrolysis was given by the initial drop in pH observed in the centre-point experiments shown in Figure 19. In an attempt to verify whether an $FeCl_2$ and FeO(OH) mix may have been formed, solid residues from experiments with t = 15, 60, and 105 min were analysed with XRD. The patterns shown in Figure 20 indicated that the metal fraction was indeed completely converted to a mixture of

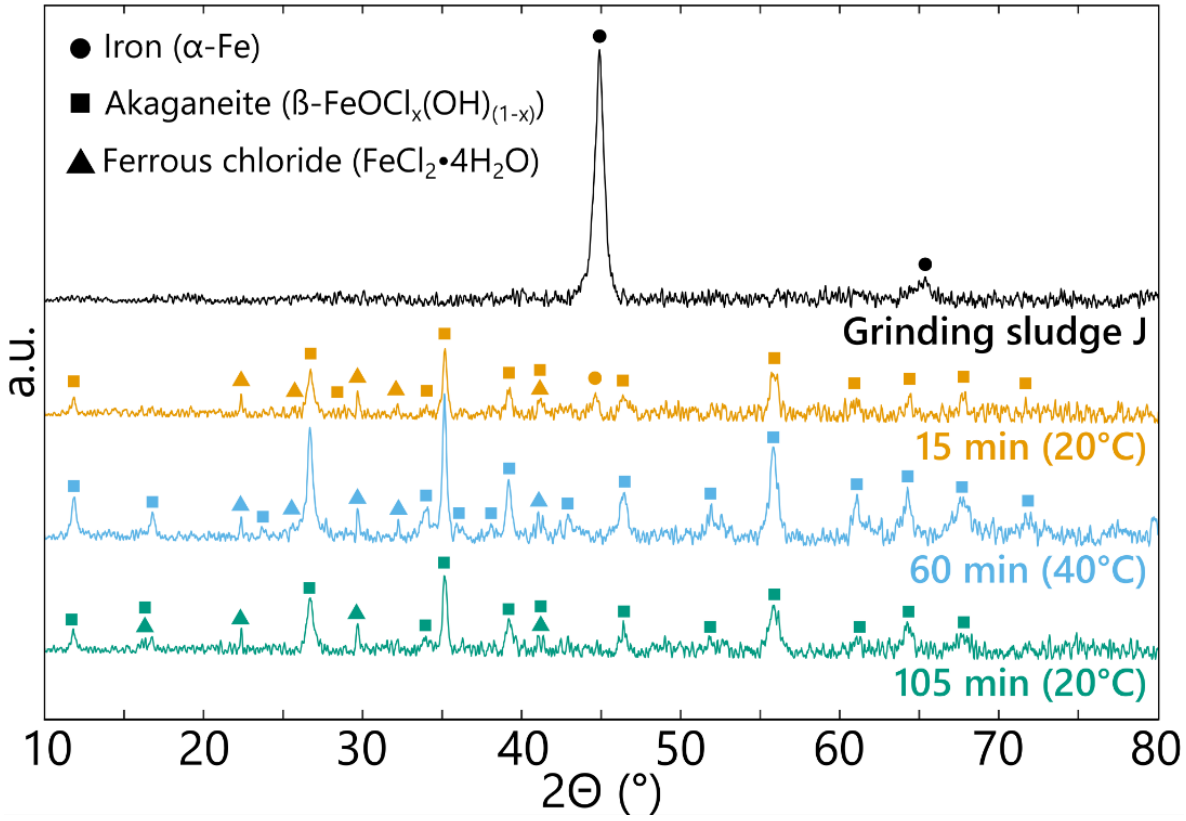

Figure 20: XRD patterns of grinding sludge J (Table 6) and solid residues from $FeCl_3$ leaching experiments of 15 (20°C), 60 (40°C), and 105 (20°C) min. In all cases, 5.8 g of sludge was leached with 35 mL of 32.5 wt% $FeCl_3$.

$FeCl_2 \cdot 4H_2O$ and akaganeite (β-$FeOCl_x(OH)_{(1-x)}$), which is a preferred hydroxide phase formed in concentrated $FeCl_2$ solutions and can contain up to 8 wt% Cl [76, 116]. No clear trend in relative peak sizes between these phases was observed, however, and it was difficult to draw firm conclusions about whether $FeCl_2$ was leached from the solids over time. A complicating factor was that some of the $FeCl_2 \cdot 4H_2O$ could have originated from aqueous $FeCl_2$ in the leachate that was not properly washed from the filter cake. Distinguishing between this $FeCl_2$ and another trapped phase was difficult without detailed analysis, which was outside the scope of the work.

Another interesting feature of this $FeCl_3$ leaching method was that any passivating corrosion inhibitors from the semisynthetic cutting fluids were circumvented. This was confirmed by leaching the grinding sludge with concentrated HCl, in which only 41% Fe was dissolved, compared to the optimum of 95% Fe in Figure 19. This had several possible explanations, including reduced adsorption efficiency due to high temperatures and a different hydrodynamic and electrostatic environment in the $FeCl_3$ solution, or a decomposition of the organic molecules in the aggressive oxidative conditions [104, 117].

The reaction with $FeCl_3$ has so far proven fast, with nearly complete conversion of the metallic swarf within 15 min, compared to 1-2 h with HCl. It was evident that less H_2 was formed as no problems with frothing were observed, and the swarf remained well mixed throughout the dissolution. Several problems were, however, foreseen with the strongly exothermic reaction, which may be more difficult to control as cooling and mixing become more challenging at scale. This could lead to even higher local temperatures, with increasing risks of hydrolysis, trapping the $FeCl_2$ product, and releasing H^+ to form H_2 indirectly with the metallic swarf.

5.4.2 Potentiostatic leaching with $FeCl_3$

Limiting Fe(III) hydrolysis was identified as crucial when dissolving swarf in $FeCl_3$. A final potentiostatic leaching method with ORP control was therefore developed in paper 4, aiming to control this reaction. Since hydrolysis is primarily favoured by high temperatures and pH, a first change from the previous method was to slowly introduce $FeCl_3$ into the slurry while simultaneously cooling to prevent rapid heat generation. The pH was more difficult to control due to the unpredictability of Fe(III) hydrolysis during leaching, but one option was to add HCl to the slurry or leaching agent to suppress this reaction. Including HCl could also help dissolve oxides and hydroxides, which were otherwise unaffected by $FeCl_3$ alone.

Considering these improvements, another DOE with three centre points was conducted with temperature (x_1), target ORP (x_2), and molar ratio of HCl to $FeCl_3$ in the reagent (n_{HCl}/n_{FeCl3}; x_3) as variables. Initially, 4 g mixed dry swarf (Table 9) was added to 18 mL of DI water, and the $FeCl_3$/HCl solution was then dosed into the system under ORP control. The slurry was stirred at 1500 rpm, and temperature and pH were continuously monitored during the 2 h experiments. The dosing rate was variable but limited to a maximum of 1 mL/min, and more than 95% of the total reagent added was typically dosed within 1 h. After 2 h, dosing rates were negligible, and the system reached a steady state in all experiments.

Measured responses again included $\%E_s$ for different metals and are reported in Appendix Table A4, but the generated regression models were relatively poor and did not fit the experimental data well. Possible reasons for the experimental variability included high dilution factors in ICP-OES, which required multiple dilution steps, and slight variations in swarf oxide content and in the leaching process. Instead, a model for the percentage of solids remaining after leaching (%FC) was produced and is given in Equation 69, with $R^2_{adj} = 0.97$ and $\sigma = \pm 1.75\%$.

$$\%FC = 23.1 + 10.6x_1 - 2.8x_2 - 2.1x_3 + 1.7x_1x_2x_3 + \varepsilon \quad (69)$$

All variables had significant effects on the leaching process, including a three-way interaction that was difficult to interpret physically but described the experimental data well. The model is valid between 20-60°C, 300-400 mV, and 1-5% HCl/$FeCl_3$, and response surfaces within these ranges are shown in Figure 21.

Temperature had the strongest influence by far, with average %FC of 13, 23, and 34% at 20, 40, and 60°C, respectively. These differences can be explained by the corresponding pictures below each plot in Figure 21. Slurries became a turbid brown, and swarf started foaming significantly at 40 and 60°C, indicating the formation of FeO(OH) and H_2. This process is best described by a combination of Equations 21 and 70, and the net reaction in Equation 71.

$$Fe^{3+} + 2H_2O \rightleftharpoons FeO(OH) + 3H^+ \quad (70)$$

$$Fe + 2H^+ \longrightarrow Fe^{2+} + H_2 \quad (21)$$

$$2Fe^{3+} + 4H_2O + 3Fe \longrightarrow 2FeO(OH) + 3Fe^{2+} + 3H_2 \quad (71)$$

Once H^+ reacts with metallic Fe, it leaves the system as H_2, preventing redissolution of FeO(OH), which makes Equation 65 irreversible. While this results in a net dissolution of Fe, only 60% of the input Fe forms soluble Fe^{2+} compared to 100% in the desired reaction pathway. The side reactions were efficiently suppressed at

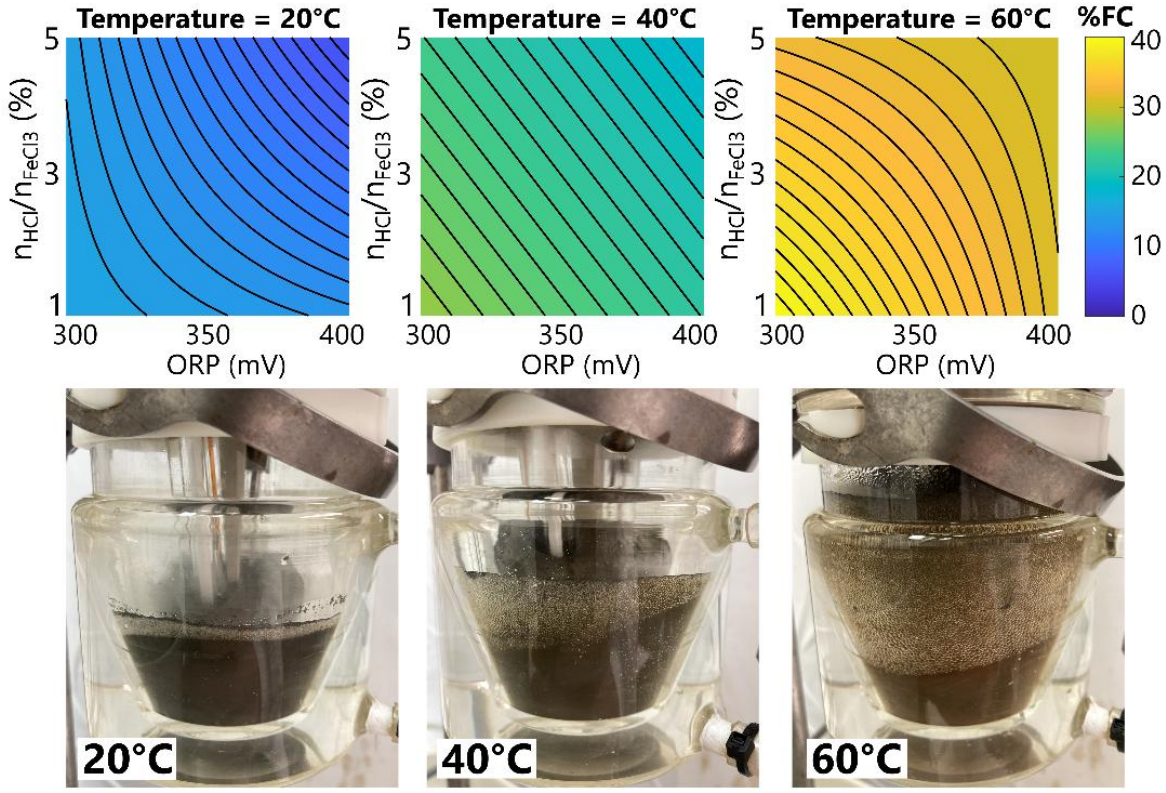

Figure 21: (Top) Response surfaces for the percentage of solids remaining as filter cake (%FC) after leaching of 4 g mixed dry swarf (Table 9) with $FeCl_3$/HCl solutions at fixed redox potentials (ORP) and temperatures of 20, 40, and 60°C. Typical pictures after 15 min of leaching at each temperature are shown below the corresponding response surfaces. The initial liquid was 18 mL of water, and leaching was conducted for 2 h while stirring at 1500 rpm.

20°C, reducing precipitation and allowing easy mixing. Correlations were weaker between %FC and n_{HCl}/n_{FeCl3}, and between %FC and ORP, but higher values generally facilitated dissolution by creating more acidic conditions that stabilised Fe(III). At the optimal conditions of 20°C, 400 mV, and 5% HCl/$FeCl_3$, only 8% solids remained, and $\%E_{s,Fe}$ = 95% with a total Fe atom economy of $\%E_{tot,Fe}$ = 98%. Other metals were also readily dissolved under these conditions, and a purification procedure is presented next to show how most impurities can be removed from $FeCl_2$ solutions via precipitation.

5.5 Leachate purification and concentration

From optimisation of the HCl leaching process, it was clear that Cr was precipitated by hydrolysis and Ni by cementation under the right conditions. Inspired by these findings, a separation process requiring only grinding sludge and no foreign chemicals was developed in paper 2 and further optimised in paper 4.

5.5.1 Hydrolysis precipitation

A first experiment was conducted to study how metal concentrations varied in a leachate when raising the pH stepwise, as shown in Figure 22. Grinding sludge B was initially leached with HCl for 3 h at 60°C, and pH 2.0, with L/S_i = 10 mL/g, before raising the pH by making smaller additions of grinding sludge to consume excess acid. Each pH level was maintained for 30 min, and the experiment was repeated twice to account for experimental variability. The ORP was found to be <-400 mV in concentrated $FeCl_2$ in the presence of swarf, at which Fe^{2+} is stable under acidic conditions according to the Eh-pH diagram in Appendix Figure A5. Practically no Fe^{3+} was therefore present, and if formed, it was assumed to have been reduced to Fe^{2+} by metallic Fe or precipitated as FeO(OH) instantaneously.

No major changes in [M] were observed between pH 2.0 and 3.5, but between pH 3.5 and 4.5, Al, Cr, and Mo began to hydrolyse and precipitate from solution. This was in good agreement with HSAB theory and only Mn^{2+}, which is also classified as a hard acid according to Table 3, did not get removed. The Eh-pH diagram in Appendix Figure A6 confirms that solid $Mn(OH)_2$ is not expected until pH >9.5.

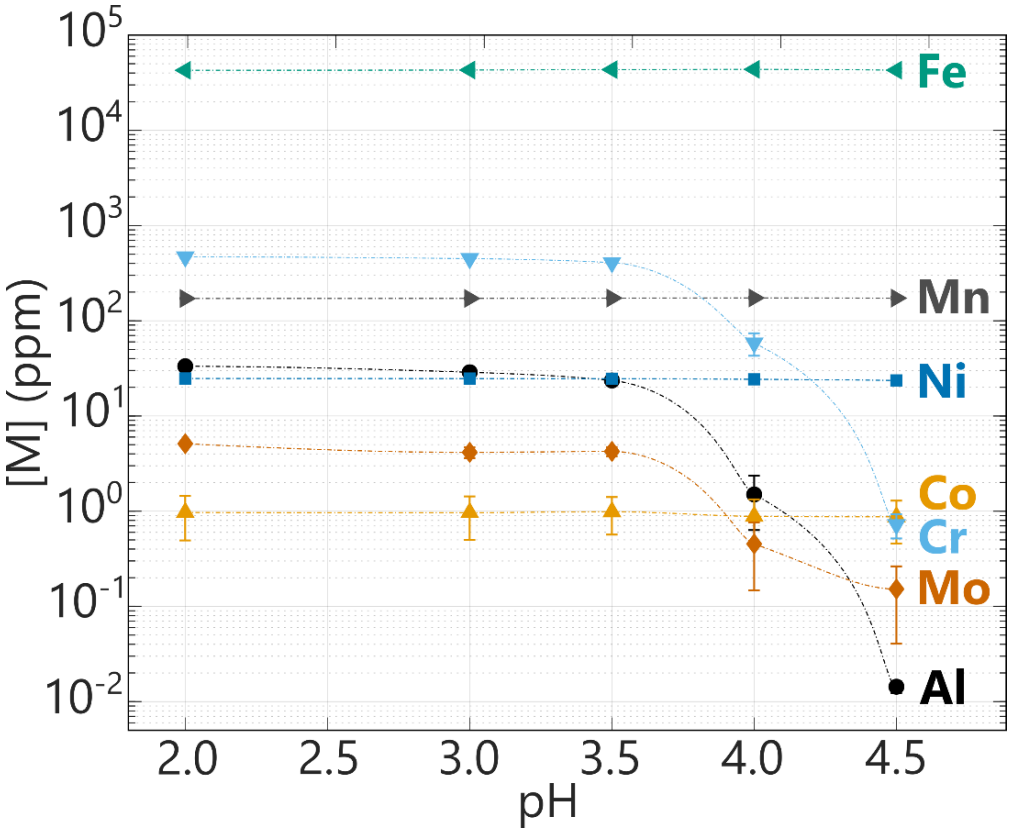

Figure 22: Metal concentrations in a solution after leaching of 30 g unwashed grinding sludge B (Table 8) at pH 2, with an initial 300 mL of water and dosing of 12 M HCl. The pH was then increased with 1 g grinding sludge additions, and maintained at 2.0, 3.0, 3.5, 4.0, and 4.5 for 30 min each. Temperatures of 60°C and stirring at 400 rpm were maintained throughout the triplicate experiments.

Importantly, Fe, as well as Mn, Ni, and Co, remained unaffected by the procedure, which allows selective separation. Desired pH intervals for hydrolysis precipitation were studied in more detail in paper 4 after potentiostatic leaching of mixed, washed sludge with $FeCl_3$. These results can be found in Appendix Figure A11, and verified the observations made in Figure 22, showing that precipitation of Al, Cr, Mo, and V (also Si) occurred more specifically at an optimum pH ≥3.7 at 60-80°C.

5.5.2 Leachate concentration by recirculation

One requirement for using $FeCl_3$ as a water treatment coagulant (standard EN 888:2023) is that it must be highly pure. Strict requirements on product concentration have recently been removed in an amendment to EN 888, but most commercial solutions are 40 wt% (193 g Fe(III)/L; see Table A2 for $FeCl_3$ solution properties) to reduce transport costs and prevent freezing in cold climates. Potentiostatic leaching with HCl, starting with 2 mL/g of grinding sludge in water, typically yielded a maximum concentration of only 160 g Fe(II)/L (see Table A1 for $FeCl_2$ solution properties). A method for concentrating the solution by partial recirculation of the $FeCl_2$ product was therefore investigated in paper 2. Grinding sludge B was subjected to consecutive HCl leaching at 60°C, pH 2.0, and L/S_i = 5 mL/g for 3 h, and precipitation with the same temperature, pH 4.0, with 5% additional sludge for 1 h. The purified $FeCl_2$ was filtered and partially reused as the initial liquid in another identical leaching and precipitation experiment. This is best described by the flowsheet in Figure 23, where [M] at the end of each cycle (R0, R1 and R2) are also shown.

Recirculation proved to be effective for concentrating Fe, and 249 g/L was reached after leaching in R2. However, it was discovered that the neutralisation was much slower at this concentration. The pH stagnated around 3.8, and reaching pH 4.0 was impossible even with the addition of bases such as NaOH or Na_2CO_3. This was suspected to be caused by hydrolysis of Fe(II), which increases with the activity of Fe^{2+}, and releases H^+ according to Equation 51. The resulting product was assumed to be soluble $FeOH^+$, since $Fe(OH)_2^0$ is less easily formed based on small β values in Table 1, and likely to precipitate, and no Fe losses were observed. Regardless, it was clear that chemical equilibria hindered the precipitation of Al, Cr, etc. After the R2 leachate was diluted to 210 g/L, pH 4.0 was easily reached. An upper limit of 220 g Fe/L for Cr(III) precipitation has previously been suggested in a patent describing a similar system [118].

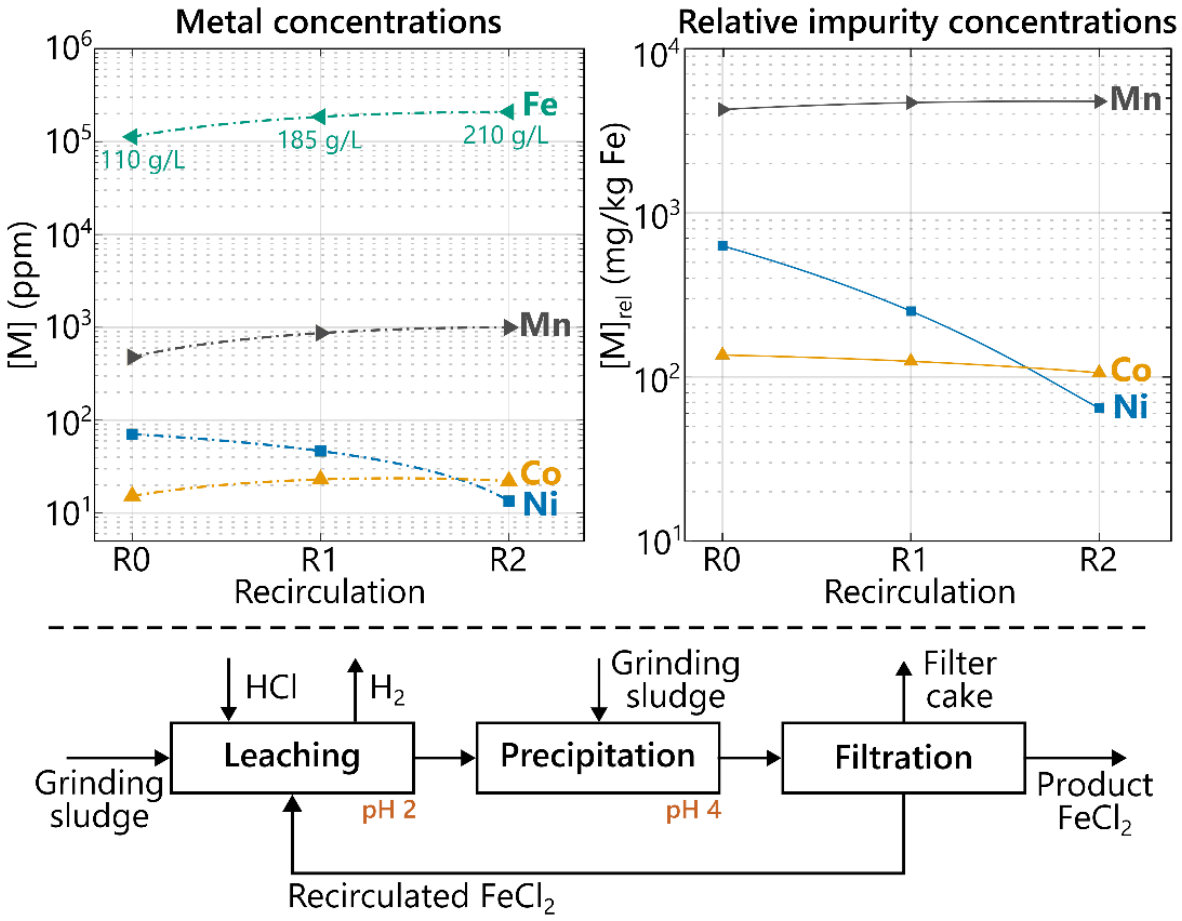

Figure 23: (Top left) Metal concentrations in a recirculated $FeCl_2$ solution after three HCl leaching and precipitation cycles, and (top right) relative impurity concentrations in the same solutions. (Bottom) A flowsheet is shown to describe the procedure. Leaching parameters: 60°C, pH 2, 3 h, 12 M HCl dosing, initial 60 g sludge per 300 mL liquid. Precipitation parameters: 60°C, pH 4, 1 h, 5 g sludge.

5.5.3 Cementation kinetics and optimisation

Concentrations of metals which were not separable by hydrolysis are also shown in the plots in Figure 23. As expected, Mn increased with Fe and was unaffected by the precipitation step, whereas the behaviours of Ni and Co were more interesting as their concentrations relative to Fe decreased from R0 to R1 and R2. Cementation of Co, Cu, and Ni was expected based on a comparison of E°, but it was concluded that this reaction became faster as $FeCl_2$ increased. Kinetically, the rate-limiting step in cementation is often reported to be the diffusion of the depositing metal to the surface, but can also be described as a mixed control process depending on surface availability, the type of sacrificial metal, and the supporting electrolyte [82, 84].

Generally, high temperatures and low L/S promote cementation, and the presence of anions such as Cl^-, SO_4^{2-}, and NO_3^- can be favourable [83, 119, 120]. The role of these ions is not well understood, but the best results are typically achieved with

Cl^-. This has been explained by its ability to dissolve passivating oxides and the formation of fast-growing porous dendrites in Cl media [121]. On a molecular level, Cl^- has also been hypothesised to reduce transport resistance for cations in the boundary layer by adsorbing to the metal surface, and by forming more readily reduced complexes such as $NiCl^+$ [122, 123]. Another theory proposed by Winand was that the Ni activity increases with [Cl], which in turn affects E for the Ni^{2+}/Ni reduction via Equation 72 [121].

$$E = E° - \frac{RT}{nF} ln\left(\frac{1}{a_{Ni^{2+}}}\right) \quad (72)$$

An increase in activity shifts E towards more positive values, thereby increasing E_{cell} for the Fe-Ni redox couple and increasing the driving force for the reaction. Their studies showed that $E_{Ni2+/Ni}$ increased to -0.058 V (from E° = -0.26 V) in a 4 M NaCl + 0.5 M HCl system, whereas $E_{Fe2+/Fe}$ shifted to -0.46 V (from E° = -0.44 V).

The temperature (x_1) and precipitant quantity (PQ; x_2) for optimal cementation and hydrolysis were further studied with a DOE including three centre points in paper 4. Prior to each precipitation experiment, 10 g of mixed, washed grinding swarf in Table 9 was mixed with 30 mL DI water and leached at 20°C with 40 wt% $FeCl_3$ at a fixed ORP of 350 mV for 1 h, yielding ~205 g Fe/L solution. The temperature was then increased to the target specified by the DOE before adding the precipitant (e.g., PQ at 5% corresponds to 0.5 g swarf). The system was left to react with aqueous-phase sampling at 15, 30, 60, and 100 min, and a model for $\%R_{100,Ni}$ with R^2_{adj} = 0.62 and σ = ±6.6% is given in Equation 73.

$$\%R_{Ni} = 21.0 + 10.7x_1 + \varepsilon \quad (73)$$

Another model was created for %FC and is shown in Equation 74, with R^2_{adj} = 0.88 and σ = ±0.7%.

$$\%FC = 22.4 + 2.3x_2 + \varepsilon \quad (74)$$

Both models are valid between 40-80°C and PQ = 2.5-7.5%. Only x_1 was significant in Equation 73, and $\%R_{100,Ni}$ is plotted versus temperature in Figure 24 on the left-hand side, while Equation 74 was independent of x_2 and is plotted versus PQ. On the right-hand side of Figure 24, $\%R_{t,Ni}$ at each sampling time is shown, as well as the increase in pH during the experiments. The red dashed line indicates the pH 3.7 threshold, which was crucial for hydrolysis precipitation.

The uncertainty in $\%R_{100,Ni}$ was relatively high, but the first response plot in Figure 24 indicates that cementation was favoured at high temperatures. Slightly higher

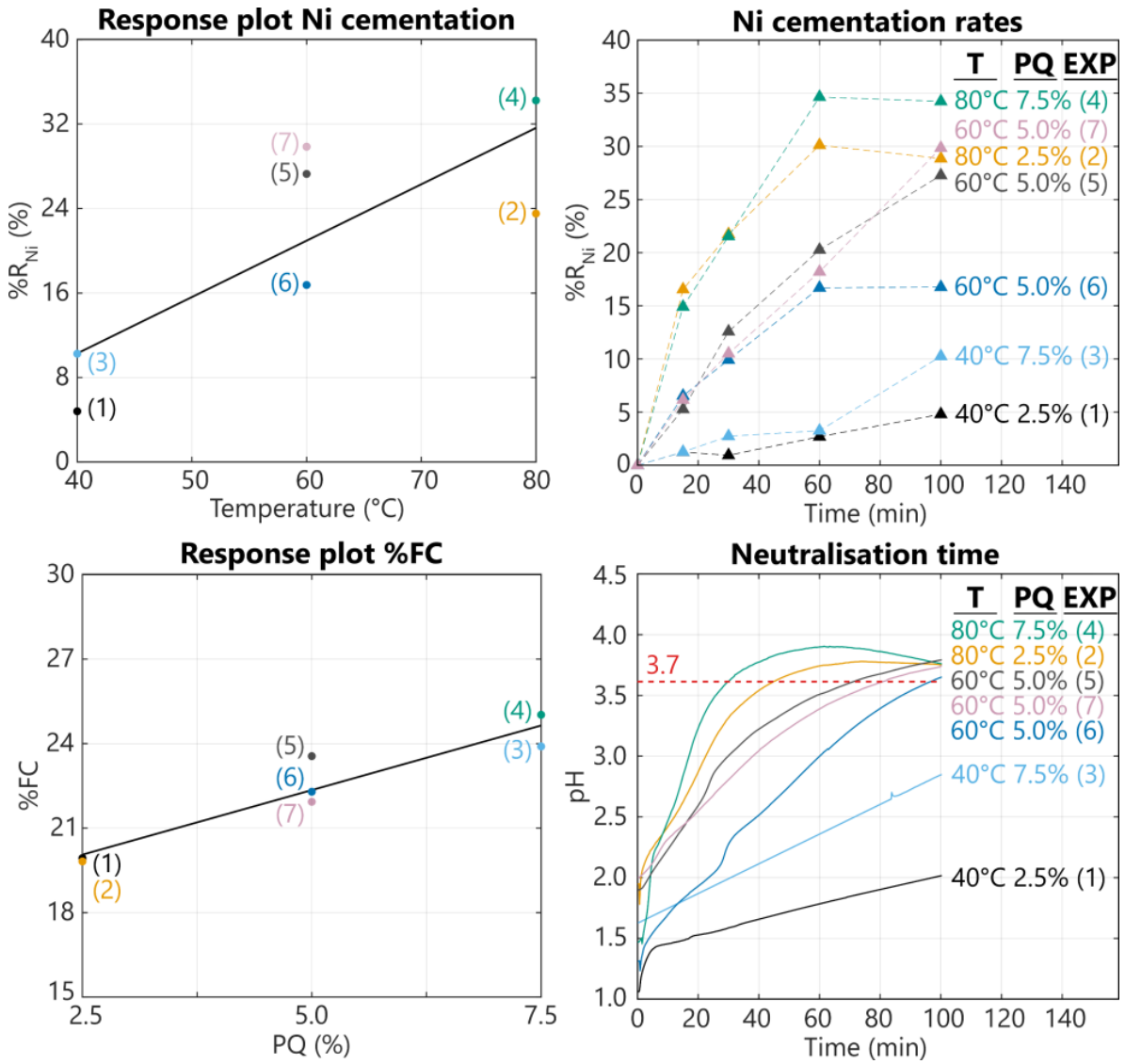

Figure 24: (Top left) Response plot with experimental data points for the removal of Ni (%R_{Ni}) from a leachate versus temperature after 100 min precipitation time, (top right) with corresponding experimental conditions and observed precipitation rates. (Bottom left) Response plot for the percentage of input grinding sludge remaining as filter cake (%FC) versus the amount of precipitant added relative to the original amount of swarf leached (PQ). (Bottom right) Measured pH during the tests are presented with a red dotted line indicating the critical pH 3.7 necessary for hydrolysis precipitation.

values were also observed with higher PQ, although the effect was not statistically significant. Neutralisation of HCl was also faster at 80°C, with pH 3.7 reached after 30 min with PQ = 7.5% and after 50 min with PQ = 2.5%. Higher PQ, therefore, seems optimal; although, the filter cake mass also increases in proportion to the added precipitant, creating a trade-off. Regardless, between 30-35% Ni could be precipitated, down to $[Ni]_{rel}$ = 170 mg/kg Fe, under optimal conditions, as well as >95% Cu, down to $[Cu]_{rel}$ = 4 mg/kg Fe. No effect was observed on Co, which remained in the leachate with Fe and Mn. The purity of this solution is discussed further in Section 5.5.5.

In conclusion, grinding sludge was found to be an excellent precipitation agent for purifying $FeCl_2$ solutions. The large surface area of the swarf not only provides ample space for cementation but also facilitates the neutralisation of excess H^+ and Fe^{3+}, and the stabilisation of Fe(II), preventing it from oxidising and precipitating as FeO(OH) as pH increases.

5.5.4 Filtration of purified $FeCl_2$ solutions

Solid-liquid separation is another crucial aspect of the precipitation process and greatly affects the final $FeCl_2$ yield. This was achieved exclusively by frontal filtration under vacuum in Büchner funnels throughout the work. Filtration rates for highly acidic solutions after leaching were relatively fast but slowed after precipitation. Hydroxide particles can exhibit poor filterability, and a previous study on the filtration of FeO(OH) particles precipitated from a $FeCl_3$ solution showed that pH and electrostatic forces between particles strongly influenced the process [89]. The electrostatic repulsion was shown to be minimised by increasing the electrolyte concentration, as in the coagulation of emulsified cutting oils. The optimal pH for FeO(OH) filtration, on the other hand, was ~7, with processing times increasing rapidly under more acidic conditions. Since the optimal pH for the purification process developed in papers 2 and 4 was 3.7, other strategies may be needed to achieve acceptable filtration rates. This may include adding a filtration aid, such as a polymer, to the solution to promote particle aggregation.

Adsorbed cutting fluids in the filter cake were also found to have a highly detrimental effect on filtration. Non-polar oils can be assumed to make the cake hydrophobic and more difficult for water solutions to pass through. This was discovered during experiments in a 5 L reactor, where filtration of purified leaching slurry with [Fe] = 200 g/L at pH 4.0 from unwashed grinding sludge required 3 h, whereas that from washed sludge with the same [Fe] and pH required only 30 min. Pictures from these tests are shown in the Appendix Figure A14 and corroborate the importance of washing the grinding sludge prior to leaching.

On an industrial scale, solid-liquid separation is preferably performed using filter presses, belt filters, centrifuges, or similar. This equipment should enable efficient filter cake washing, as significant amounts of highly concentrated $FeCl_2$ can remain in the solids. The dry matter in wet filter cakes from washed sludges was around 20 wt%. Product loss to the filter cake may otherwise reduce recycling rates and increase secondary waste. Washing can be performed with water or dilute acid to

stabilise Fe without redissolving precipitated impurities, after which the wash liquid is recirculated to the leaching step to recover additional product.

5.5.5 Analysis of $FeCl_2$ intermediate products and filter cakes

Filtered $FeCl_2$ intermediates were generally clear, blueish-green, but after several weeks in a sealed container, they took on a more brownish colour, typical of $FeCl_3$, due to air oxidation. The solutions were usually acidified to pH <1 with HCl to stabilise Fe^{3+}, as the reaction (Equation 26) continued to consume H^+. A faint, fishy oil-like smell was noted in most recycled $FeCl_2$, regardless of whether the grinding sludges were washed, suggesting that some cutting fluid components remained despite the coagulation and adsorption mechanisms observed during hydrometallurgical processing.

Relative metal concentrations in grinding sludges and leachates before and after precipitation in experiment R2 (Figure 23) and DOE experiment (4) (Figure 24) are presented in Table 11. Leachate impurities after precipitation were compared with the coagulant standard EN 888:2023 and found to be within the limits of Grade 2. In both cases, Cr was the most important element to remove, and it could be reduced well below 350 mg/kg Fe, with $\%R_{Cr}$ >95%. The table confirmed that the process was generally also capable of separating Al, Cu, Mo, Ni, Si, and V from Fe to varying extents. Only Co, Mn, and Zn could not be removed, but may be controlled by mixing the grinding sludge input at suitable ratios. It should be noted that the standards in Table 11 are for $FeCl_3$, whereas the leachates were >99% $FeCl_2$. Impurities were, however, found to be unaffected by the following oxidation processes and can be assumed to be identical in the final product.

Analysis of the filter cake was important for completing the overall process mass balance and determining the recyclability of this byproduct. Several XRD patterns were already shown for residues from $FeCl_3$ leaching in Figure 20, but more representative diffractograms from R0 and R2 after precipitation are shown in Figure 25. As expected, the chemically resistant Al_2O_3 abrasives were mostly intact. The ferrite and austenite phases observed in the grinding sludge in Figure 11 were completely dissolved, but a metallic high-carbon cementite phase remained, appearing more resistant to HCl. Similar to $FeCl_3$ leaching, part of the Fe was lost to FeO(OH); although, the hydroxide phase was mostly lepidocrocite (γ-FeO(OH)) instead of akaganeite (β-FeO(OH)). Lepidocrocite has been shown to form exclusively in concentrated $FeCl_2$, while akaganeite is typically formed at low

Table 11: Relative metal concentrations in grinding sludges and leachates before and after purification compared with EN 888:2023 standards. Limits for As, Cd, Hg, Pb, and Sb are also specified in the standard, but were not detected in the grinding sludges and were therefore irrelevant (NA = not available).

Experiment R2						
Element	Composition (mg/kg Fe(II))			EN 888:2023 (mg/kg Fe(III))		
	Sludge B	Leachate R2	Purified leachate	Grade 1	Grade 2	Grade 3
Cr	14400	1440	25	50	350	500
Mn	4720	4230	4770	5000	10000	20000
Si	4340	210	90	NA	NA	NA
Mo	1150	107	17	NA	NA	NA
Ni	1280	140	65	60	350	500
Cu	1280	18	20	NA	NA	NA
Al	510	45	<1	NA	NA	NA
Co	130	107	105	NA	NA	NA
Fe content (wt%)						
Fe	78.4	17.2	15.2	13.8	13.8	13.8

Purification DOE experiment (4)						
Element	Composition (mg/kg Fe(II))			EN 888:2023 (mg/kg Fe(III))		
	Washed F+H+K	Leachate	Purified leachate	Grade 1	Grade 2	Grade 3
Cr	17800	3630	150	50	350	500
Mn	6630	2760	2950	5000	10000	20000
Si	1450	1150	100	NA	NA	NA
Mo	1790	200	10	NA	NA	NA
Ni	1360	260	170	60	350	500
Cu	770	73	4	NA	NA	NA
Al	290	650	29	NA	NA	NA
V	380	170	1	NA	NA	NA
Zn	250	64	70	NA	NA	NA
Co	105	39	39	NA	NA	NA
Fe content (wt%)						
Fe	90.6	14.9	14.9	13.8	13.8	13.8

$[Fe^{2+}]$, $[Cl^-]$, and $[OH^-]$ [116]. A possible explanation for the observed difference is therefore that FeO(OH) was formed during leaching with $FeCl_3$, whereas with HCl, it was formed by oxidation of residual $FeCl_2$ in the filter cake after washing. This argument is supported by the presence of $FeCl_3$ peaks in the R2 diffractogram.

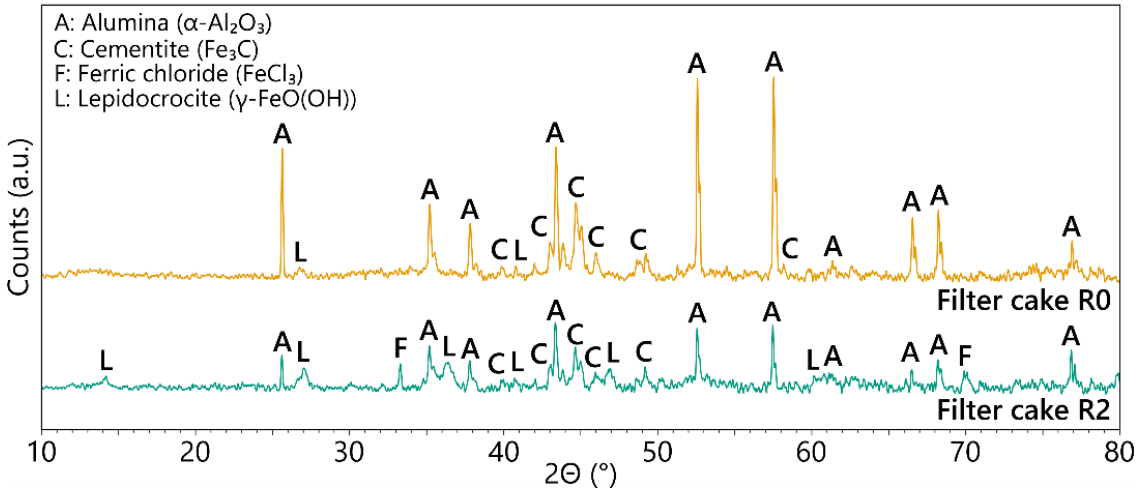

Figure 25: XRD analysis of filter cakes from experiments R0 and R2 (see Figure 23) based on grinding sludge B (Figure 11). Few peaks for metallic Fe were detected after leaching and precipitation, and mainly alumina abrasives, FeO(OH), and traces of iron chloride were detected.

Either way, the FeO(OH) phase may be relevant due to known Cl inclusions in akaganeite, which could complicate the filter cake recycling. A further observation from Figure 25 was that no Cr related peaks were identified, indicating that these were under the LOD for XRD, but more likely that this metal precipitated as amorphous $Cr(OH)_3$ [124].

With more knowledge about the different phases likely to be present, XRF analysis of filter cakes from R0, R1, R2, and from processing of washed swarf in a 5 L demonstration experiment (Demo; Appendix Figure A14) was performed and is presented in Table 12. A majority of the material was FeO(OH) in each case, and the Fe content increased with increasing [$FeCl_2$] in the leachate. A similar trend was observed for Cl, indicating that residual iron chloride was less efficiently washed out of the cake in R2, as confirmed by an $FeCl_3$ peak in Figure 25. A possibility that the hydroxide phase had Cl inclusions could not be ruled out, however, as these have been proposed in similar green rust containing mixed Fe(II) and Fe(III) hydroxides [125].

For unwashed grinding sludges in R0, R1 and R2, %FC was typically ~50%, and considering an approximate Fe content of 30 wt% in the R2 filter cake, the overall Fe recycling rate was 85%. This corresponds well to %E observed in the leaching of unwashed sludge B in Figure 16. Grinding sludge washing can substantially reduce these Fe losses, given that %FC was lower with pretreated swarf. Taking the 31.22 wt% FeO(OH) (~20 wt% Fe) from Demo in Table 12 where %FC was 20%, the overall Fe recovery rate was estimated to ≥95%, which was again in good agreement with $\%E_{s,Fe}$ observed in potentiostatic leaching with $FeCl_3$ in Section 5.4.2.

Table 12: XRF analysis of filter cakes from processing of unwashed grinding sludges in R0, R1, and R2, and washed grinding sludge processed in a scale-up demonstration trial (Demo; Appendix Figure A14). Standard deviations reported for R0, R1, and R2 are based on repeat measurements of the same samples, while Demo was measured only once.

Compound	R0 (wt%)	R1 (wt%)	R2 (wt%)	Demo (wt%)
FeO(OH)	40.45 ± 0.30	46.98 ± 0.30	57.93 ± 0.30	31.22
$Cr(OH)_3$	9.23 ± 0.10	5.08 ± 0.01	7.11 ± 0.09	5.22
Al_2O_3	8.38 ± 0.10	2.22 ± 0.05	4.63 ± 0.07	5.35
SiO_2	2.57 ± 0.05	1.12 ± 0.04	1.90 ± 0.04	12.38
MoO_3	1.68 ± 0.04	1.19 ± 0.04	1.25 ± 0.04	0.78
Cl	1.59 ± 0.04	1.99 ± 0.05	2.62 ± 0.05	2.34
Cu	0.53 ± 0.03	0.43 ± 0.03	0.37 ± 0.02	0.48
Ni	0.35 ± 0.03	0.30 ± 0.03	0.36 ± 0.02	0.73
MnO	0.28 ± 0.02	0.24 ± 0.02	0.37 ± 0.02	0.46
TC	11.57 ± 0.12	8.60 ± 0.24	8.31 ± 0.18	n/a
C	2.00	2.00	2.00	n/a
Org. ($C_{15}H_{32}ON$)	12.10	9.50	8.00	n/a
Other	20.84	28.94	13.47	41.04

In terms of secondary waste management, a main priority should be to minimise Fe losses in the hydrometallurgical process, in accordance with the waste hierarchy (Figure 1), as well as the washing, dewatering, and drying of the filter cake. This reduces the material's final mass and further concentrates the valuable alloying elements, thereby increasing its potential recyclability. When dried, the cake turned into a fine dust, and the most promising alternative identified for recycling was therefore to process it along with other similar steelmaking dusts. Several commercial technologies are available for smelting ferrous oxide dusts and sludges [126]. In these processes, Fe and alloying elements may be recovered as new steel, while abrasive materials would form slag, and organic carbon would be combusted, providing energy and a potential reduction source to the melt. The contents of Cl and Al_2O_3 have to be reduced sufficiently, however, as these can corrode equipment and damage acidicly lined furnaces [38]. If recycling is not possible, the waste needs to be properly disposed of. Given the high organic content in Table 12, filter cakes from unwashed sludge may not be eligible for direct landfilling and require incineration [44]. In addition to mineral oils, the numerous alloying elements, including Ni and Cr, may also warrant classifying the filter cake as hazardous waste under Directive 2008/98/EC (EWC 11 01 09). This could make the disposal both difficult and expensive.

5.6 Oxidation of $FeCl_2$ intermediate products

Two oxidation methods were tested to verify that the $FeCl_2$ was suitable for producing $FeCl_3$ solutions. Pressure oxidation in a setup similar to industrial equipment was done in collaboration with an industrial partner as part of the demonstration project presented in the Appendix Figure A12-Figure A14. Electrolysis was studied later in paper 4, inspired by the work of Marconi et al. [96].

5.6.1 Pressure oxidation

Two $FeCl_2$ solutions were oxidised with O_2: one based on unwashed grinding sludge B, and the other on a 1:1 mix of sludges B and J, washed with detergents. Both were leached with HCl and purified by precipitation. A summary of the $FeCl_2$ intermediates and final $FeCl_3$ products is shown in Table 13. Oxidation generally took 2-3 h, and the final $FeCl_3$ solutions both had satisfactory residual Fe(II) and HCl concentrations (<2.5% Fe(II)/Fe(III) and 0-1 wt% HCl) conforming to EN 888:2023. No Fe precipitation was observed either during the process or after several months of storage, suggesting that the product was relatively stable. The total [Fe] was, however, <13.8 wt%, typical of commercial $FeCl_3$, as the solutions were significantly diluted by the added HCl and reaction water (Equation 26). Higher concentrations could be reached by starting with a more concentrated $FeCl_2$ solution, but, as mentioned in Section 5.5.2, the system is constrained to ~220 g Fe/L (15.6 wt% Fe(II)) to allow hydrolysis precipitation. This is insufficient to reach 40 wt% $FeCl_3$ based on calculations with data in Appendix Table A1 and Table A2. Partial water evaporation or mixing the recycled product with solutions containing >40 wt% $FeCl_3$ may therefore be required.

Table 13: Concentrations of Fe, Fe(II), total organic carbon (TOC), and total nitrogen (TN) in two $FeCl_2$ solutions before and after O_2 oxidation with 34 wt% HCl.

Parameter	Unwashed B	Washed B+J (1:1)
Purified $FeCl_2$ intermediate		
Total Fe (wt%)	14.4	13.5
Fe(II) (wt%)	14.4	13.5
TOC (mg/L)	550	330
TN (mg/L)	100	<50
Final $FeCl_3$ product		
Total Fe (wt%)	11.3	10.5
Fe(II) (wt%)	0.15	0.24
HCl (wt%)	<1	<1
TOC (mg/L)	480	300
TN (mg/L)	84	<50

Relative metal impurity concentrations in both solutions were similar to those presented for R2 in Table 11 and were unaffected by the oxidation process. Both TOC and total nitrogen (TN) were also measured before and after oxidation, indicating that the process had a negligible effect on the residual organic fraction. The values shown in Table 13 are lower for iron chloride from washed sludges, where TOC can be assumed to originate from residual detergents. Stronger oxidants, such as H_2O_2 or O_3, may break down these substances and could, if necessary, be added after O_2 oxidation [32]. While EN 888:2023 is not clear regarding TOC and TN, it states that the contents of organic pollutants, such as cyanides, pesticides, and polycyclic aromatic hydrocarbons, are irrelevant, since the raw materials used for $FeCl_3$ production are free of them. To be on the safe side, grinding sludge should therefore be washed to ensure that any such substances are removed in compliance with the directive.

5.6.2 Electrolysis in a membrane cell

A possible solution to the dilution problem encountered during pressure oxidation was to perform oxidation in an electrolytic cell, where $FeCl_2$ is separated from, rather than mixed with, HCl via an AEM [96]. This method was proposed by Marconi et al., who studied oxidation of $FeCl_2$ pickling liquors from steelmaking in a flow cell. The setup used as a proof of concept in this work, shown in Figure 10, was simpler and did not have any circulating anolyte or catholyte. Its electrochemical properties and possible reactions were initially studied with CV and EIS.

Voltammograms for $FeCl_2$ based on mixed, washed swarf in Table 9, using the GCD WE are shown in Figure 26a. Peaks for Fe^{2+}/Fe^{3+} were observed at around +1.0 V vs Ag/AgCl in anodic sweeps and +0.1 V in cathodic sweeps. At anodic potentials >+1.5 V, undesired O_2 or Cl_2 gas evolution began, whilst in the cathodic direction, H_2 formation and nucleation of magnetic Fe particles were observed at <-0.8 V. Narrower sweeps of the area of interest are shown in Figure 26b with dashed lines representing simulated voltammograms for the 3.5 M $FeCl_2$ system. The peak heights were similar in the anodic and cathodic sweeps, but the peak separation was >59 mV and increased with the sweep rate. This indicates either quasi-reversible charge-transfer kinetics in the redox reaction or significant solution resistance. Comparing modelled voltammograms with fast and slow kinetics (high or low k_s), and low and high solution resistances (R_{sol}) in Figure 26b showed that high resistance (R_{sol} = 27.7 Ω based on EIS) and low k_s gave the best fits. This was

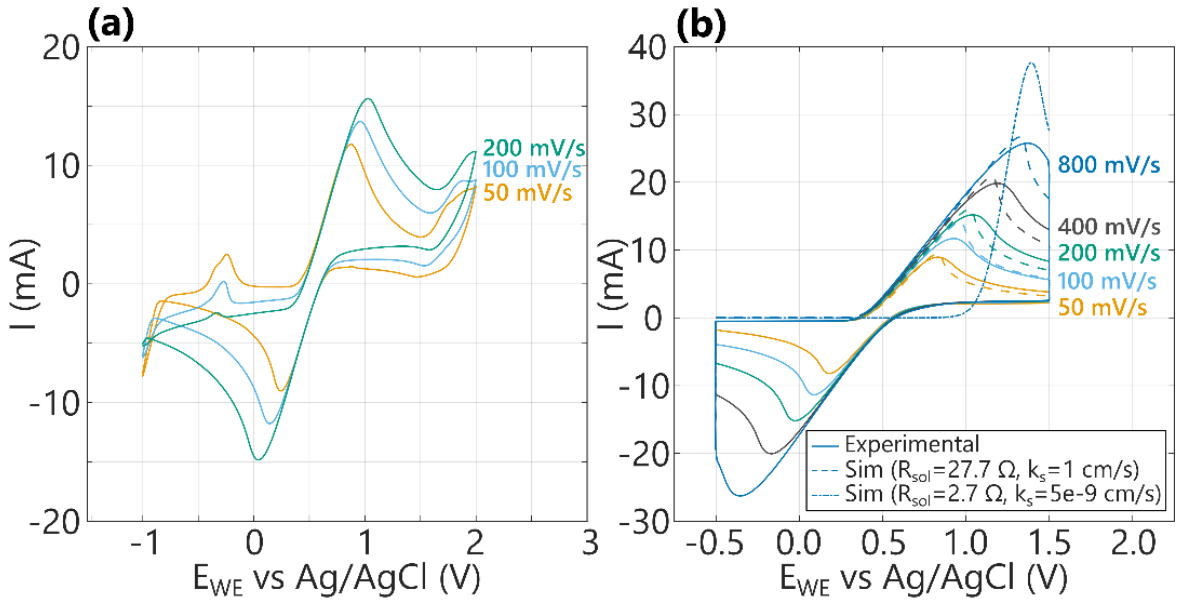

Figure 26: Voltammetry with a glassy carbon disc working electrode in a $FeCl_2$ (200 g Fe/L) solution, separated by an anion exchange membrane from a Pt counter electrode in 4 M HCl. Sweep ranging from (a) -1.0 to +2.0 V and (b) -0.5 to +1.5 V with a 30 s waiting time between anodic and cathodic sweeps. Dashed/dotted lines represent simulated voltammograms with combinations of high and low solution resistances (27.7 and 2.7 Ω) and high and low electron transfer rates (1 and $5 \cdot 10^{-9}$ cm/s).

unexpected, given the high ionic strength (>10 M) of the electrolyte, but may be explained by partial complexation of Fe^{2+} with Cl^-, which can reduce the number of charge carriers present. The distance between the WE and RE was also relatively large (1 cm) due to constraints in the cell, thereby amplifying the resistance effect.

In further electrolysis experiments, the GCD WE used in CV was replaced with a larger GCR anode, which was more sensitive to gas formation. The anodic potential was therefore set to a maximum of +1.5 V. Both a recycled and a synthetic $FeCl_2$ solution were oxidised to investigate the influence of impurities from grinding sludges on the process. Measured currents during electrolysis are shown in Figure 27a for both solutions, and corresponding measured E_{cell} and R_{cell} determined by Ohm's law for the recycled solution in Figure 27b. Irregularities can be seen in the graphs, caused by temporary breaks in the experiment for sampling. Constant bubbling was observed in the catholyte, while the anolyte slowly changed from transparent blue to green, yellow-brown, opaque dark brown, and then once again became transparent with a lighter brown colour.

The reaction times were 48 h and 88 h for complete oxidation of the synthetic and recycled solutions, respectively, and were relatively long compared to Marconi's 3 h. One reason was likely a difference in E_{cell}, which was set to 8 V in the setup used by Marconi, whereas a value around 4 V was maintained in the H-cell. Another possible rate-limiting factor in the cell was transport of Cl^- through the AEM, which

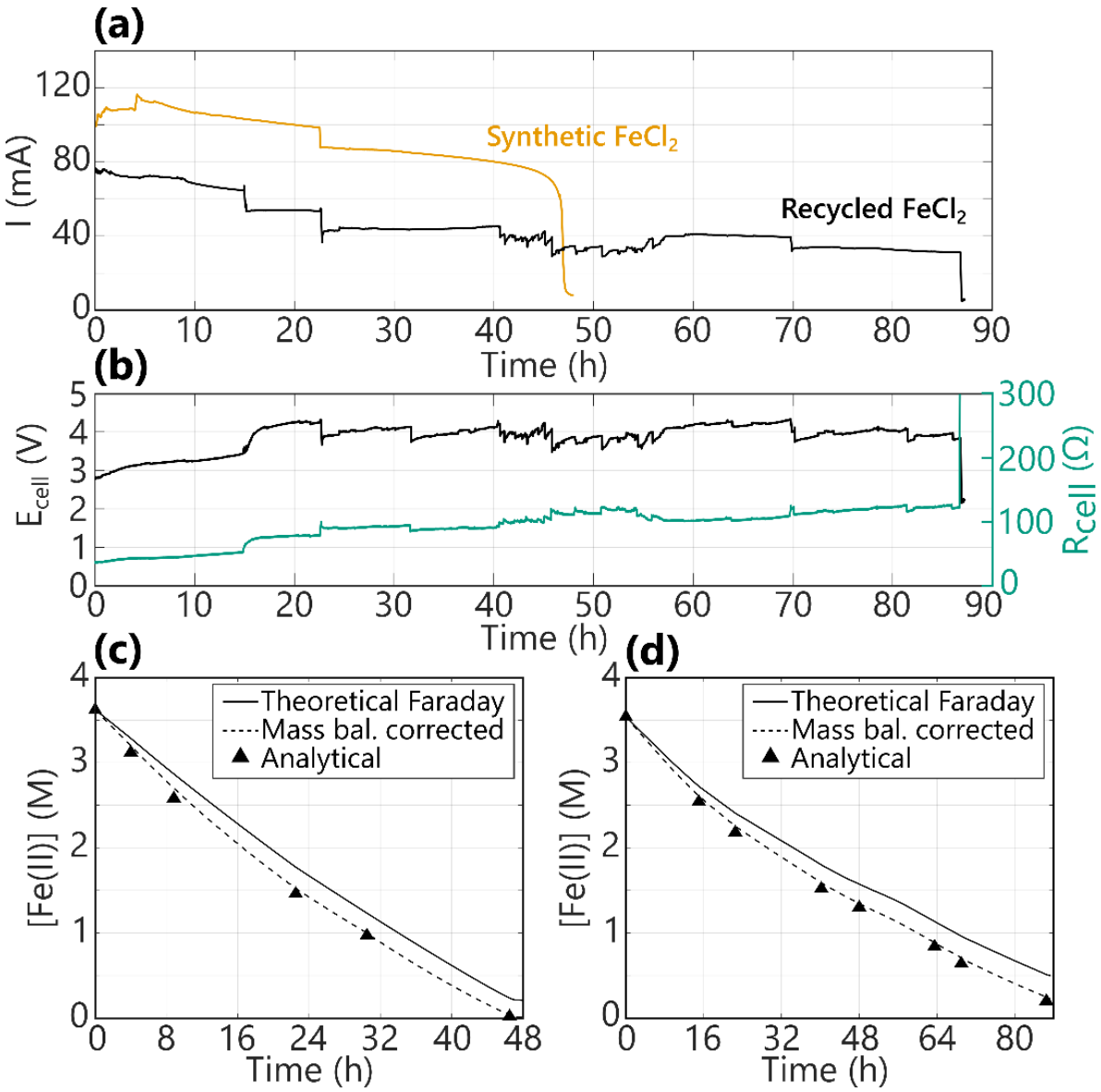

Figure 27: (a) Measured current (I) versus time in electrolysis of recycled and synthetic $FeCl_2$ (200 g Fe/L) at 1.5 V anodic potential, with (b) corresponding cell potential (E_{cell}) and resistance (R_{cell}) for the recycled solution. Analytical and modelled [Fe(II)] (Equations 62 and 75) over time are shown for (c) synthetic and (d) recycled solutions. Initial volumes of the anolyte and catholyte (4 M HCl) were 48 mL.

had a relatively small area compared to the electrodes. However, further testing with other electrodes and membrane sizes is needed to verify this claim. While E_{cell} remained more or less constant in Figure 27b, R_{cell} slowly increased from around 50 Ω to 120 Ω after 88 h. A similar doubling of R_{sol} was also observed between $FeCl_2$ and $FeCl_3$ in EIS results presented in paper 4. A possible explanation is given by a stronger tendency of Fe^{3+} to complex with Cl^-, as seen from β-values in Table 1. This could have reduced the number of charge carriers upon the conversion of Fe^{2+} to Fe^{3+}. Another reason for the R_{cell} increase in Figure 27b was that H^+ and Cl^- decreased in the catholyte as the reaction progressed.

Comparing the electrolysis of recycled and synthetic solutions showed that the former took almost twice as long, suggesting that impurities from the grinding sludge affected the process. Further evidence for this was found when the GCR was washed with acetone after electrolysis of the recycled solution, where a white salt was released from the electrode surface. This was not observed with the synthetic solution, indicating that some impurities had adsorbed onto the electrode during electrolysis. A qualitative FTIR inspection of the salt is shown in Figure 28. The main peaks were located in the single-bond region at 2800-3000 cm^{-1}, with a single peak in the double-bond region at around 1700 cm^{-1}, most likely stemming from acetone from GCR rinsing. Besides noise and smaller peaks in the fingerprint region, many similarities were observed with the cutting fluid oil. The salt was therefore concluded to be a mixture of saturated hydrocarbons that likely originated from the cutting fluids and adsorbed on the glassy carbon. This adsorption was not necessarily bad, as organic molecules such as surfactants have been shown to improve the electrode properties in several cases [127]. However, organic compounds can also foul and partially block the AEM pores, thereby inhibiting Cl^- transport and slowing the electrolysis process. The AEM was composed of crosslinked aromatic compounds, not unlike the GCR, which could have served as adsorption sites [128]. While this phenomenon was strictly negative in electrolysis, these observations more generally demonstrate that carbon adsorbents can be used to remove organic impurities from iron chloride solutions.

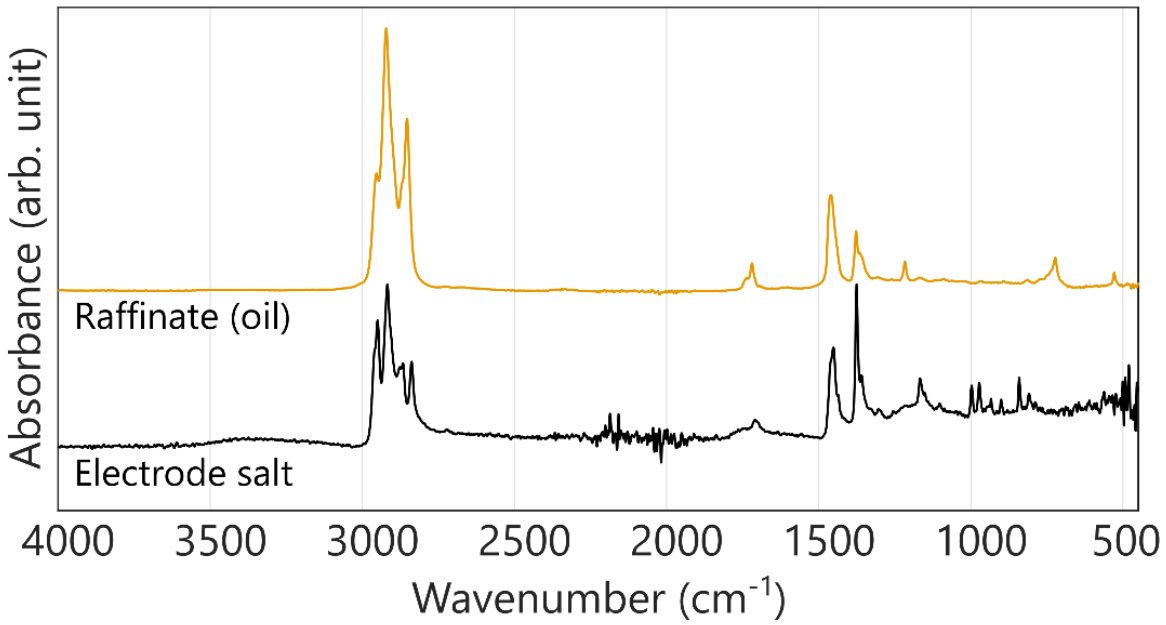

Figure 28: FTIR spectra of white salts recovered from rinsing the reticulated glassy carbon electrode with acetone after electrolysis of $FeCl_2$ solution based on grinding sludges. The spectra of lubricant oil recovered during pretreatment of the grinding sludge is given for comparison.

Returning to Figure 27, η_F are presented in Figure 27c and d, and were determined using Equation 56 and by measuring Fe(II) in the anolytes. Despite the longer electrolysis time, these results were similar to those obtained by Marconi and suggested that η_F >100%. This meant the reaction consumed fewer electrons than predicted theoretically, which was unrealistic. Marconi proposed that Fe(II) was partially oxidised by O_2 during electrolysis; although, as mentioned in the theory (Section 3.4.3), this reaction is negligible at ambient conditions and could not have been responsible for the significant decrease in [Fe(II)] within 3 h.

The system was modelled to explain the high η_F, and two additional experimental observations were relevant in this context: (1) the final catholyte had a slightly yellow colour, indicating unwanted crossover of Fe, and (2) the anolyte/catholyte volume increased/decreased by 20-25% during electrolysis, indicating net water transport. These phenomena are usually observed in similar redox flow battery systems [129], and were accounted for in a new model based on Faraday's law in Equation 75.

$$C_{\mathrm{Fe(II)}}(t) = C_i - \frac{\int_0^t I\,dt}{FV_a(t)} - \frac{\dot{n}_{CO}t}{V_a(t)} \tag{75}$$

Here, C_i and $C_{Fe(II)}$ are [Fe(II)] in the initial solution and after time t, V_a is the time-dependent anolyte volume, and $\dot{n}_{CO}$ is the Fe(II) crossover rate (~2 mg/cm^2/h). The AEM's area-specific water transport rates were estimated from final electrolyte volumes and were 59 and 154 µL/cm^2/h for the recycled and synthetic solutions, respectively. Modelled mass-balance-corrected [Fe(II)] values, derived from Equation 75, are shown in Figure 27 and fit the experimental data well. Sensitivity analysis indicated that anolyte dilution was primarily responsible for the observed decrease in [Fe(II)], and that Fe crossover was negligible.

Water transport through semi-permeable membranes is governed by several effects, including osmosis driven by a [H_2O] gradient across the membrane, electro-osmosis arising from the drag exerted on water by ions moving in an electric field, and cotransportation of hydration water [130, 131]. During Fe(II) oxidation, predominantly Cl^- was transported through the membrane, resulting in a net ion flux from the catholyte to the anolyte and possible electro-osmosis. Moreover, Cl^- can hold up to 6 H_2O molecules in its inner hydration sphere, thereby increasing the likelihood of additional water being drawn into the anolyte [132]. In addition to active transport mechanisms, there was a large, increasing

difference in ionic strength between the anolyte and the catholyte, which could have driven passive water osmosis into the anolyte.

The active water transport mechanisms can be assumed to lead to dilution of $FeCl_3$ regardless of the electrolysis time, as confirmed by the similarities between Marconi's results and those in Figure 27c and d. In total, [Fe] was found to decrease from 204 (14.8 wt%) to 153 (11.9 wt%) g/L with synthetic, and 203 (14.7 wt%) to 159 (12.3 wt%) g/L with recycled $FeCl_2$. These values are only slightly better than those in Table 13 which disproves the initial hypothesis that electrochemical oxidation can be conducted without significant dilution of the $FeCl_3$ product. The situation may be improved with a different membrane, reverse osmosis, or adding a draw solute in the catholyte, but further testing is needed to verify this assumption [130, 131]. To end this section on a more positive note, it should be restated that electrolysis remains a promising method for oxidation because of the possibility to continuously generate H_2. Especially when leaching with $FeCl_3$, where oxidation is needed both to obtain the final product and to regenerate the leaching agent. Another advantage is that any [HCl] between 0.1 and 12 M can be used, incentivising the use of more dilute waste acid solutions [96].

5.7 Recycling process design

After testing each individual unit operation required to produce $FeCl_3$ from grinding sludges, the final objective was to propose a more complete process with mass and energy balances. This was a central objective in paper 4, and a flowsheet developed in this work is shown in Figure 29. It comprises three main interchangeable blocks, where A represents sludge pretreatment, for which the acetone washing with magnetic separation from Section 5.2 was selected. This method synergises with the $FeCl_3$ leaching part of block B, described in Section 5.4, where significant amounts of heat are released by exothermic reactions that could be used in the distillation. The choice of $FeCl_3$ as a leaching agent was also made for safety reasons, given its limited generation of H_2. Leachate purification was assumed to be performed in the same reactor using the precipitation techniques described in Section 5.5, followed by consecutive filtration and filter cake washing, as discussed in Section 5.5.4. The electrolysis method in Section 5.6.2 was selected as the final step in block C due to its synergy with $FeCl_3$ leaching, providing a continuous stream of H_2 at significant volumes. A water mixing point, e.g., a storage tank from which process water can be supplied, was also included in the flowsheet to ensure efficient water use and minimise waste generation.

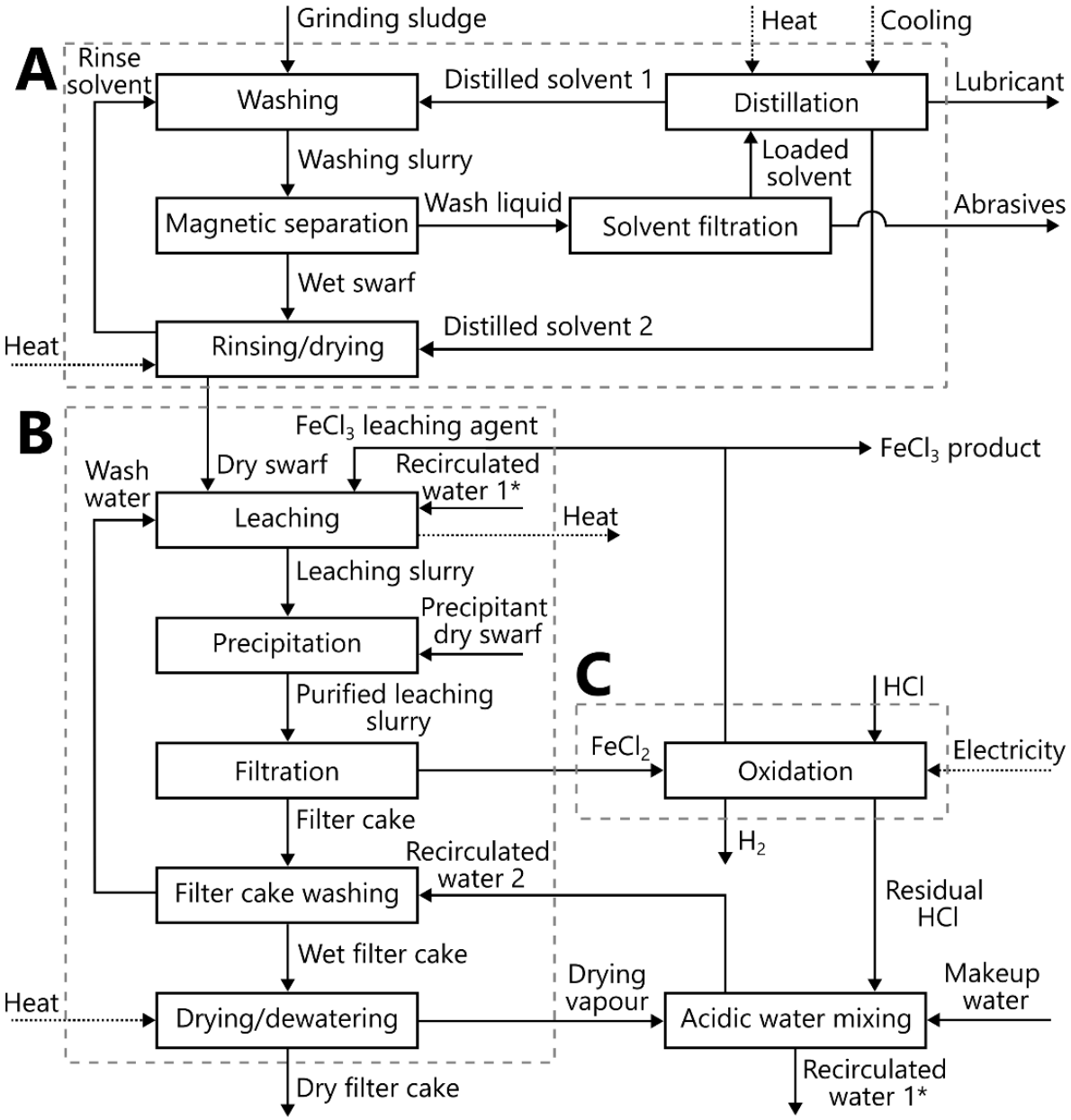

Figure 29: Proposed flowsheet for producing $FeCl_3$ from grinding sludges. The interchangeable blocks represent: (A) pretreatment with recovery of lubricants and abrasives via solvent washing; (B) hydrometallurgical processing, including FeCl3 leaching, precipitation, filtration, and filter cake management; and (C) oxidation of FeCl2 via electrolysis, with coproduction of H_2. A water mixing and distribution point is included for efficient water management in the process.

5.7.1 Mass and energy balances and OPEX calculation

A summary of the recycling process inputs and outputs based on mass and energy balances is given in Table 14. The grinding sludge gate fee was an average of typical disposal costs of 100-500 €/ton encountered in Sweden, Austria, Germany, Poland, Spain, and Italy, as shared in personal interviews with manufacturers in these countries [4]. Values on the higher end of this range can generally be expected if the sludges contain oils and are classified as hazardous waste. No data

Table 14: Input and output streams from mass and energy balances based on the flowsheet in Figure 29. Unit prices for materials and energy have been estimated or obtained from market data and used to calculate revenue from each stream and for the whole process.

Input	Quantity	Unit	Price/unit (€/unit)	Revenue (€)	Reference
Grinding sludge	1.00	ton	300	+300	N/A
HCl (32 wt%)	4.25	ton	100	-425	[133]
Water	0.05	ton	4	0	[134]
Cooling water	0.87	ton	4	-3	[134]
Output	**Quantity**	**Unit**	**Price/unit (€/unit)**	**Revenue (€)**	**Reference**
$FeCl_3$ (40 wt%)	4.92	ton	200	+985	[135]
Dry filter cake	0.16	ton	500	-80	N/A
Cutting fluid	0.17	ton	500	-85	N/A
Abrasives	0.02	ton	100	-2	N/A
H_2	36.19	kg	3	+109	[114]
Cooling water	0.87	ton	-	-	N/A
Energy	**Quantity**	**Unit**	**Price/unit (€/kJ)**	**Revenue (€)**	**Reference**
Distillation reboiler	3003	MJ	17	-51	[136]
Other heating	1031	MJ	17	-18	[136]
Cooling (elec.)	16	MJ	55	-1	[137]
Oxidation (elec.)	3590	MJ	55	-197	[137]
Mixing (elec.)	220	MJ	55	-12	[137]
			Net revenue:	+520	

were available on the disposal of filter cake, cutting fluids, and abrasives, and high estimates of 500 €/ton and 100 €/ton were assumed. Selected modelled process stream compositions from the mass balances are provided in Appendix Table A5. Further justifications and assumptions for the balances are given in paper 4.

Mass balances showed that up to 5 tons of 40 wt% $FeCl_3$ could theoretically be produced per ton of grinding sludge. Assuming the product is used as a coagulant at an active substance dose of 100 mg/L, this is sufficient to treat 6900 m^3 of water [138]. Around 36 kg of H_2 is also generated, enough to, e.g., power a hydrogen fuel cell truck consuming 8-10 kg H_2/100 km for 360-450 km [139]. To validate the environmental benefits of these products, hydrometallurgical recycling was compared to state-of-the-art waste management methods with life cycle assessment (LCA). The study indicated that hydrometallurgical recycling had a relatively low global warming potential (-120 to -830 kg CO_2 eq./ton depending on modelling assumptions, with an average -350 kg CO_2 eq./ton) compared to

recycling in steelmaking using EAFs (-17 to -73 kg CO_2 eq./ton) and incineration (+120 kg CO_2 eq./ton) [140]. The economic feasibility was also examined in more detail by comparing revenue streams with OPEX in Figure 30.

This bar diagram shows that $FeCl_3$ accounts for around 71% of the income, with 21% from gate fees, and only 8% from H_2. Main expenses included HCl, accounting for 52% of OPEX, and electricity for the oxidation process. These numbers show that the profitability is less dependent on grinding sludge fees and more on chemical costs. Given that $FeCl_3$ is indispensable in water treatment, this can provide a reliable, stable income stream for recycling. The net revenue was approximately 500 €/ton of grinding sludge processed, increasing in proportion to the gate fee. This showed that recycling can be profitable, even with a minimal fee of 100 €/ton. Higher fees may, however, be required during the payback period in the first years after commissioning. More work, including capital expenditure (CAPEX) calculations, is needed to assess the potential long-term profitability of hydrometallurgical recycling across different industrial landscapes.

Several key areas for improvement were identified to further increase profitability. Sourcing of cheap HCl should be prioritised, and, where possible, secondary streams with lower concentrations may be included to reduce environmental imp-

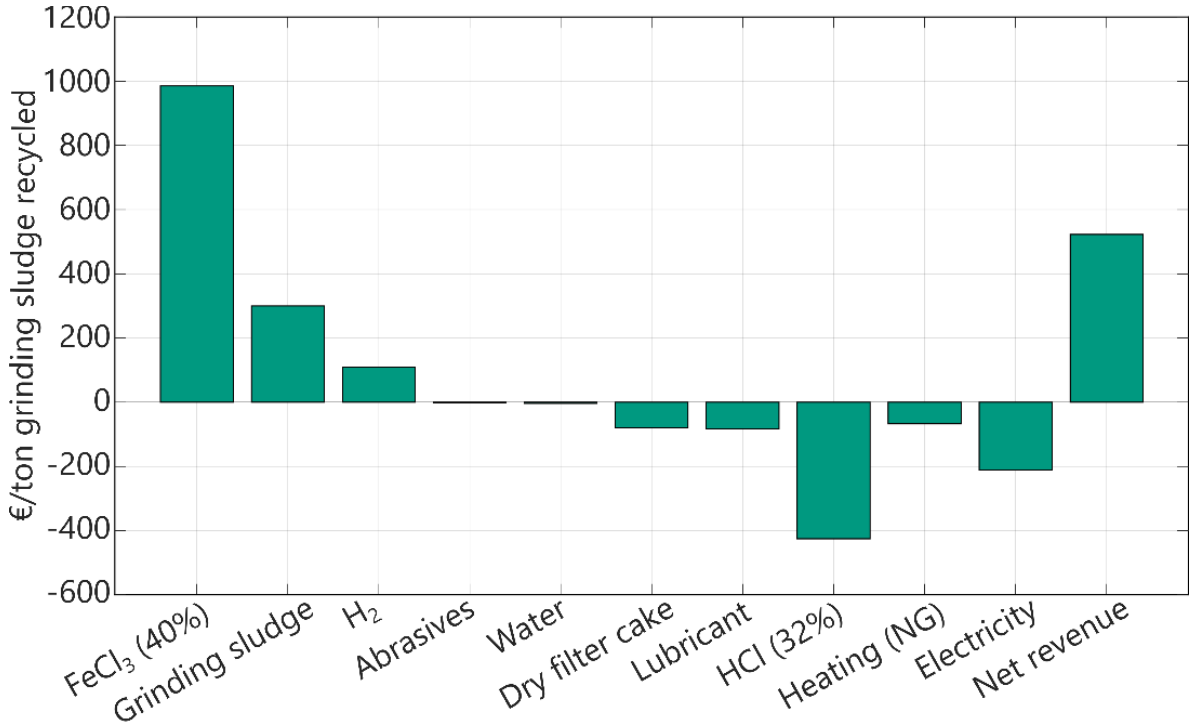

Figure 30: Comparison of profit and OPEX for the recycling process presented in Figure 29, based on economic calculations in Table 14. (NG = natural gas).

acts. Given that HCl and $FeCl_3$ were the largest streams by far, the recycling plant is ideally located near the HCl source to minimise transportation costs. Energy loads in the distillation column can be reduced further by optimising the washing process to minimise the L/S ratio. Heat integration was not considered in the energy balance, and it may be possible to make the process self-sufficient in heat by integrating the reboiler with the leaching process, in which approximately 2000 MJ/ton of heat is released via exothermic reactions. Cutting fluids and filter cake waste also represented substantial costs in Figure 30, and their recycling is important from both economic and environmental perspectives. As mentioned in previous sections, the filter cake may be eligible for recycling in the steel industry, while lubricating oil could be refined and reused in machining or as fuel.

5.8 Testing of recycled $FeCl_3$ for commercial applications

As a final measure, the applicability of the recycled $FeCl_3$ product was validated through proof-of-concept testing in water purification and LFP synthesis. Commercial Grade 1 40 wt% $FeCl_3$ coagulant was used as a reference in both cases.

5.8.1 Water treatment coagulation

Recycled $FeCl_3$ from washed grinding sludge in Table 13 was used in coagulation trials carried out by an industrial partner. Two natural waters from Ödåkra brook (ÖB) and Västersjön lake (VL) mixed with clay were tested. The waters were added to a flocculator and dosed with 50-150 µmol Fe(III)/L, then stirred for 20 s at 350 rpm and for 20 min at 40 rpm to initiate flocculation. Suspended solids were sedimented, and two water samples were taken for analysis, of which one was passed through a 0.45 µm membrane filter. The effects of recycled and commercial $FeCl_3$ on the pH, residual [Fe], turbidity, and colour of each water are compared in Figure 31.

No difference was observed between recycled and commercial coagulants in terms of pH and residual Fe concentrations in either water. The turbidity and colour values in sedimented ÖB were slightly lower with commercial $FeCl_3$, but both coagulants were equally effective at the maximum dose of 150 µmol Fe/L, and after filtration. Water from VL contained more particles, which could be removed effectively with an optimal dose of 100 µmol Fe/L of either coagulant. The conclusion was that no clear difference between recycled and commercial $FeCl_3$ could be identified, and that a coagulant based on grinding sludges was practically identical to current products on the market.

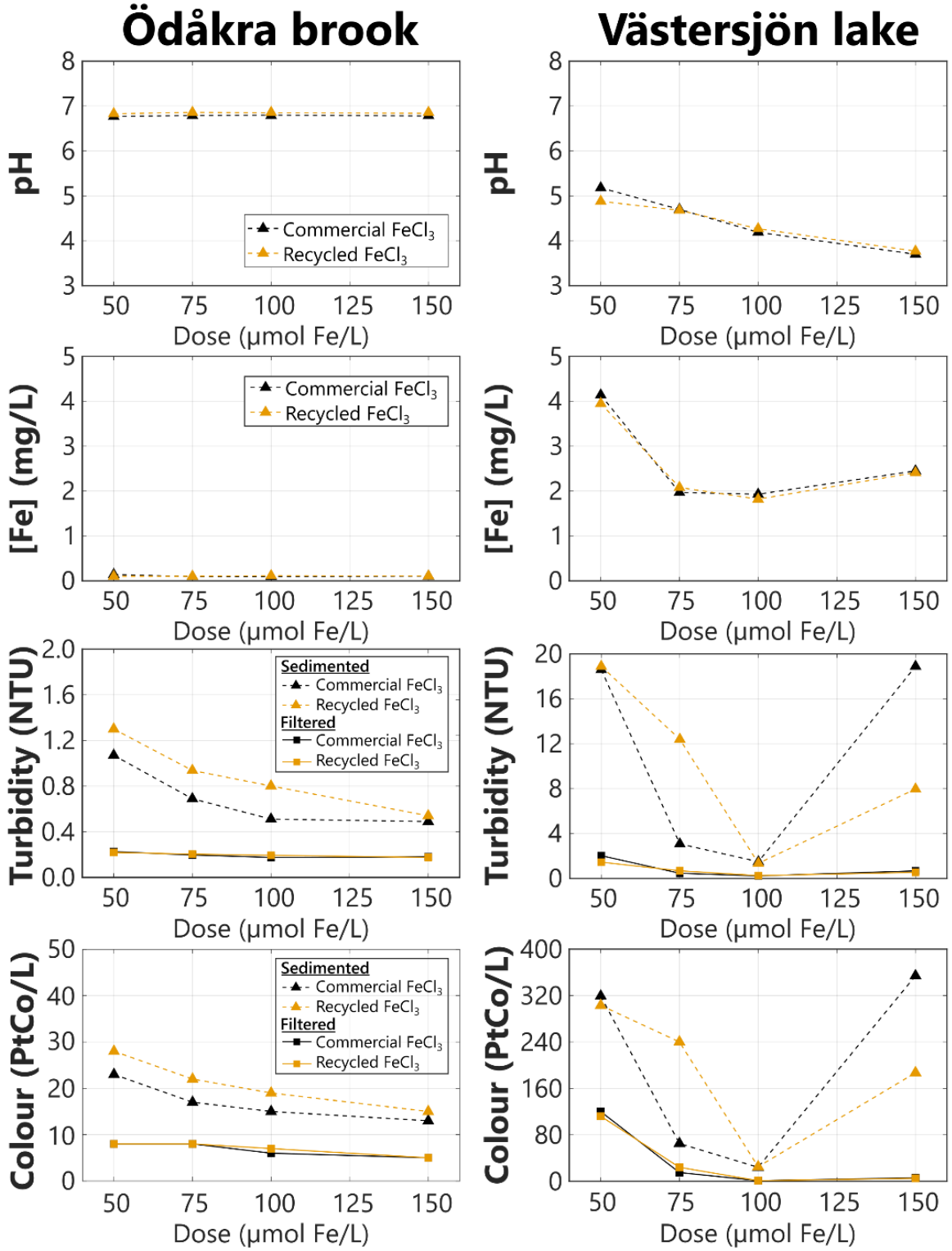

Figure 31: Assays of pH, Fe concentration, turbidity, and colour in waters from Ödåkra brook and Västersjön lake after coagulation with varying doses of recycled or commercial $FeCl_3$.

5.8.2 Synthesis of iron phosphate precursors for LFP

The same $FeCl_3$ was also tested as a precursor in synthesis of iron phosphate (FP) for LFP. The work by Yuan et al. (2024) was used as inspiration to develop a method for precipitation tests [141]. These authors synthesised three FP polymorphs from

$FeCl_3$: amorphous, monoclinic, and trigonal, which were lithiated, carbon-coated and tested for their electrochemical properties. The LFP based on monoclinic FP was found to exhibit the most promising morphology and performance as a cathode active material. To obtain this particular polymorph, 1 L of 0.1 M solution of recycled $FeCl_3$ with a 2:1 molar excess of H_3PO_4 was prepared and heated to 90°C while stirring at 400 rpm. The initial solution was yellow, transparent, and highly acidic (pH ~0), and was neutralised with an NaOH solution to precipitate FP. A strong complex is formed between Fe^{3+} and PO_4^{3-} (a hard base), which precipitates as a highly insoluble FP dihydrate according to Equation 76 [142].

$$Fe^{3+} + PO_4^{3-} + 2H_2O \longrightarrow FePO_4 \cdot 2H_2O(s) \quad (76)$$

This is the same principle behind the removal of PO_4^{3-} and similar arsenates (AsO_4^{3-}) by coagulation in wastewater treatment [143]. The stability region for solid $FePO_4{\cdot}2H_2O$ can be determined with chemical equilibria and Eh-pH diagrams [144]. If the solution is too acidic, the precipitate is easily redissolved by the formation of soluble complexes between FP and H^+ via Equation 77 [145].

$$FePO_4 \cdot 2H_2O(s) + xH^+ \rightleftharpoons H_xFePO_4^{x+} + 2H_2O \quad (77)$$

Under alkaline conditions (pH ≥7), however, $Fe(OH)_3$ can form preferentially. Experimentally, beige flocs formed at pH 0.7-0.8, and NaOH was added until the pH rose beyond this point, reaching pH ~1, indicating that precipitation was complete. This first precipitate was likely amorphous and required recrystallisation to obtain the monoclinic phase as described in Equation 78.

$$FePO_4 \cdot 2H_2O(am) \longrightarrow FePO_4 \cdot 2H_2O(mono) \quad (78)$$

Previous work in SO_4^{2-} media has shown that this reaction occurs after an induction period of <1 h at 90°C, with longer times required at lower temperatures [145]. This was in good agreement with the experiments, where a sudden colour transition from beige to pinkish white was observed after 1 h. Attempts to synthesise monoclinic FP at $FeCl_3$:H_3PO_4 of 1:1 and 1.5:1 were also tested, but no recrystallisation took place even after 4 h at 90°C, suggesting that an excess of H_3PO_4 may be required in Cl^- solutions.

The pink $FePO_4{\cdot}2H_2O$ crystals were easily filtered and washed with water, yielding a free-flowing powder upon drying. Around 98% of the Fe was converted to FP, and residual Fe in the solutions was primarily Fe(II), which is less easily precipitated by PO_4^{3-}. Other divalent impurities, including Mn, Ni, and Co, were also unaffected by the precipitation procedure, and the $FePO_4{\cdot}2H_2O$ was 99.98% pure according

to XRF analysis. In collaboration with the Chalmers Materials Chemistry group, the FP powder was lithiated by calcining with $LiOH{\cdot}H_2O$ at 700°C for 4 h using H_2 as the reducing agent, as described in Equation 79.

$$2FePO_4 \cdot 2H_2O(s) + 2LiOH \cdot H_2O(s) + H_2(g) \longrightarrow 2LiFePO_4(s) + 8H_2O(g) \qquad (79)$$

Both FP and LFP were analysed with XRD, as seen in Figure 32a-b, and the recycled FP was further analysed with SEM in Figure 32c and d. Diffractograms of FP and

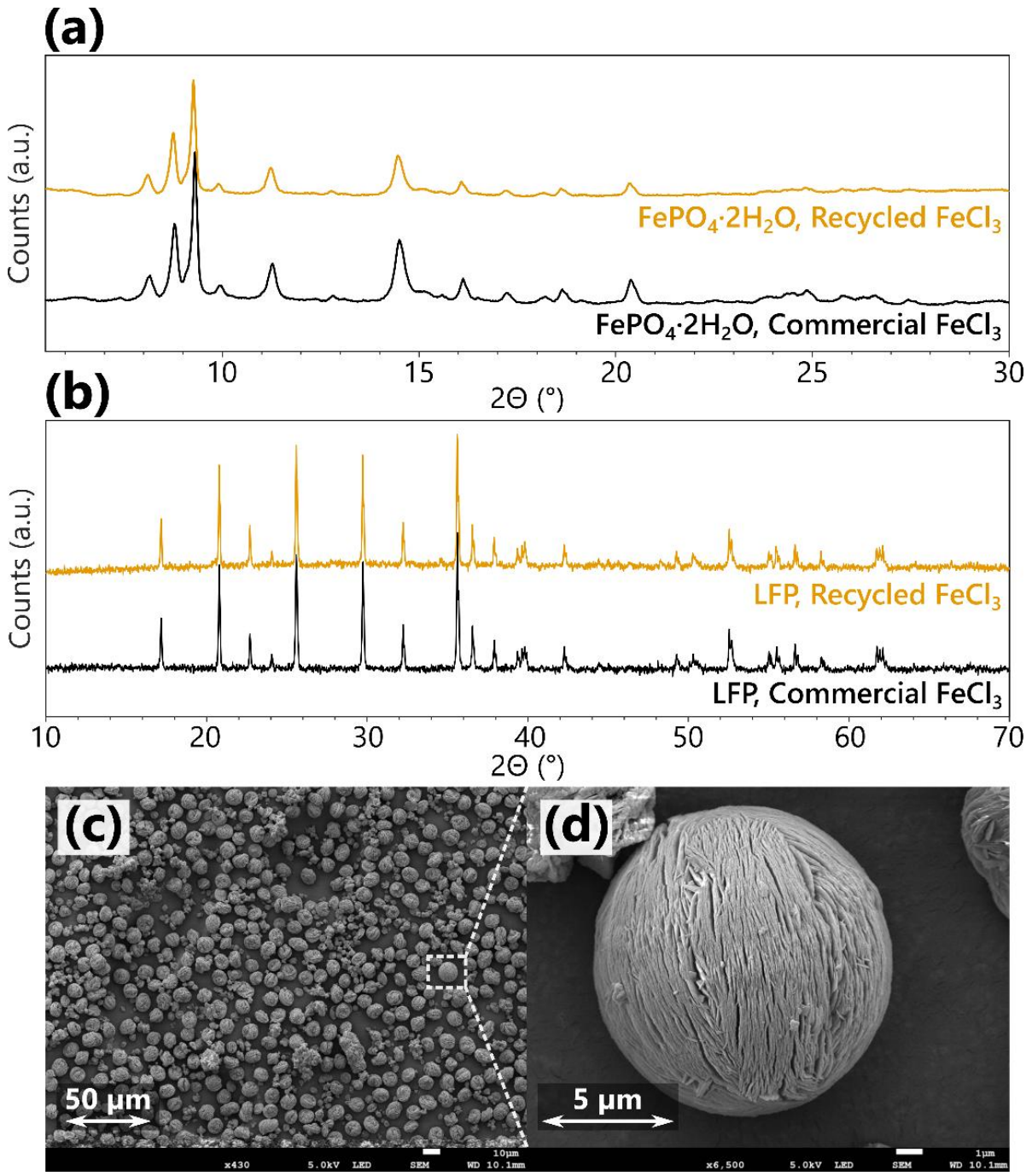

Figure 32: Diffractograms of (a) iron phosphate dihydrate (FP) and (b) lithium iron phosphate (LFP) synthesised from recycled and commercial $FeCl_3$. SEM analysis of FP particles based on recycled $FeCl_3$, showing the morphology (c) 430x and (d) 6500x magnification.

LFP synthesised using the same methods, but with commercial Grade 1 $FeCl_3$, are shown for comparison to demonstrate that the final products were similar. The SEM shows that FP particles were spherical, with a relatively uniform size of around 10 μm, composed of smaller plates. Further optimisation of the LFP morphology and electrochemical testing is ongoing and part of future work.

6 Conclusion

The feasibility of using a hydrometallurgical approach to recycle grinding sludges has been investigated, and initial economic and environmental assessments have been conducted. A flexible process capable of handling variations in waste input was developed to convert Fe in the sludges to $FeCl_3$, and the chemistry behind the necessary unit processes was explained. The work shows that high-quality $FeCl_3$ solutions meeting drinking water-grade coagulant purity standards can be produced at concentrations up to 36 wt% $FeCl_3$, just below the typical commercial solutions of 40 wt%. The final product is identical in performance to commercial $FeCl_3$ and is deemed suitable for water treatment and FP synthesis.

More than 95% Fe in grinding sludges can be converted to $FeCl_2$ by dissolution in HCl, or a mixture of $FeCl_3$ and HCl with slow addition of the leaching agent. Using HCl is simpler but generates H_2, which can be undesirable from a safety perspective. Alloying elements are generally also dissolved during leaching and can be separated from $FeCl_2$ using the purification process that was developed. Grinding swarf is an excellent precipitation agent and provides large metal surfaces for rapid deposition of nobler metals such as Cu and Ni, and for neutralising remaining HCl and $FeCl_3$, thereby precipitating Al, Cr, Mo, and other higher-valency metals via hydrolysis at pH ≥3.7. Emulsified lubricant oils are also destabilised during leaching and are adsorbed onto solid residues or precipitates. After precipitation, these impurities can be removed from the $FeCl_2$ solution via filtration. Pretreatment of grinding sludges prior to leaching is not strictly necessary, provided they are briquetted, but is nonetheless highly recommended. Removing cutting fluids early on yields a more uniform input material, faster leaching with higher Fe recovery, easier filtration, and fewer unknown organic substances in the iron chloride product. Both pressure oxidation and electrolysis are feasible for oxidising $FeCl_2$ to $FeCl_3$, but result in dilution of the product. The solution is slightly less diluted via electrolysis, and this method also allows for the use of lower-grade HCl and the coproduction of H_2.

In theory, 5 tons of 40 wt% $FeCl_3$ solution and 36 kg of H_2 can be obtained per ton of sludge recycled, representing around 70% and 10% of the potential incomes, respectively. This makes the process relatively robust economically and less dependent on waste gate fees. The environmental benefits of waste disposal prevention and recycling products are also significant, making hydrometallurgical recycling a strong competitor to current waste management options.

Future work

A relatively complete recycling process has been proposed at the research level so far, but several improvements remain. Firstly, the washing procedure should be further optimised by using more technically relevant equipment, given its importance for subsequent treatment steps. Both aqueous and solvent washing procedures can be developed here to accommodate regional constraints, such as limited energy or water supply. The electrolysis process was another promising addition that was not studied sufficiently and should be further developed in relevant equipment, such as a flow cell, to determine whether reaction time, energy use, and water transport can be reduced. Furthermore, several questions remain regarding the products, including whether the filter cake can be recycled and if simple measures can be taken during or after the process to promote its recyclability. Removal of residual organics from the $FeCl_3$ product may also be necessary, where carbon adsorption seemed a promising alternative.

Newer research avenues should also be explored, such as incorporating other waste streams into the process. Chloride-based pickle liquors from steelmaking may, for instance, be highly compatible and could be included in the leaching process and purified via precipitation with grinding swarf. An analogous process for preparing iron sulphate solutions from grinding sludges can also be developed for situations where H_2SO_4 is more readily available or a sulphate product is preferred. Continuing the development of LFP and other electrode materials from grinding sludges also helps diversify potential applications, thereby providing a more stable foundation for recycling.

In a potential future scale-up, a more in-depth study of the $FeCl_2$ filtration (or other liquid-solid separation) process should be conducted, as this step can be difficult to study at small scales. At this point, safety measures for handling H_2 also become more relevant, and capture of the gas can be considered. Once the dimensions and types of required equipment are better known, OPEX calculations should be complemented by CAPEX estimates to evaluate the profitability of recycling in the short and long term. From a regulatory standpoint, it can also be necessary to investigate whether the current $FeCl_3$ product is acceptable for water treatment and whether more dilute solutions are marketable. A proposal to update the current EN:888 standard can also be made to make it easier to replace virgin magnetite used in coagulant production with waste materials more generally.

Acknowledgements

This work would not have been possible without the countless people who have supported me throughout the project.

First and foremost, I'd like to thank my supervisor, Dr Martina Petranikova, for giving me the opportunity to work in the field of recycling I'm so passionate about. I'm grateful that you let me take the reins and trusted me to steer the project in the right direction, while also listening and supporting me when needed. A special thanks also to Dr Léa Rouquette for your tireless positivity and friendship, and Prof. Christian Ekberg for your time and attention. Both your careful reviewing and commenting have been a great help and have undoubtedly improved the quality of the thesis. I'm also thankful to my examiner, Prof. Teodora Retegan Vollmer, and all my colleagues and friends in the group, especially Andrea, Dogac, Nils, Luis, and Nathalia, who have made me feel welcome from the very start.

Within Chalmers entrepreneurial sphere, I would like to thank Ana, Lotta, and Fredrik at Chalmers Ventures, and in particular Anne Alsholm at Chalmers Innovations Office. You've helped me explore the commercial potential of my technology, which has been a great motivator in my academic work. Without you, our startup Anferra, through which I've learned so much, would not have existed. To my dear friends and future colleagues, Ebba, Max, and Julie, as well as Sofia, Ingrid, and others who have contributed to Anferra in the past, I'm truly impressed by each and every one of you and very proud of how far we've come.

Besides the people at Chalmers and Anferra, I'd like to thank Linda Widbro and Peter Boussard at SKF, and Anders Krantz at Husqvarna, who have both been early advocates for the project, and whose enthusiasm has been infectious. The insights you've shared about the industry have been invaluable in writing the thesis. The same thanks are extended to Kalle Pelin at Feralco and Håkan Wiktorsson, Jakob Smusin, and Fazlollah Azarnoush at Kemira. I'm grateful for your collaboration and for the projects we've worked on together that have inspired me to continue seeking new solutions.

Lastly, none of this work would have been possible without the daily happiness and support I've received outside of work from my parents Judith and Roel, siblings Anna, David and Eva, and all of my good friends. Most importantly, I'd like to thank my wife, Hanna, for her patience, understanding, and being a constant in my life. You are my best friend, and I love you to the moon and back.

References

[1] World Steel Association. *World Steel in Figures*. 2025.

[2] Pauliuk S, Milford RL, Müller DB, et al. The steel scrap age. *Environ Sci Technol* 2013; 47: 3448–3454.

[3] Ritchie H. Sector by sector: where do global greenhouse gas emissions come from? *OurWorldinData.org*, https://archive.ourworldindata.org/20251125-173858/ghg-emissions-by-sector.html (2020, accessed 20 January 2026).

[4] Ottink T. Personal market research as part of Vinnova's SPiRiT program, https://www.vinnova.se/p/swedish-platforms-for-advanced-infrastructures-in-research-innovation-and-technology-spirit-fas-i/ (accessed 2026-03-04) (2024).

[5] Großwendt F, Bürk V, Kopanka B, et al. A novel powder-metallurgical eco-friendly recycling process for tool steel grinding sludge. *J Clean Prod* 2023; 392: 136329.

[6] Smil V. *Still the Iron Age: Iron and Steel in the Modern World*. Elsevier Inc., 2016. Epub ahead of print February 2016. DOI: 10.1016/C2014-0-04576-5.

[7] Wayman ML. Archaeometallurgical contributions to a better understanding of the past. *Mater Charact* 2000; 45: 259–267.

[8] Spoerl JS. *A Brief History of Iron and Steel Production*. Manchester, 2004.

[9] Johansson PO, Kriström B. "Green" steel investments in the EU: Pie in the sky? *Resour Energy Econ*; 82. Epub ahead of print May 2025. DOI: 10.1016/j.reseneeco.2025.101494.

[10] Zhou G, Wang Q, Li J, et al. Removal of polystyrene and polyethylene microplastics using PAC and FeCl3 coagulation: Performance and mechanism. *Science of The Total Environment* 2021; 752: 141837.

[11] Kong Y, Huang A, Lu F, et al. Enhanced removal of organic arsenic by using potassium ferrate coupled with metal coagulants: Role of iron species and effect of AlCl3 and FeCl3. *Chemical Engineering Journal* 2023; 475: 146109.

[12] Malakootian M, Yazdanpanah G, Poorjahanshahi M. A comparison of the effectiveness of electrocoagulation to coagulation processes using ferric chloride for the removal of cadmium from aqueous solution. *Desalination Water Treat* 2017; 78: 215–220.

[13] de Raús Maúre E, Terauchi G, Ishizaka J, et al. Globally consistent assessment of coastal eutrophication. *Nature Communications 2021 12:1* 2021; 12: 6142-.

[14] Incopa. Iron-based coagulant: A good example of the circular economy. *2020*.

[15] Miao XF, Zhou XT, Wang RX, et al. Study on closed recycling regeneration process of FeCl3 waste etching solution and recovery of Copper. *IOP Conf Ser Earth Environ Sci* 2016; 39: 012046.

[16] O'Malley ML, Liddell KC. Leaching of CuFeS2 by aqueous FeCl3, HCl, and NaCl: Effects of solution composition and limited oxidant. *Metallurgical Transactions B* 1987; 18: 505–510.

[17] Wesselborg T, Virolainen S, Sainio T. Recovery of lithium from leach solutions of battery waste using direct solvent extraction with TBP and FeCl3. *Hydrometallurgy*; 202. Epub ahead of print June 2021. DOI: 10.1016/j.hydromet.2021.105593.

[18] Seisko S, Lampinen M, Aromaa J, et al. Kinetics and mechanisms of gold dissolution by ferric chloride leaching. *Miner Eng* 2018; 115: 131–141.

[19] Yuzir A, Yaacob SS, Tijani HI, et al. Addition of ferric chloride in anaerobic digesters to enhance sulphide removal and methanogenesis. *Desalination Water Treat* 2017; 79: 64–72.

[20] Ahn BK, Kim TH, Seon J, et al. Mill Scale Addition to Reduce Hydrogen Sulfide Production in Anaerobic Digestion. *Energies 2021, Vol 14, Page 6542* 2021; 14: 6542.

[21] Hwang JY, Myung ST, Sun YK. Sodium-ion batteries: Present and future. *Chemical Society Reviews* 2017; 46: 3529–3614.

[22] Darley J. The Rust Revolution: Can Iron-Air Batteries Save the Planet? *Sustainability Magazine*, 1 December 2025.

[23] Li Z, Yu J, Liu X. Materials and Devices for Iron Batteries: Recent Progress and Perspectives. *ACS Appl Energy Mater* 2025; 8: 9965–9982.

[24] Dorri M, Nekahi A, Ahmed S, et al. Exploring sustainable lithium iron phosphate cathodes for Li-ion batteries: From mine to precursor and cathode production. *J Power Sources* 2025; 656: 238041.

[25] Wijareni AS, Yunita FE, Ichlas ZT, et al. Advanced review on FePO4 synthesis process from various Fe sources for LiFePO4 battery cathode precursor material. *Ionics* 2025; 31: 12545–12573.

[26] Azarhoushang B. Abrasive tools. *Tribology and Fundamentals of Abrasive Machining Processes: Third Edition* 2022; 31–73.

[27] El Baradie MA. Cutting fluids: Part I. Characterisation. *J Mater Process Technol* 1996; 56: 786–797.

[28] Azarhoushang B. Abrasives. *Tribology and Fundamentals of Abrasive Machining Processes: Third Edition* 2022; 3–30.

[29] Irani RA, Bauer RJ, Warkentin A. A review of cutting fluid application in the grinding process. *Int J Mach Tools Manuf* 2005; 45: 1696–1705.

[30] Fuchs. Cutting Fluids Manual - Collected Knowledge on Cutting Fluids for Metalworking.

[31] Said Z, Gupta M, Hegab H, et al. A comprehensive review on minimum quantity lubrication (MQL) in machining processes using nano-cutting fluids. *International Journal of Advanced Manufacturing Technology* 2019; 105: 2057–2086.

[32] Wu X, Li C, Zhou Z, et al. Circulating purification of cutting fluid: an overview. *The International Journal of Advanced Manufacturing Technology 2021 117:9* 2021; 117: 2565–2600.

[33] Li H, Zhang Y, Li C, et al. Cutting fluid corrosion inhibitors from inorganic to organic: Progress and applications. *Korean Journal of Chemical Engineering 2022 39:5* 2022; 39: 1107–1134.

[34] Lopes JC, Ávila BN, de Souza Rodrigues M, et al. Grinding comparative analysis between different proportions of water-oil applied to MQL technique and industrial production cost towards a green manufacturing. *International Journal of Advanced Manufacturing Technology* 2021; 113: 1281–1293.

[35] Lee CM, Choi YH, Ha JH, et al. Eco-friendly technology for recycling of cutting fluids and metal chips: A review. *International Journal of Precision Engineering and Manufacturing - Green Technology* 2017; 4: 457–468.

[36] Hess MJ, Kawatra SK. Environmental Beneficiation of Machining Wastes-Part I: Material Characterization of Machining Swarf. *J Air Waste Manage Assoc* 1999; 49: 207–212.

[37] Xiao Y, Reuter MA. Recycling of distributed aluminium turning scrap. *Miner Eng* 2002; 15: 963–970.

[38] Nayström P. *Brikettering av stål-och gjutjärnspån samt slipmull*. Gjuteriföreningen, 1998.

[39] Nakamura K, Hayashi S. Grinding Sludge Recycling to Reduce Environmental Load Analysis of Disturbing Factor for Briquetting of Grinding Sludge. *Tetsu-to-Hagane* 2006; 92: 535–538.

[40] Lauenstein Å. *Cirkulära materialflöden i svenska gjuterier: slutrapport från projektet HANS*. 2025.

[41] El Baradie MA. Cutting fluids: Part II. Recycling and clean machining. *J Mater Process Technol* 1996; 56: 798–806.

[42] Punmatharith T, Rachakornkij M, Imyim A, et al. Co-processing of grinding sludge as alternative raw material in portland cement clinker production. *Journal of Applied Sciences* 2010; 10: 1525–1535.

[43] Magistri M. Hexavalent chromium in cement, 15 years later. *ZKG International*.

[44] European Environment Agency. *Technical note accompanying the EEA briefing 'Economic instruments and separate collection-key instruments to increase recycling'*. 2023.

[45] Fu H, Matthews MA, S. Warner L. Recycling steel from grinding swarf. *Waste Management* 1998; 18: 321–329.

[46] Chang JI, Lin JJ, Huang JS, et al. Recycling oil and steel from grinding swarf. *Resour Conserv Recycl* 2006; 49: 191–201.

[47] Ruffino B, Zanetti MC. Recycling of steel from grinding scraps: Reclamation plant design and cost analysis. *Resour Conserv Recycl* 2008; 52: 1315–1321.

[48] Lee H, Jung M, Bae M, et al. Removal of oil from ferrous grinding swarf of automobile industry by aqueous washing process. *Waste Management* 2020; 111: 51–57.

[49] Hankel J, Jäger S, Weber S. Development of a recycling strategy for grinding sludge using supersolidus liquid phase sintering. *J Clean Prod* 2020; 263: 121501.

[50] Dankoff JD, Snyder DK. *Reclamation of components from grinding swarf*. US3865629A, United States, 1975.

[51] Großwendt F, Bram M, Treppmann M, et al. Materials scientific challenges of a circular economy of high-alloy tool steels. *Practical Metallography* 2025; 62: 634–649.

[52] Anastas P, Eghbali N. Green Chemistry: Principles and Practice. *Chem Soc Rev* 2010; 39: 301–312.

[53] Free ML. *Hydrometallurgy: Fundamentals and Applications*. Second Edi. Salt Lake City: Springer, 2021.

[54] Cerrillo-Gonzalez M del M, Villen-Guzman M, Vereda-Alonso C, et al. Towards Sustainable Lithium-Ion Battery Recycling: Advancements in Circular Hydrometallurgy. *Processes*; 12. Epub ahead of print July 2024. DOI: 10.3390/pr12071485.

[55] Porvali A, Ojanen S, Wilson BP, et al. Nickel Metal Hydride Battery Waste: Mechano-hydrometallurgical Experimental Study on Recycling Aspects. *Journal of Sustainable Metallurgy* 2020; 6: 78–90.

[56] Tunsu C, Petranikova M, Gergorić M, et al. Reclaiming rare earth elements from end-of-life products: A review of the perspectives for urban mining using hydrometallurgical unit operations. *Hydrometallurgy* 2015; 156: 239–258.

[57] Sethurajan M, van Hullebusch ED, Fontana D, et al. Recent advances on hydrometallurgical recovery of critical and precious elements from end of life electronic wastes - a review. *Crit Rev Environ Sci Technol* 2019; 49: 212–275.

[58] Tang J. *Removal and Recovery of Metals from Municipal Solid Waste Incineration ashes by a Hydrometallurgical Process*. Chalmers University of Technology, 2017.

[59] Binnemans K, Jones PT, Manjón Fernández Á, et al. Hydrometallurgical Processes for the Recovery of Metals from Steel Industry By-Products: A Critical Review. *Journal of Sustainable Metallurgy 2020 6:4* 2020; 6: 505–540.

[60] Petranikova M, Ssenteza V, Lousada CM, et al. Novel process for decontamination and additional valorization of steel making dust processing using two-step correlative leaching. *J Hazard Mater* 2020; 384: 121442.

[61] Virolainen S, Salmimies R, Hasan M, et al. Recovery of valuable metals from argon oxygen decarburization (AOD) dusts by leaching, filtration and solvent extraction. *Hydrometallurgy* 2013; 140: 181–189.

[62] Liu B, Zhang SG, Tian JJ, et al. New technology for recycling materials from oily cold rolling mill sludge. *International Journal of Minerals, Metallurgy and Materials* 2013; 20: 1141–1147.

[63] Devi A, Singhal A, Gupta R, et al. A study on treatment methods of spent pickling liquor generated by pickling process of steel. *Clean Technologies and Environmental Policy* 2014; 16: 1515–1527.

[64] Liu C, Wang X, Ma P, et al. A new application of oily cold rolling mill sludge for preparing Fe2O3/graphene as anodes for lithium-ion batteries. *RSC Adv* 2015; 5: 57383–57388.

[65] Sipos P. Application of the Specific Ion Interaction Theory (SIT) for the ionic products of aqueous electrolyte solutions of very high concentrations. *J Mol Liq* 2008; 143: 13–16.

[66] Outotec® HSC Chemistry™ 10 (2020).

[67] Weller M, Rourke J, Armstrong F, et al. *Inorganic Chemistry*. 8th ed. Oxford University Press, 2025.

[68] Brown P, Ekberg C. *Hydrolysis of metal ions*. John Wiley & Sons, 2016.

[69] Pearson RG. Hard and Soft Acids and Bases. *J Am Chem Soc* 1963; 85: 3533–3539.

[70] Zhao R, Pan P. A spectrophotometric study of Fe(II)-chloride complexes in aqueous solutions from 10 to 100°C. *Can J Chem* 2001; 79: 131–144.

[71] Testemale D, Brugger J, Liu W, et al. In-situ X-ray absorption study of Iron(II) speciation in brines up to supercritical conditions. *Chem Geol* 2009; 264: 295–310.

[72] Lee MS. Chemical equilibria in ferrous chloride acid solution. *Metals and Materials International* 2004; 10: 387–392.

[73] Liu W, Etschmann B, Brugger J, et al. UV–Vis spectrophotometric and XAFS studies of ferric chloride complexes in hyper-saline LiCl solutions at 25–90 °C. *Chem Geol* 2006; 231: 326–349.

[74] Jamett NE, Hernández PC, Casas JM, et al. Speciation in the Fe(III)-Cl(I)-H2O System at 298.15 K, 313.15 K, and 333.15 K (25 °C, 40 °C, and 60 °C). *Metallurgical and Materials Transactions B: Process Metallurgy and Materials Processing Science* 2018; 49: 451–459.

[75] Knight RJ, Sylva RN. Precipitation in hydrolysed iron(III) solutions. *Journal of Inorganic and Nuclear Chemistry* 1974; 36: 591–597.

[76] Dutrizac JE, Riveros PA. Precipitation of hematite from ferric chloride media at atmospheric pressure. *Metallurgical and Materials Transactions B: Process Metallurgy and Materials Processing Science* 1999; 30: 993–1001.

[77] Havlík T. *Hydrometallurgy*. Woodhead Publishing, 2008. Epub ahead of print 2008. DOI: 10.1533/9781845694616.242.

[78] Lundström M. *Chalcopyrite Dissolution in Cupric Chloride Solutions*. Helsinki University of Technology, 2009.

[79] Einar Mattsson. *Basic Corrosion Technology for Scientists and Engineers*. Second Edition. London: Maney Publishing for IOM3, the Institute of Materials, Minerals and Mining, 1996, 1996.

[80] Cappuyns V, Swennen R. The application of pHstat leaching tests to assess the pH-dependent release of trace metals from soils, sediments and waste materials. *J Hazard Mater* 2008; 158: 185–195.

[81] Larsson K, Ekberg C, Ødegaard-Jensen A. Dissolution and characterization of HEV NiMH batteries. *Waste Management* 2013; 33: 689–698.

[82] Sędzimir JA. Precipitation of metals by metals (cementation)—kinetics, equilibria. *Hydrometallurgy* 2002; 64: 161–167.

[83] Addy S, Fletcher AJ. The deposition of cobalt on iron powder by means of the cementation reaction. *Hydrometallurgy* 1987; 17: 269–280.

[84] Sareyed-Dim NA. *The cementation of nickel onto iron at elevated temperatures*. Monash University, 1974.

[85] Agrawal RD. Theoretical considerations of the cementation of copper with iron. *Journal of the South African Institute of Mining and Metallurgy* 1982; 84: 106–111.

[86] Makhloufi L, Saidani B, Hammache H. Removal of lead ions from acidic aqueous solutions by cementation on iron. *Water Res* 2000; 34: 2517–2524.

[87] Anacleto AL, Carvalho JR. Mercury cementation from chloride solutions using iron, zinc and aluminium. *Miner Eng* 1996; 9: 385–397.

[88] Pearson RG. Hard and soft acids and bases, HSAB, part 1: Fundamental principles. *J Am Chem Soc*; 45. Epub ahead of print September 1968. DOI: 10.1021/jacs.5c18963.

[89] Lewandowski GA, Linford HB. Filtration of Ferric Hydroxide. *Environ Sci Technol* 1972; 6: 169–172.

[90] Pesic B, Oliver DJ, Wichlacz P. An electrochemical method of measuring the oxidation rate of ferrous to ferric iron with oxygen in the presence of Thiobacillus ferrooxidans. *Biotechnol Bioeng* 1989; 33: 428–439.

[91] Crabtree JH, Schaefer WP. The Oxidation of Iron(II) by Chlorine. *Inorg Chem* 1966; 5: 1348–1351.

[92] Miki H, Nicol M. The kinetics of the oxidation of iron(II) by chlorate in the leaching of uranium ores. *Hydrometallurgy* 2009; 100: 47–49.

[93] Kearney MJ, Parks CA. Oxidation Of Iron And Manganese By Ozone. *Ozone Sci Eng* 1991; 13: 675–695.

[94] Abdel-Fatah MA, Hawash SI, Shaarawy HH. Cost-effective Clean Electrochemical Preparation of Ferric Chloride and its Applications. *Egypt J Chem* 2021; 64: 3841–3851.

[95] Morgan B, Lahav O. The effect of pH on the kinetics of spontaneous Fe(II) oxidation by O2 in aqueous solution – basic principles and a simple heuristic description. *Chemosphere* 2007; 68: 2080–2084.

[96] Marconi PF, Meunier V, Vatistas N. Recovery of pickling effluents by electrochemical oxidation of ferrous to ferric chloride. *J Appl Electrochem* 1996; 26: 693–701.

[97] Weng F-T, Ho - C-T, Kong Y, et al. FeCl3 coagulant production from waste pickle liquor using electrolysis. *IOP Conf Ser Mater Sci Eng* 2020; 823: 012058.

[98] Johansson K, Liljenroth A. *Carbon footprints of inorganic coagulants*. October 2023.

[99] Westcott C. *Ph Measurements*. Academic Press Inc, 1978.

[100] Montgomery DC. *Design and analysis of experiments*. 10th ed. John Wiley & Sons, 2020.

[101] Fortune WB, Mellon MG. Determination of Iron with o-Phenanthroline: A Spectrophotometric Study. *Industrial and Engineering Chemistry - Analytical Edition* 1938; 10: 60–64.

[102] Lucchesi CA, Hirn CF. EDTA Titration of Total Iron in Iron(II) and Iron(III) Mixtures Application to Iron Driers.
[103] Knop J. Diphenylamine as indicator in the titration of iron with dichromate solution. *The Journal of the American Chemical Society* 1924; 46: 263–269.
[104] Ma IAW, Ammar S, Kumar SSA, et al. A concise review on corrosion inhibitors: types, mechanisms and electrochemical evaluation studies. *Journal of Coatings Technology and Research 2021 19:1* 2021; 19: 241–268.
[105] Reichardt C. Empirical Parameters of the Polarity of Solvents. *Angewandte Chemie International Edition in English* 1965; 4: 29–40.
[106] Byrne FP, Jin S, Paggiola G, et al. Tools and techniques for solvent selection: green solvent selection guides. *Sustainable Chemical Processes*; 4. Epub ahead of print December 2016. DOI: 10.1186/s40508-016-0051-z.
[107] Seader JD, Henley EJ, Roper DK. *Separation Process Principles*. 1998.
[108] Bayu A, Nandiyanto D, Oktiani R, et al. How to Read and Interpret FTIR Spectroscope of Organic Material. *Indonesian Journal of Science and Technology* 2019; 4: 97–118.
[109] Shen WF, Benyounes H, Song J. A review of ternary azeotropic mixtures advanced separation strategies. *Theoretical Foundations of Chemical Engineering 2016 50:1* 2016; 50: 28–40.
[110] Hu B, Chen B, Zhang C, et al. Separation and Recovery of Chromium from Solution After Vanadium Precipitation. DOI: 10.1007/s42461-020-00342-2/Published.
[111] Rihan R, Shawabkeh R, Al-Bakr N. The effect of two amine-based corrosion inhibitors in improving the corrosion resistance of carbon steel in sea water. *J Mater Eng Perform* 2014; 23: 693–699.
[112] Guimarães AP, Maia DAS, Araújo RS, et al. Destabilization and Recuperability of Oil Used in the Formulation of Concentrated Emulsions and Cutting Fluids. *Chem Biochem Eng Q* 2010; 24: 43–49.
[113] Ríos G, Pazos C, Coca J. Destabilization of cutting oil emulsions using inorganic salts as coagulants. *Colloids Surf A Physicochem Eng Asp* 1998; 138: 383–389.
[114] Iea. Global Hydrogen Review 2025.
[115] Watari T, McLellan B. Global demand for green hydrogen-based steel: Insights from 28 scenarios. *Int J Hydrogen Energy* 2024; 79: 630–635.
[116] Rémazeilles C, Refait P. On the formation of β-FeOOH (akaganéite) in chloride-containing environments. *Corros Sci* 2007; 49: 844–857.
[117] Verma C, Hussain CM, Ebenso EE. *Organic corrosion inhibitors: Synthesis, characterization, mechanism, and applications*. wiley, 2021. Epub ahead of print 7 November 2021. DOI: 10.1002/9781119794516.
[118] Kitazawa T, Ishita T, Nagashima M, et al. *Method for purifying iron chloride-base waste liquid containing chromium or the like*. JPH05138178A, 1991.
[119] Lienhardt WS. *Process of recovering nickel*. Patent application no. 1592307, 1925.
[120] Saylam H. *Deposition of cobalt on iron powder*. Sheffield City Polytechnic, 1982.

[121] Winand R. Chloride hydrometallurgy. *Hydrometallurgy* 1991; 27: 285–316.
[122] Jinxing J. *Fundamental aspects of nickel electrowinning from chloride electrolytes*. The University of British Columbia, 1982.
[123] Hurlen T. Kinetics and thermodynamics of Ni/Ni(II) reactions in concentrated solutions of nickel and calcium chlorides. *Electrochim Acta* 1975; 20: 499–505.
[124] Rai D, Sass BM, Moore DA. Chromium(III) Hydrolysis Constants and Solubility of Chromium(III) Hydroxide. *Inorg Chem* 1987; 26: 345–349.
[125] Refait P, Génin JMR. The transformation of chloride-containing green rust one into sulphated green rust two by oxidation in mixed Cl- and SO42- aqueous media. *Corros Sci* 1994; 36: 55–65.
[126] Rieger J, Schenk J. Residual Processing in the European Steel Industry: A Technological Overview. *Journal of Sustainable Metallurgy* 2019; 5: 295–309.
[127] Vittal R, Gomathi H, Kim KJ. Beneficial role of surfactants in electrochemistry and in the modification of electrodes. *Adv Colloid Interface Sci* 2006; 119: 55–68.
[128] Giovanelli A, Pozio A, Pucci A, et al. Fumasep FAA-3-PK-130: Exploiting multinuclear solid-state NMR to shed light on undisclosed structural properties. *Polymer (Guildf)* 2024; 311: 127536.
[129] Bock R, Kleinsteinberg B, Selnes-Volseth B, et al. A Novel Iron Chloride Red-Ox Concentration Flow Cell Battery (ICFB) Concept; Power and Electrode Optimization. *Energies 2021, Vol 14, Page 1109* 2021; 14: 1109.
[130] Spiegler KS. Transport processes in ionic membranes. *Transactions of the Faraday Society* 1958; 54: 1408–1428.
[131] Yan L, Li D, Li S, et al. Balancing Osmotic Pressure of Electrolytes for Nanoporous Membrane Vanadium Redox Flow Battery with a Draw Solute. *ACS Appl Mater Interfaces* 2016; 8: 35289–35297.
[132] Powell DH, Barnes AC, Enderby JE, et al. The hydration structure around chloride ions in aqueous solution. *Faraday Discuss Chem Soc* 1988; 85: 137–146.
[133] Business Analytiq. Hydrochloric Acid price index.
[134] EurEau. *Europe's Water in Figures*. 2021.
[135] imarc. *Ferric Chloride Prices, Trend, Chart, Demand, Market Analysis, News, Historical and Forecast Data Report 2025 Edition*. 2025.
[136] Eurostat. Natural gas price statistics.
[137] Eurostat. Electricity price statistics.
[138] Leentvaar J, Yweema TSJ, Roersma RE. Optimalization of coagulant dose in coagulation-flocculation of sewage. *Water Res* 1979; 13: 229–236.
[139] Basma H, Rodríguez F. *Fuel cell electric tractor-trailers: Technology overview and fuel economy*. 2022.
[140] Johansson K. *LCA of recovered ferric chloride from grinding swarf: Environmental performance of Anferra's process compared to State-of-the-Art processes*. IVL Svenska Miljöinstitutet, 2025.

[141] Yuan Y, Hu J, Wang L, et al. Structural properties and electrochemical performance of different polymorphs of FePO 4 as raw materials for lithium ion electrodes. *J Mater Chem C Mater* 2024; 12: 6511–6518.
[142] Zhang T, Lu Y, Luo G. Effects of temperature and phosphoric acid addition on the solubility of iron phosphate dihydrate in aqueous solutions. *Chin J Chem Eng* 2017; 25: 211–215.
[143] Qiao J, Jiang Z, Sun B, et al. Arsenate and arsenite removal by FeCl3: Effects of pH, As/Fe ratio, initial As concentration and co-existing solutes. *Sep Purif Technol* 2012; 92: 106–114.
[144] Jing Q, Zhang J, Liu Y, et al. E-pH Diagrams for the Li-Fe-P-H2O System from 298 to 473 K: Thermodynamic Analysis and Application to the Wet Chemical Processes of the LiFePO4 Cathode Material. *Journal of Physical Chemistry C* 2019; 123: 14207–14215.
[145] Wang H, Guo M, Niu Y, et al. Study on Precipitation Processes and Phase Transformation Kinetics of Iron Phosphate Dihydrate. *Crystals (Basel)* 2022; 12: 1369.
[146] Solvay. Ferric Chloride product characteristics - density.
[147] BASF. Amines for Metalworking Fluids.

Appendix

Pourbaix diagrams

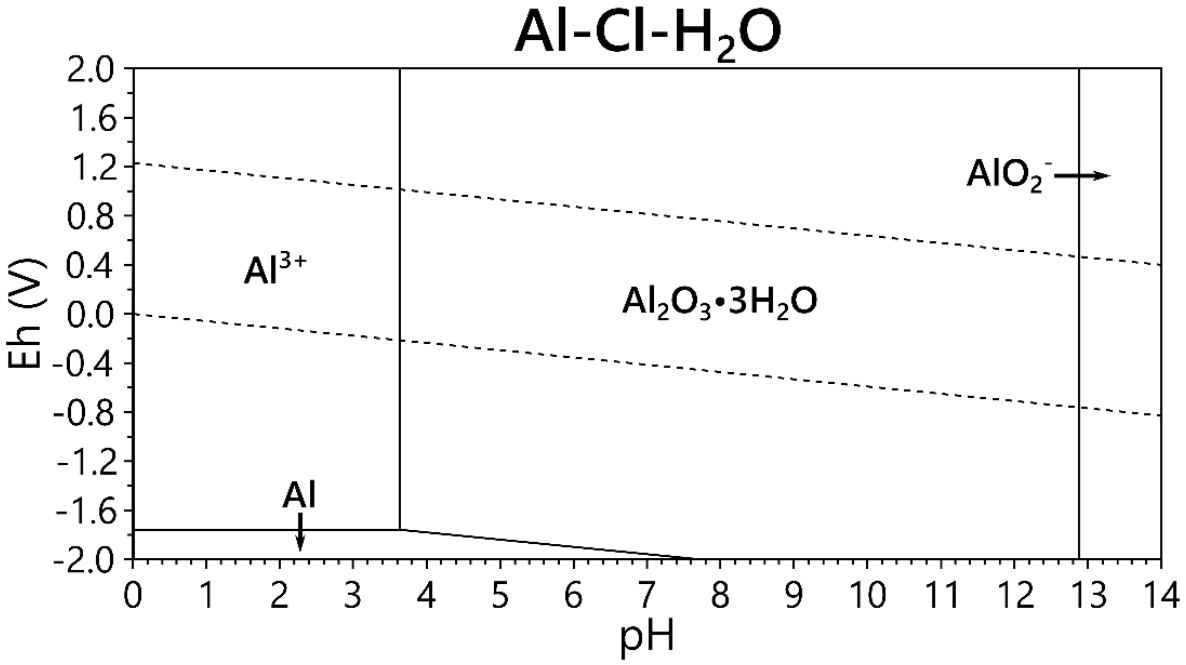

Figure A1: Pourbaix diagram for the Al-Cl-H_2O system with 1 mM Al and 10 M Cl at 25°C and 1 atm.

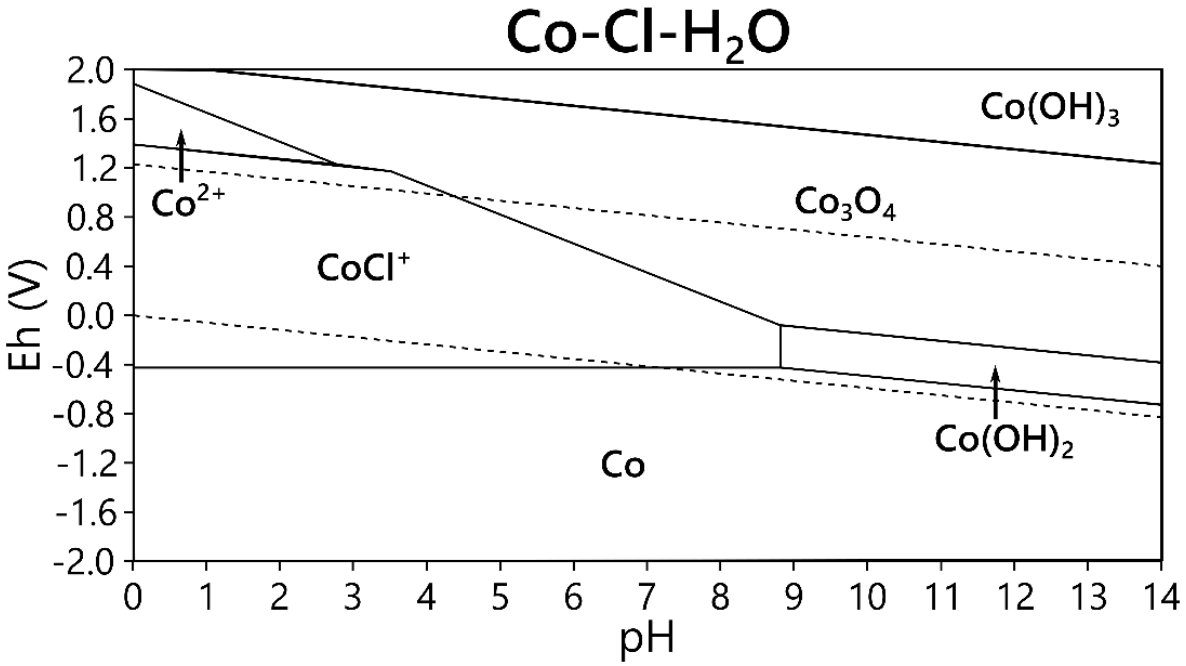

Figure A2: Pourbaix diagram for the Co-Cl-H_2O system with 1 mM Co and 10 M Cl at 25°C and 1 atm.

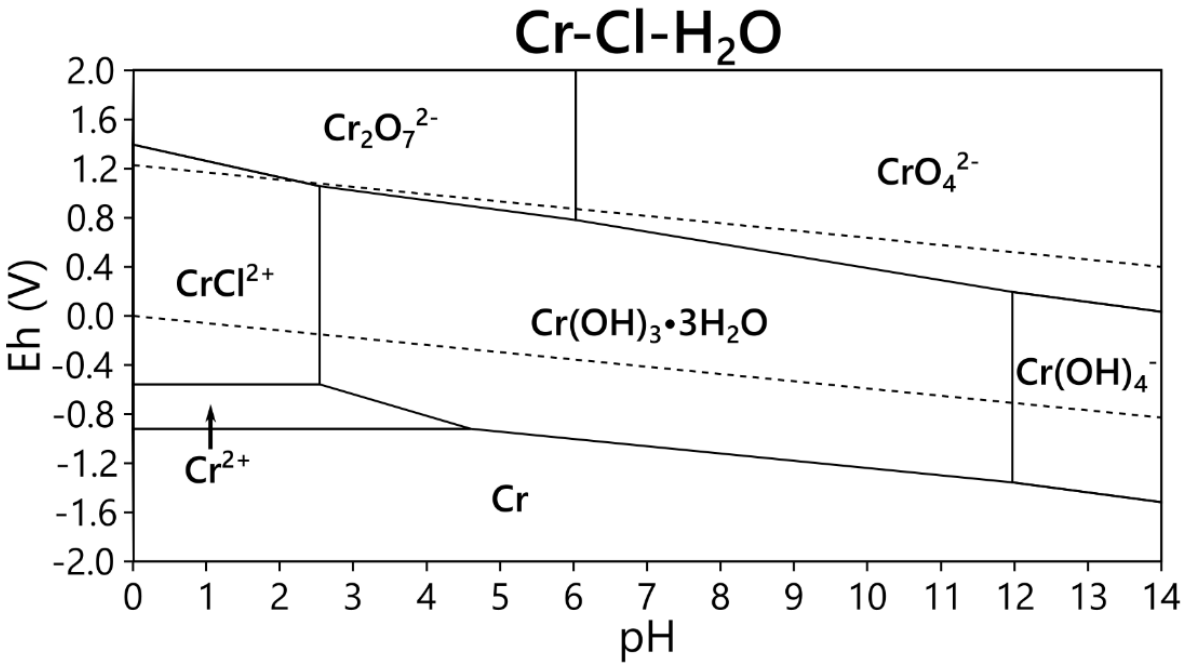

Figure A3: Pourbaix diagram for the Cr-Cl-H_2O system with 1 mM Cr and 10 M Cl at 25°C and 1 atm.

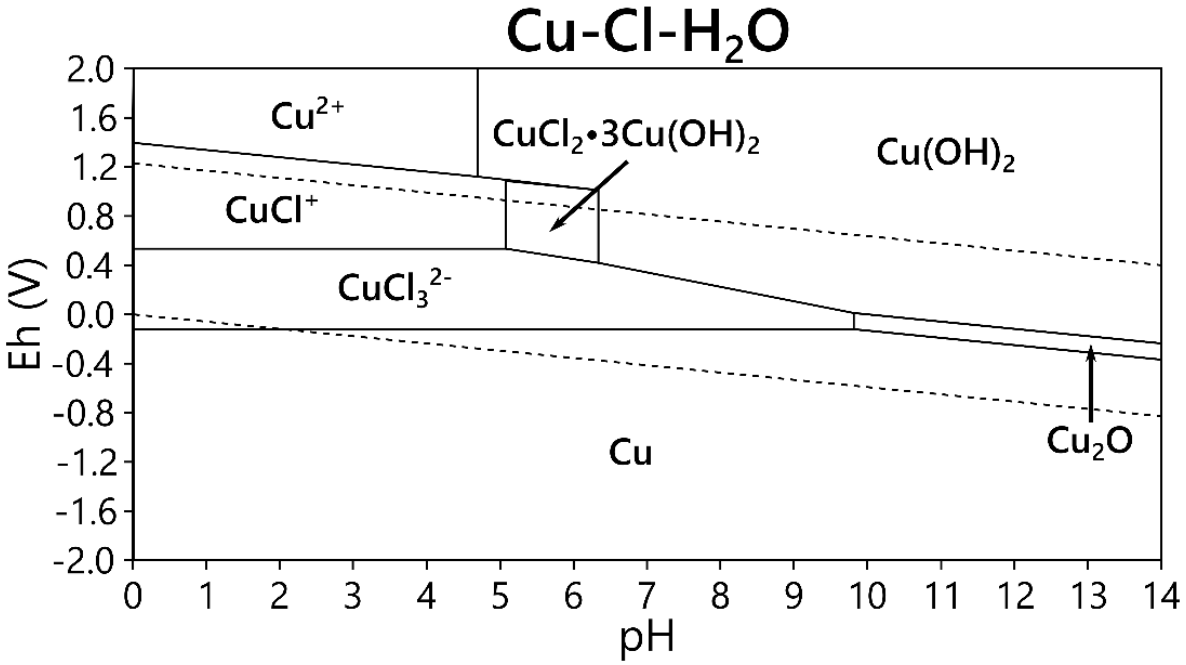

Figure A4: Pourbaix diagram for the Cu-Cl-H_2O system with 1 mM Cu and 10 M Cl at 25°C and 1 atm.

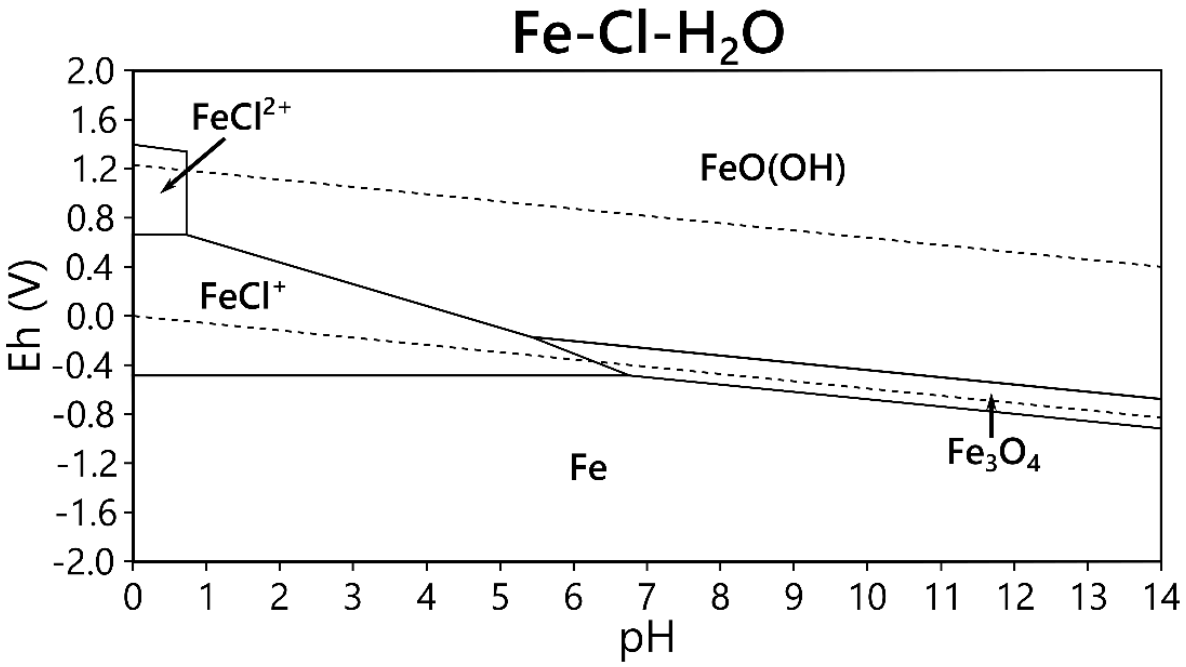

Figure A5: Pourbaix diagram for the Fe-Cl-H_2O system with 3.5 M Fe and 10 M Cl at 25°C and 1 atm.

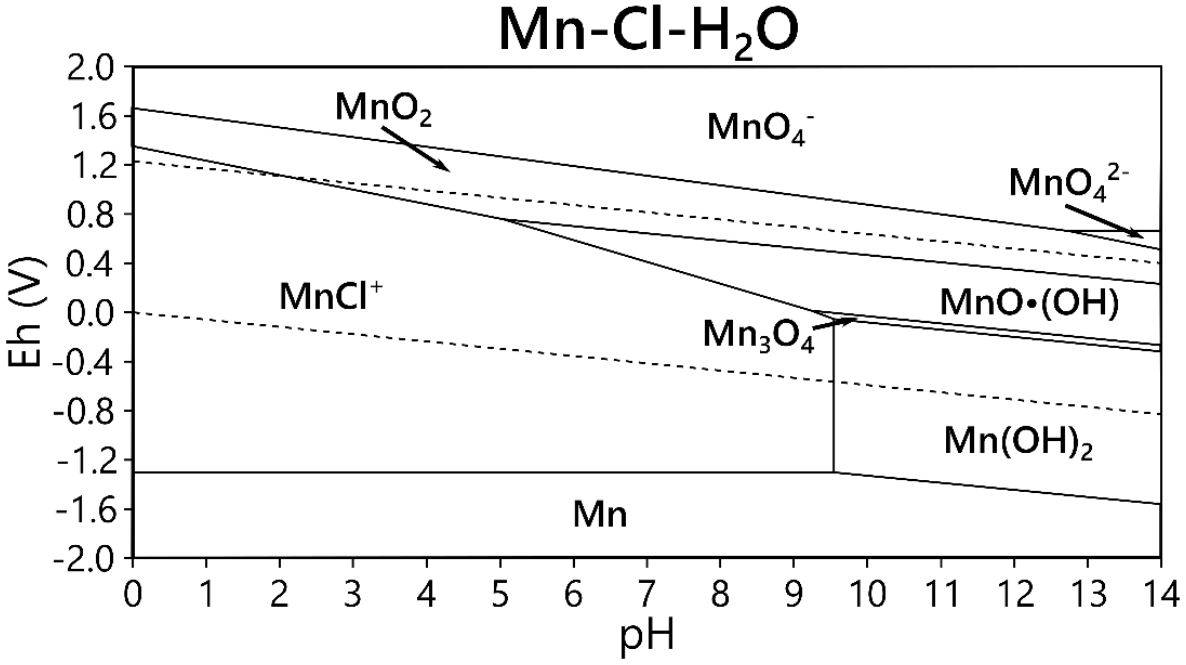

Figure A6: Pourbaix diagram for the Mn-Cl-H_2O system with 1 mM Mn and 10 M Cl at 25°C and 1 atm.

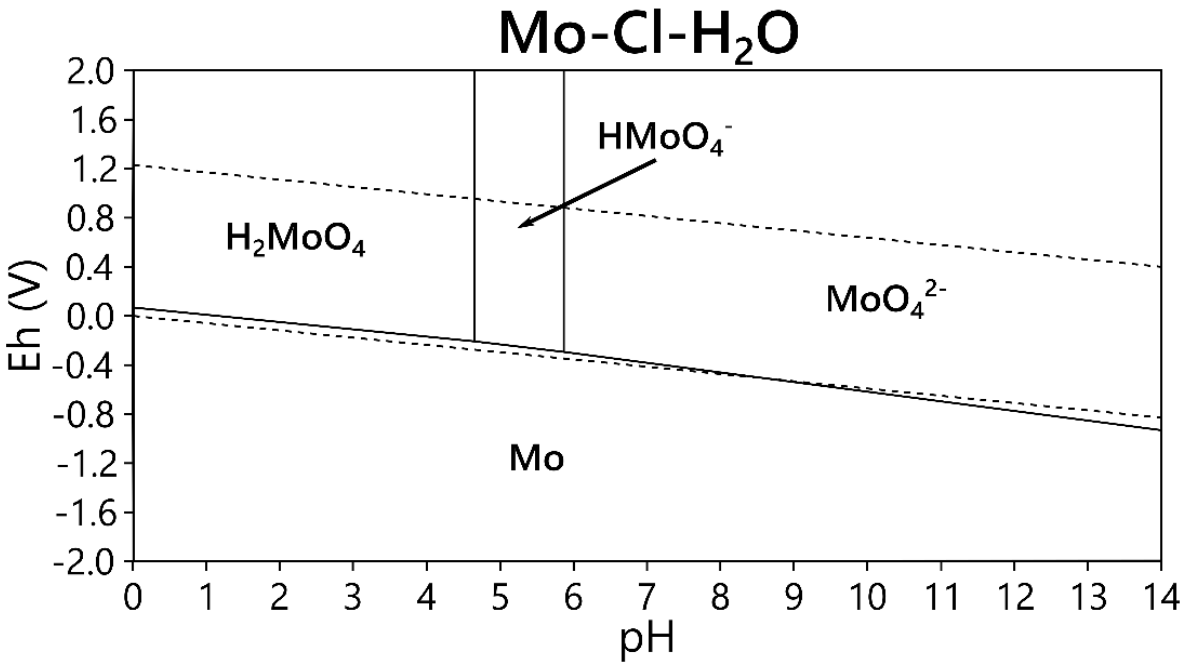

Figure A7: Pourbaix diagram for the Mo-Cl-H_2O system with 1 mM Mo and 10 M Cl at 25°C and 1 atm.

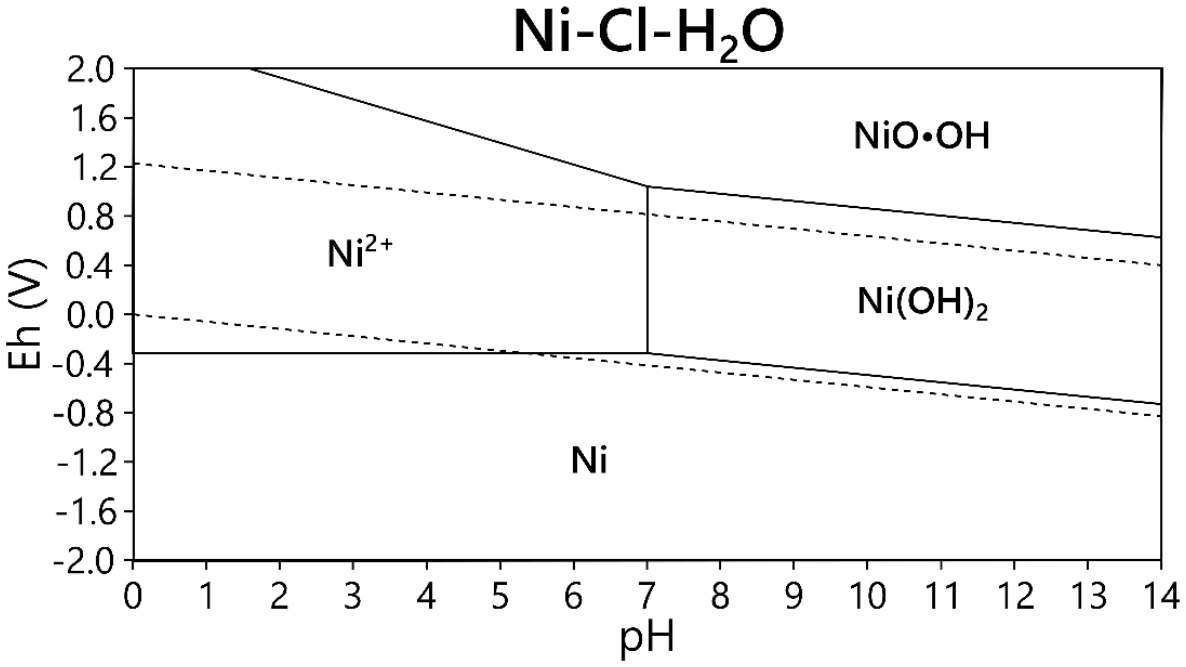

Figure A8: Pourbaix diagram for the Ni-Cl-H_2O system with 1 mM Ni and 10 M Cl at 25°C and 1 atm.

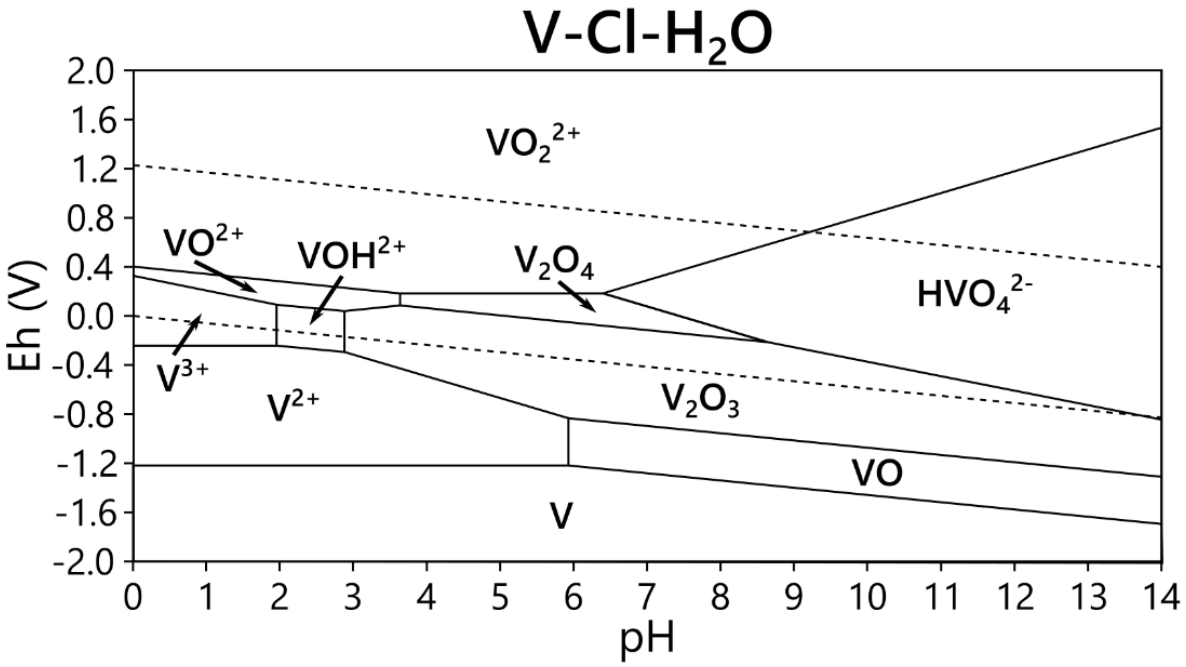

Figure A9: Pourbaix diagram for the V-Cl-H_2O system with 1 mM V and 10 M Cl at 25°C and 1 atm.

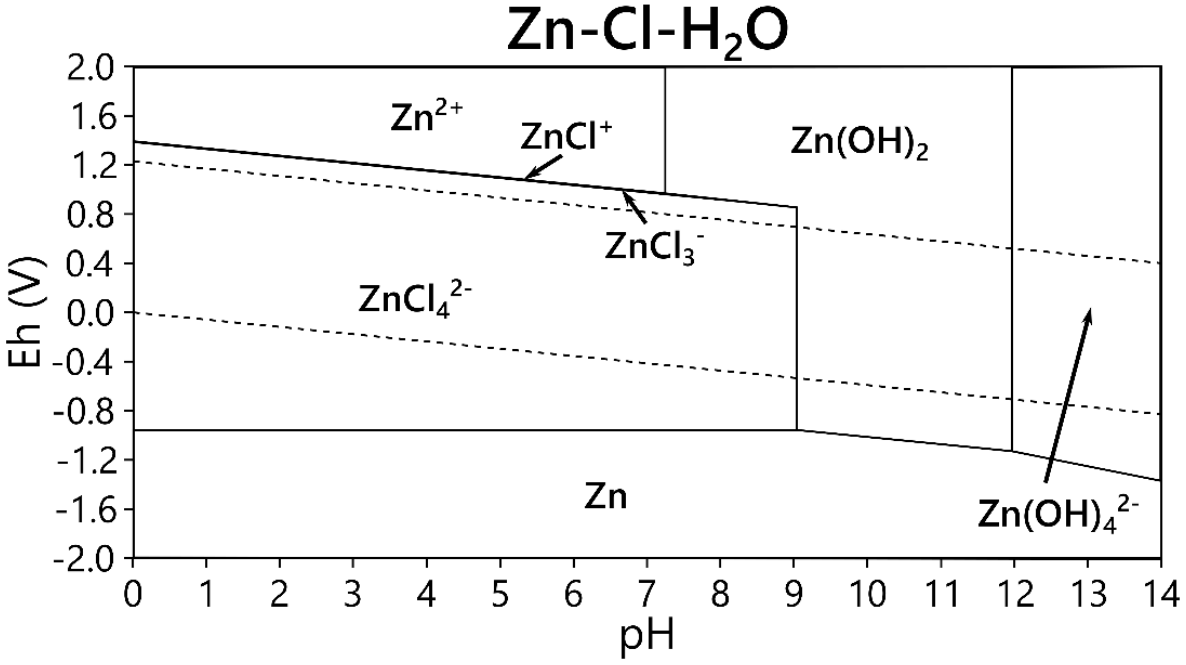

Figure A10: Pourbaix diagram for the Zn-Cl-H_2O system with 1 mM Zn and 10 M Cl at 25°C and 1 atm.

Iron chloride solution properties

Table A1: Properties of $FeCl_2$ solutions at 20°C with densities (ρ) based on a linear model fitted to empirical determinations at 50, 100, 150, 200, and 250 g Fe/L.

[Fe] (g/L)	ρ_{FeCl2} (g/mL)	x_{Fe} (wt%)	x_{FeCl2} (wt%)	[$FeCl_2$] (M)
10	1024	1.21	2.62	0.18
20	1042	2.06	4.56	0.36
30	1060	2.90	6.48	0.54
40	1078	3.72	8.35	0.72
50	1096	4.52	10.19	0.90
60	1114	5.31	11.99	1.07
70	1132	6.08	13.76	1.25
80	1150	6.84	15.48	1.43
90	1168	7.58	17.17	1.61
100	1186	8.30	18.83	1.79
110	1204	9.01	20.45	1.97
120	1222	9.71	22.03	2.15
130	1240	10.38	23.57	2.33
140	1258	11.05	25.08	2.51
150	1276	11.69	26.55	2.69
160	1295	12.32	27.98	2.87
170	1313	12.93	29.38	3.04
180	1331	13.53	30.74	3.22
190	1349	14.11	32.06	3.40
200	1367	14.68	33.35	3.58
210	1385	15.23	34.60	3.76
220	1403	15.77	35.81	3.94
230	1421	16.28	36.99	4.12
240	1439	16.79	38.13	4.30
250	1457	17.27	39.23	4.48
260	1475	17.74	40.30	4.66
270	1493	18.20	41.33	4.83
280	1511	18.64	42.32	5.01
290	1529	19.06	43.28	5.19
300	1547	19.47	44.19	5.37

Table A2: Properties of $FeCl_3$ solutions at 20°C with densities (ρ) based on [146].

[Fe] (g/L)	ρ_{FeCl3} (g/L)	x_{Fe} (wt%)	x_{FeCl3} (wt%)	[$FeCl_3$] (M)
10	1028	1.04	3.01	0.18
20	1049	1.91	5.56	0.36
30	1070	2.77	8.05	0.54
40	1091	3.61	10.48	0.72
50	1113	4.42	12.84	0.90
60	1134	5.21	15.14	1.07
70	1155	5.98	17.38	1.25
80	1176	6.73	19.56	1.43
90	1197	7.46	21.67	1.61
100	1218	8.17	23.72	1.79
110	1239	8.85	25.71	1.97
120	1260	9.52	27.64	2.15
130	1281	10.16	29.50	2.33
140	1302	10.78	31.30	2.51
150	1323	11.38	33.04	2.69
160	1345	11.95	34.71	2.87
170	1366	12.51	36.33	3.04
180	1387	13.04	37.87	3.22
190	1408	13.55	39.36	3.40
200	1429	14.04	40.78	3.58
210	1450	14.51	42.15	3.76
220	1471	14.96	43.44	3.94

Analytical methods

Quantification of total Fe by complexometric titration

Total Fe in a solution can be obtained by complexometric titration with EDTA and $ZnCl_2$ using Eriochrome black T indicator [102]. An iron chloride sample containing ~10 mg Fe was weighed and diluted to 50 mL with water in a beaker. The solution was further diluted with 150 mL 95 wt% ethanol, and the pH was adjusted to ≤2 with 25 wt% HCl. Exactly 40 mL of 0.01 M EDTA was added from a burette, and the solution was neutralised with 25 wt% ammonia until a colour shift from yellow to reddish occurred. A volume of 10 mL ammonium buffer (350 mL 25 wt% NH_4OH and 54 g NH_4Cl in 1 L water) and 0.3 g indicator (0.2 g/100 g Eriochrome black T in NaCl) were then added, after which excess EDTA was immediately back-titrated with 0.01 M $ZnCl_2$ until a colour change from blue to red.

Supplementary information and data

Table A3: Compositions of Hysol SL 35 XBB (B) and Hysol SL 36 XBB (G) according to safety data sheets.

Constituent	B (wt%)	G (wt%)	Function	Reference
Petroleum distillates	25-50	25-50	Lubricant	PubChem
Ethanolamine	≤13	≤8	Corrosion inhibitor, pH regulator	PubChem, [147]
Dicyclohexylamine	≤10	≤10	Corrosion inhibitor, lubricant	PubChem, [147]
Neodecanoic acid	-	≤10	Corrosion inhibitor, pH regulator	PubChem
(Z)-octadec-9-enol	≤5	-	Solvent, lubricant	PubChem
Methyldiethanolamine	≤5	≤5	Corrosion inhibitor, pH regulator	PubChem, [147]
Triethanolamine	≤5	≤10	Corrosion inhibitor, pH regulator	PubChem, [147]
Alcohols, C16-C18	≤3	-	Emulsifier	PubChem
Glycolic acid ethoxylate oleyl ether	≤3	-	Emulsifier	Sigma
Alkyl ether carboxylic acid	≤3	-	Emulsifier	Sigma
2-Octadec-9-enoxyethanol phosphoric acid	-	≤3	Solvent, emulsifier	PubChem
Oleic acid	-	≤3	Emulsifier	PubChem
Aminomethyl propanol	-	≤3	Emulsifier, lubricant	PubChem
5-Carboxy-4-hexyl-2-cyclohexene-1-octanoic acid	-	≤3	Corrosion inhibitor, surfactant	PubChem
Tolyltriazole sodium salt	≤0.3	≤0.3	Corrosion inhibitor	Sigma

Table A4: Data from an experimental design for potentiostatic leaching of mixed, washed grinding sludge with a $FeCl_3$/HCl solution.

Experiment	Variables			Response (%$E_{s,M}$)				Other
	T (°C)	ORP (mV)	n_{HCl}/ n_{FeCl3} (%)	Fe	Cr	Mn	Ni	%FC
1	20	300	1	59	86	54	61	17
2	60	300	1	71	89	15	68	45
3	20	400	1	86	89	60	66	12
4	60	400	1	66	87	31	66	31
5	20	300	5	61	85	59	61	16
6	60	300	5	61	90	20	67	32
7	20	400	5	95	88	66	69	8
8	60	400	5	92	89	37	67	30
9	40	350	3	81	87	44	67	21
10	40	350	3	61	88	41	67	23
11	40	350	3	61	88	40	67	24
12	40	350	3	71	92	42	68	24
13	11.7	350	3	87	88	63	65	11
14	68.3	350	3	51	89	25	67	42
15	40	279.3	3	57	88	39	66	26
16	40	420.7	3	31	88	45	68	23
17	40	350	0.2	66	91	42	67	25
18	40	350	5.8	81	88	46	67	21

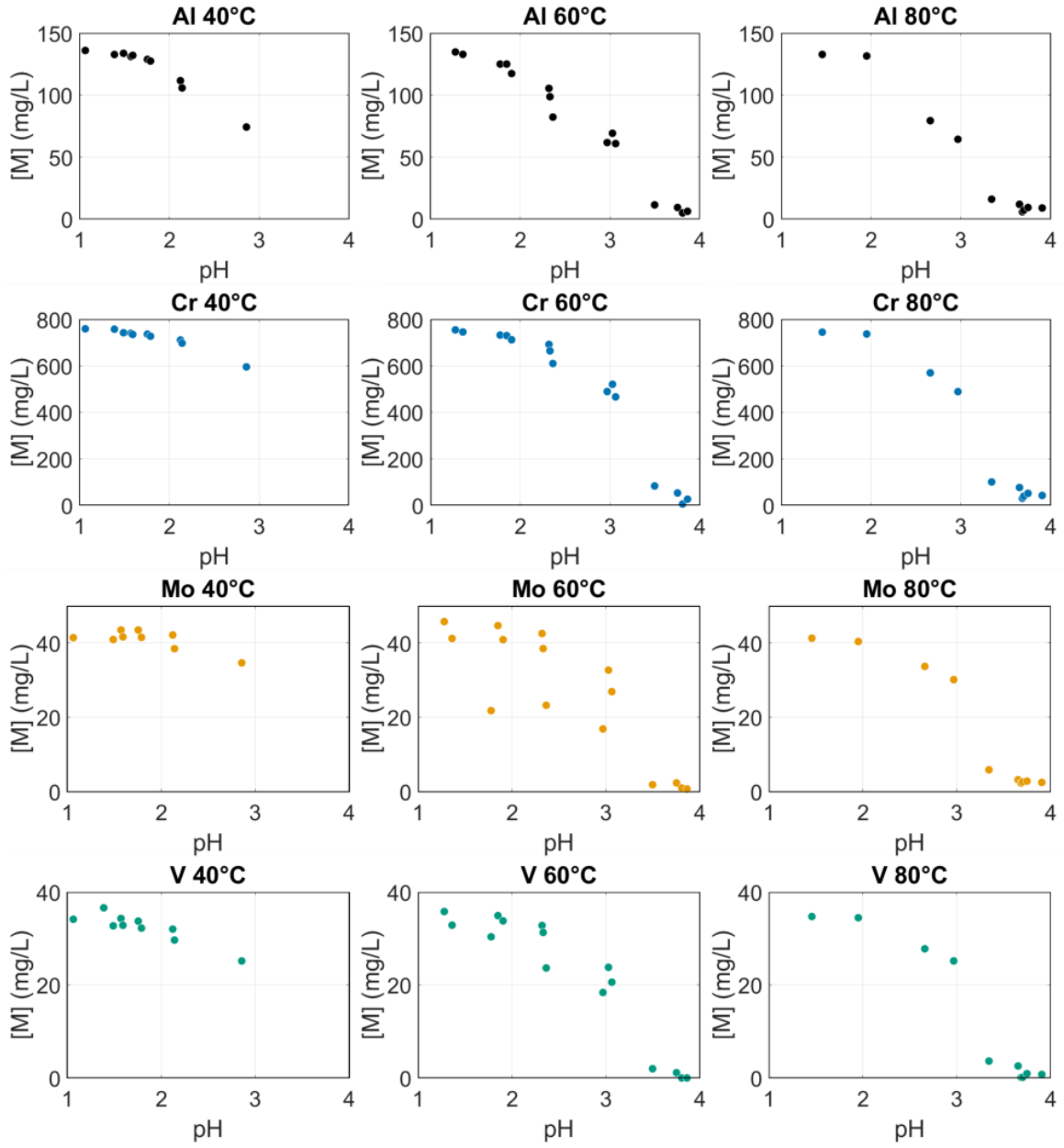

Figure A11: Concentrations of Al, Cr, Mo, and V versus pH in $FeCl_2$ solutions ([Fe] ≈ 200 g/L) at 40, 60, and 80°C. Data was obtained in the impurity precipitation experimental design presented in Section 5.5.3.

Table A5: Compositions of modelled process streams in the mass balances in Section 5.7.1.

Solids (wt%)														
Stream	Mass (kg)	Fe	Cr	Mn	Mo	Si	Ni	Cu	V	Al	Zn	Co	Cl	Other
Grinding sludge	1000	75.6	1.39	0.48	0.13	0.15	0.09	0.05	0.03	0.03	0.01	0.01	-	22.0
Dry swarf	815	90.6	1.61	0.60	0.16	0.13	0.12	0.07	0.03	0.03	0.02	0.01	-	6.6
Dry filter cake	162	35.1	8.22	0.68	0.83	0.67	0.56	0.36	0.18	0.14	0.04	0.01	-	53.3
Liquids (mg/kg Fe)														
Stream	Mass (kg)	Fe (wt%)	Cr	Mn	Mo	Si	Ni	Cu	V	Al	Zn	Co	Cl (wt%)	H_2O (wt%)
Leachate $FeCl_2$ (aq)	13730	15.1	4580	5400	264	555	426	85	68	96	181	11	19.2	65.5
Purified leachate (aq)	13730	15.1	230	5400	13	28	170	4	1	5	181	11	19.2	65.6
Product $FeCl_3$	5006	13.8	230	5400	13	28	170	4	1	5	181	11	26.2	59.9
Recirculated $FeCl_3$	9780	13.8	230	5400	13	28	170	4	1	5	181	11	26.2	59.9

Scale-up demonstration project

Pictures from a scale-up demonstration project with an aqueous washing pretreatment step, leaching and precipitation in a 5 L reactor, and pressure oxidation are shown in Figure A12 to Figure A14.

Figure A12: Weighing of mixed grinding sludges B and J (top left), washing with a detergent solution (top right), washing slurry after cleaning (bottom left), and HCl leaching and precipitation reactor setup with gas scrubbing (bottom right).

Figure A13: Leaching of grinding sludges B and J with HCl (top left), filtration of leaching slurry after precipitation (top right), filtered intermediate product $FeCl_2$ (bottom left), and pressure oxidation with O_2 (bottom right).

Figure A14: Filter cakes from the leaching of mixed unwashed sludges B and J (top left), and from the same sludges with aqueous washing (top right). Grinding sludge, intermediate product $FeCl_2$, and final product $FeCl_3$ (bottom).